UNIVERSIDADE DE LISBOA
FACULDADE DE CIÊNCIAS
DEPARTAMENTO DE ENGENHARIA GEOGRÁFICA, GEOFÍSICA E ENERGIA

Compound dry and hot extreme events in the Mediterranean region

André Filipe Correia Lourenço

Mestrado em Ciências Geofísicas

Dissertação orientada por:
Doutora Ana Russo
Doutor Virgílio Bento

2024

Agradecimentos

Gostaria de começar por agradecer aos meus orientadores, Ana Russo e Virgílio Bento, por todo o apoio que demonstraram ao longo deste ano, pelo tempo disponibilizado e pelos conselhos que me fizeram crescer enquanto cientista.

Gostaria de fazer um agradecimento especial ao João Geirinhas, pelo acompanhamento que fez da minha dissertação e pelas ideias que fizeram aprimorar este trabalho, também à Raquel Santos e ao João Careto, pela disponibilização de material importante no desenvolvimento deste trabalho.

O desenvolvimento desta dissertação não teria sido o mesmo sem os meus colegas e amigos de escritório, são eles a Mariana Oliveira, o Tomás Gaspar, a María Molina, o Miguel Lima, a Sílvia Nunes, o Tiago Ferreira e o João Cruz. O bom ambiente que sempre proporcionaram foi crucial para me sentir acolhido e em casa desde o primeiro dia.

Quero deixar um forte agradecimento aos meus amigos de orquestra, em especial à professora Catarina e ao professor César, que todas as semanas tiveram uma palavra de apoio e conforto.

Deixo também um agradecimento aos meus amigos de licenciatura e mestrado que estiveram presentes nesta jornada para momentos de descontração.

Por fim, agradeço à minha mãe e ao meu irmão que foram a base de tudo e uma peça fundamental para encarar de forma positiva todas as adversidades que surgiram.

This work was supported by the Fundação para a Ciência e a Tecnologia (FCT) I.P./MCTES through national funds (PIDDAC, grant no. UIDB/50019/2020, https://doi.org/10.54499/UIDP/50019/2020, and LA/P/0068/2020, https://doi.org/10.54499/LA/P/0068/2020, to Instituto Dom Luiz; project DHEFEUS, https://doi.org/10.54499/2022.09185.PTDC).

Abstract

In recent decades, extreme events such as heatwaves and droughts have increased in number, duration and severity, and these trends are expected to continue to increase under climate change scenarios. These events can occur simultaneously or consecutively, and have severe impacts on ecosystems and human health, with significant reported losses.

The objectives of this work are twofold: 1) to make a historical characterization of single and compound dry and hot extreme events (CDHEs) between 1979 and 2022 in Mediterranean Europe, and 2) to analyze the driving mechanisms conducive of CDHEs. The year 2022 is defined in the literature as one of the most severe CDHEs in recent years, and thus is presented here as a case study. For the purpose of this study, ERA5 data of temperature, total precipitation, volumetric soil water layers 1, 2 and 3, temperature at 850 hPa, geopotential height at 850 hPa, and vertical integrate of eastward and northward water vapor flux, with a spatial resolution of 0.25º x 0.25º, is used.

Heatwaves were identified when maximum temperature is above its 90th percentile during at least 5 days. The Standardized Precipitation Index (SPI) on a 12-months accumulation scale (hereafter, SPI-12) was used to identify drought conditions at a monthly scale. Drought events were identified when SPI-12 was below -1 during at least 2 months. CDHEs were identified with a cooccurrence matrix, with 1 in each grid point under heatwave and drought.

The results show positive trends for the duration and intensity of heatwaves and droughts and, conversely, negative trends for soil moisture. Most of the study area show statistically significant negative trends when aggregating spatially for soil moisture. On the other hand, the annual temperature means present an increase and precipitation means show a small decrease on decadal trends. The bivariate analysis shows a shift on temperature and soil moisture towards dry and hot conditions. Heatwaves occupy smaller areas than droughts, which in turn influences the areas of the CDHEs, due to different reaction times of the atmosphere and soil. The combination of the high temperature, low soil moisture and precipitation, and anticyclonic conditions, associated with subsidence and clear-sky conditions, is the main driver to the development and maintenance of extreme events, as in 2022 CDHE event.

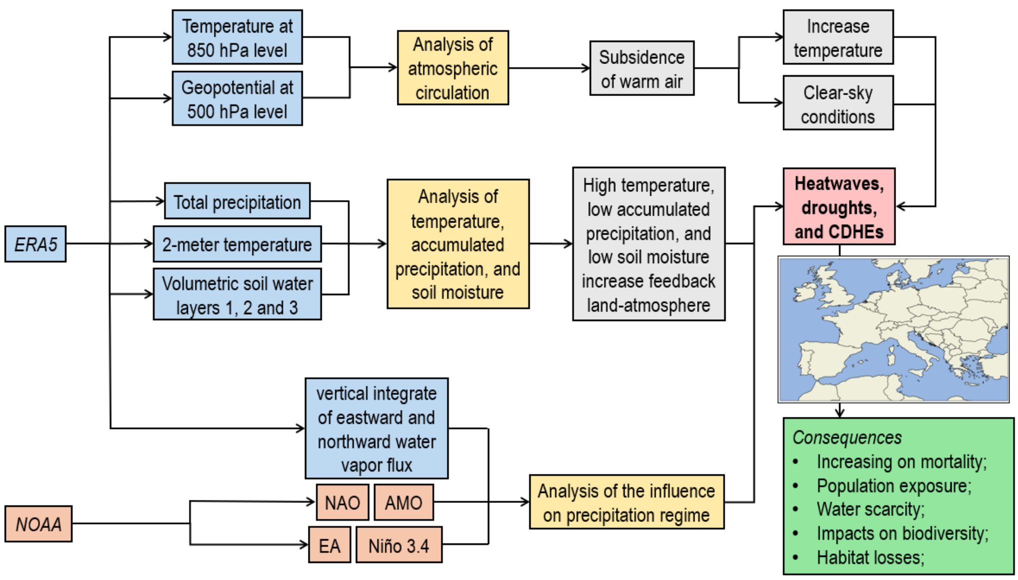

Figure A: Graphical abstract about this work.

Keywords: Heatwaves, Droughts, Temperature, Soil moisture and Precipitation.

Resumo

Nas últimas décadas, tanto a ocorrência de ondas de calor como de secas tem aumentado em número, duração e intensidade. Esse incremento tem conduzido ao aumento da coocorrência de ondas de calor e secas. Estes eventos, denominados em português, eventos compostos quentes e secos (ou, em inglês, compound dry and hot events, CDHEs) têm impactos profundos em vários setores da nossa sociedade como, por exemplo, na saúde humana, na produção agrícola ou na destruição da biodiversidade e habitats naturais. Desta forma, o entendimento de como as ondas de calor, as secas e os CDHEs se desenvolvem e quais são os mecanismos que estão na sua génese, torna-se muito relevante. Particularmente, na região Mediterrânica, que é caracterizada por ser um potencial foco de desenvolvimento deste tipo de eventos.

Os objetivos deste trabalho são: 1) fornecer uma caracterização histórica das ondas de calor, das secas e dos CDHEs, entre 1979 e 2022, fazendo uma caracterização baseada nas análises de tendências da temperatura, precipitação acumulada e da humidade no solo e também um estudo probabilístico dessas variáveis; 2) identificar os mecanismos de desenvolvimento desses mesmos tipos de eventos para o mesmo período de estudo, analisando a circulação atmosférica para cada tipo de evento, identificando os centros de alta pressão e relacionando-os com o aumento de temperatura e o transporte de humidade, a fim de analisar os mecanismos que potenciam o desenvolvimento de eventos extremos e identificar as regiões mais propensas a estes fenómenos; 3) por fim, analisar em detalhe o ano de 2022, que foi caracteristicamente quente e seco e está definido na literatura como um forte CDHE. Este trabalho foca-se na Europa Mediterrânica, entre os 13º e 32º W de longitude e os 32º e 60º N de latitude, e em duas sub-regiões, a Ibéria e a França.

Os dados utilizados neste trabalho, temperatura do ar a 2 metros, precipitação total, volume de água no solo nas camadas 1, 2 e 3 (correspondendo a 1 metro de profundidade), temperatura aos 850 hPa, a altura geopotencial aos 500 hPa e integração vertical do fluxo de vapor de água para leste e para norte, foram extraídos da 5ª geração de dados de reanálise do *European Centre for Medium-Range Weather Forecasts* (Hersbach et al., 2020).

Um determinado período foi considerado como uma onda de calor quando a temperatura máxima se encontrou acima do percentil 90 durante pelo menos 5 dias. Teve-se também em consideração que os eventos separados temporalmente por 2 ou menos dias são o mesmo evento. As secas foram identificadas através do índice de seca, *Standardized Precipitation Index* (SPI), calculado com base em dados mensais de precipitação acumulada. Considerou-se um evento de seca sempre que o SPI esteve abaixo de -1 durante, pelo menos, 2 meses. Como nas ondas de calor, também se consideraram eventos separados temporalmente por apenas 1 mês como o mesmo evento. As ondas de calor foram de seguida caracterizadas quanto à sua frequência, duração, intensidade e intensidade cumulativa, enquanto as secas foram caracterizadas quanto à sua duração e tendo em conta os meses sob seca, considerando o período climatológico 1981-2010. Quanto aos CDHEs, foram obtidos através da interseção das matrizes de identificação das ondas de calor e secas, i.e. em cada ponto de grelha assinalou-se com o valor 1 a coocorrência dos dois tipos de eventos num determinado período. Desta forma, apresentaram-se os resultados sob a forma de área para os três tipos de eventos extremos. Tendo em conta o segundo objetivo deste trabalho, realizou-se uma análise das tendências decadais, bem como uma análise bivariada com ajuste de Kernel da temperatura, da precipitação acumulada e da humidade no solo acompanhada por *Probability Density Functions* (PDFs) de forma a entender a evolução de cada variável nos dois subperíodos e como isso pode influenciar o aumento da ocorrência de eventos extremos. As configurações atmosféricas também foram estudadas de forma a perceber quais as características da atmosfera que estiveram na génese destes três tipos de eventos. Para isso calcularam-se os compósitos

médios da temperatura aos 850 hPa e da altura geopotencial aos 500 hPa, considerando os meses de cada distribuição cujo valor está acima do percentil 90 da respetiva distribuição. Esta análise foi dividida em meses de inverno (de dezembro a fevereiro) e de verão (de junho a agosto). O último mecanismo estudado neste trabalho foi o fluxo de vapor de água que entra pela fronteira oeste da área de estudo, denominado por *Western Moisture Flux* (WMF). Neste caso utilizou-se a fronteira oeste devido à maior influência do movimento atmosférico oeste-este sentida no Atlântico Norte, que afeta as regiões estudadas. Este fluxo foi correlacionado com quatro teleconexões de forma a identificar a teleconexão que mais influencia a variação deste fluxo. São elas a fase positiva da *North Atlantic Oscillation* (NAO+), a *Atlantic Multidecadal Oscillation* (AMO), a *Eastern Atlantic* (EA) e o *Niño 3.4* (N3.4). Os resultados obtidos mostraram que a NAO+ e a EA são as teleconexões que influenciam mais fortemente a WMF na Europa e também nas duas subregiões. Calcularam-se as anomalias sazonais do *Integrated Water Vapor Transport* (IVT) e da divergência de vapor de água.

Os resultados obtidos apresentaram grande variabilidade interanual e tendências decadais positivas. Também se analisaram estas características tendo em conta dois subperíodos, 1979-2000 e 2001-2022. Os resultados mostraram que em 2001-2022 houve um aumento dos valores das características estudadas nas ondas de calor relativamente a 1979-2000, enquanto nas secas essas variações não são tão percetíveis. Os CDHEs mostraram uma distribuição de valores máximos durante mais meses para as secas do que para as ondas de calor. Assim, a distribuição dos CDHEs é fortemente influenciada pela das ondas de calor, devido aos tempos de resposta da atmosfera serem muito mais rápidos do que do solo, ou mesmo devido aos limites utilizados para identificar cada evento.

Os resultados das tendências decadais evidenciam o aumento de temperatura, e o decréscimo de precipitação acumulada e de humidade no solo. Após a análise bivariada, também se observou uma migração dos valores para condições mais secas e mais quentes, demonstrando uma propensão ao desenvolvimento de ondas de calor, secas e CDHEs. Os resultados mostraram uma persistência de centros de altas pressões sobre a Europa durante os meses mais intensos. Estas condições anticiclónicas provocam o aumento da temperatura à superfície e condições de céu limpo através de processos de subsidência nas regiões afetadas.

Durante o ano de 2022, identificaram-se condições muito quentes, com anomalias superiores a 2 ºC sobre toda a Europa, promovidas por condições anticiclónicas onde ocorreu subsidência de ar mais quente na baixa troposfera. Isto levou a condições de céu limpo e, portanto, a défices de precipitação. Estas condições foram complementadas através de anomalias de precipitação acumulada e de humidade no solo muito negativas no sul da Europa, que atingiram os -1 mm e -0.1 m^3/m^3, respetivamente. As anomalias sazonais de IVT e da divergência de vapor de água mostraram que o aumento da divergência está diretamente relacionado com a subsidência atmosférica, levando à dissipação do vapor de água sobre a Europa central durante a primavera e sobre a Ibéria no verão. Esta humidade abaixo do esperado e o aumento da divergência do vapor de água, ao mesmo tempo que se encontraram padrões de circulação anticiclónica sobre a Europa central, constituiu o mecanismo de desenvolvimento principal para as condições excecionalmente quentes e secas observadas no ano de 2022.

Palavras-chave: Ondas de calor, Secas, Temperatura, Humidade no solo e Precipitação.

Contents

Agradecimentos i

Abstract ii

Resumo iii

Contents v

List of Acronyms and Abbreviations vi

List of Figures viii

List of Tables xii

Chapter 1 – Introduction 1

1.1 Extreme events 1

1.2 Objectives and motivations 4

Chapter 2 – Data and Methodology 6

2.1 Data 6

2.2 Methodology 7

2.2.1 Heatwaves and droughts 7

2.2.2 Identification of CDHEs 8

2.2.3 Analysis of driving mechanisms 9

Chapter 3 – Results 13

3.1 Historical characterization of extreme events 13

3.2 Study case: 2022 CDHE 22

Chapter 4 – Discussion 26

Chapter 5 – Conclusions 30

References 32

Supplementary material 42

List of Acronyms and Abbreviations

AMO – Atlantic Multidecadal Oscillation

CDHE – Compound dry and hot event

CMIP – Coupled Model Intercomparison Project

DJF – December, January, and February months

EA – Eastern Atlantic Pattern

ECMWF – European Centre for Medium-Range Weather Forecasts

ENSO – El Niño-Southern Oscillation

ERA5 – ECMWF's 5th generation reanalysis dataset

ET – Evapotranspiration

IPCC – Intergovernmental Panel on Climate Change

IVT – Integrated Water Vapor Transport

JJA – June, July, and August months

LH – Latent heat

MAM – March, April, and May months

N – North

NAO – North Atlantic Oscillation

NASA – National Aeronautics and Space Administration

NCAR – National Center for Atmospheric Research

NOAA – National Oceanic and Atmospheric Administration

N3.4 – Niño 3.4 Pattern

PDF – Probability Density Function

PDSI – Palmer Drought Standardized Index

PET – Potential Evapotranspiration

RCP – Representative Concentration Pathway

SH – Sensible heat

SON – September, October, and December months

SPI – Standardized Precipitation Index

TOA – Top of atmosphere

W – West

WMF – Western Moisture Flux

List of Figures

Figure A: Graphical abstract about this work…………………………………………………………...ii

Figure 1: Schematic representation of the development of heatwaves, droughts, and CDHEs. SH represents sensible heat, LH represents latent heat and ET represents evapotranspiration (Hao et al., 2022).. 2

Figure 2: Study area representation, showing Central and Southern Europe... 6

Figure 3: Schematic representation of the procedure applied to identify a heatwave (following Hobday et al., 2016). The blue line represents the climatology, the green represents the 90th percentile and the black represents the observed temperatures. Font: https://www.marineheatwaves.org/all-about-mhws.html.. 7

Figure 4: Schematic representation of zonal and meridional components of IVT............................... 10

Figure 5: Schematic representation of the boundaries. F_W represents western boundary, F_N represents northern boundary, F_E represents eastern boundary, and F_S represents southern boundary.................. 11

Figure 6: Time series of annual spatial means of temperature (a), daily accumulated precipitation (b) and soil moisture (c) accompanied by decadal trend values, with the value of the respective trends labelled “m”. Trends of soil moisture (dots depict statically significant trends at a 5% level) (d). 13

Figure 7: SPI time series for Europe. Positive SPI values are shown in blue, representing months with wet conditions. Negative SPI values are shown in red, representing months with dry conditions. 14

Figure 8: Frequency (a and e), duration (b and f), intensity (c and g) and cumulative intensity (d and h) of heatwaves with decadal trends and divided in two subperiods, 1979-2000 and 2001-2022, considering the whole domain. 15

Figure 9: Months under drought (a and c), and magnitude (b and d) of droughts with decadal trends and divided in two subperiods, 1979-2000 and 2001-2022, considering the whole domain. 16

Figure 10: Europe’s area affected by each type of drought. Continuous (green) line indicates mild drought, long dashed (orange) line indicates moderate drought, dot dashed (red) line indicates severe drought and dotted (black) line indicates extreme events. 17

Figure 11: Plots of the bivariate distributions with kernel fit plots accompanied by univariate PDFs with kernel fit of each variable: temperature and accumulated precipitation (a) and temperature and soil moisture (b), considering whole domain.. 18

Figure 12: Incidence (%) of heatwaves, droughts and CDHEs occurrences in Europe (vertical colorbar), with trends for each month between 1979 and 2022 ('X’ marking statically significant trends at a 5% level; horizontal colorbar). 19

Figure 13: Mean composite of temperature anomalies at 850 hPa level (color shading) and geopotential height at 500 hPa level (m) (contours). The red zones and continuous lines indicate positive anomalies and blue zones and discontinuous lines indicate negative anomalies. “Composite” indicates an annual

composite, “Winter season” indicates a composite of the DJF months, and “Summer season” indicates a composite of the JJA months. 20

Figure 14: Time series from 1979 to 2022 of the NAO (blue and continuous line), the AMO (green and dot line), the EA (red and long dash line), and the N3.4 (purple and dot dash line) and of the anomalies of western moisture flux in Europe (yellow and shaded line) filtered by a 10-year low pass Lanczos filter. 21

Figure 15: Spatial anomalies of temperature (a), accumulated precipitation (b), and soil moisture (c) for 2022, regarding 1981-2010 climatological period. 23

Figure 16: Composite of temperature anomalies at 850 hPa level (color shading) and geopotential height at 500 hPa level (m) (contours), considering all months, winter and summer of 2022, regarding 1981-2010 climatological period. 23

Figure 17: Seasonal IVT anomaly (regarding the 1981 - 2010 climatology) during 2022 (absolute field – color shading; direction – vectors). 24

Figure 18: Seasonal anomalies of moisture divergence (regarding the 1981 - 2010 climatology) during 2022. 25

Figure S1: Time series of mean temperature (a and d), accumulated precipitation (b and e) and soil moisture (c and f) accompanied by decadal trend values, The first line corresponds to Iberia and the second line correspond to France. viii

Figure S2: Seasonal mean temperature with decadal trend, considering Europe. 43

Figure S3: Seasonal mean accumulated precipitation with decadal trend, considering Europe. 43

Figure S4: Seasonal mean soil moisture with decadal trend, considering Europe. 44

Figure S5: As in Fig. S2, but considering Iberia. 44

Figure S6: As in Fig. S3, but considering Iberia. 45

Figure S7: As in Fig. S4, but considering Iberia. 45

Figure S8: As in Fig. S2, but considering France. 46

Figure S9: As in Fig. S3, but considering France. 46

Figure S10: As in Fig. S4, but considering France. 47

Figure S11: As in Fig. 7, but considering Iberia. 47

Figure S12: As in Fig. 7, but considering France. 48

Figure S13: As in Figs. 8 and 9, but considering Iberia. 49

Figure S14: As in Figs. 8 and 9, but considering France. 50

Figure S15: As in Fig. 10, but considering Iberia. 51

Figure S16: As in Fig. 10, but considering France. 51

Figure S17: As in Fig. 11, but considering Iberia. 52

Figure S18: As in Fig. 11, but considering France. 52

Figure S19: As in Fig. 12, but considering Iberia. 53

Figure S20: As in Fig. 12, but considering France. 54

Figure S21: As in Fig. 13, but considering Iberia. 55

Figure S22: As in Fig. 13, but considering France. 56

Figure S23: As in Fig. 14, but considering Iberia. 57

Figure S24: As in Fig. 14, but considering France. 58

Figure S25: Annual spatial frequency of heatwaves between 1979 and 1993. 59

Figure S26: Annual spatial frequency of heatwaves between 1994 and 2008. 60

Figure S27: Annual spatial frequency of heatwaves between 2009 and 2022. 61

Figure S28: Annual spatial duration of heatwaves between 1979 and 1993. 62

Figure S29: Annual spatial duration of heatwaves between 1994 and 2008. 63

Figure S30: Annual spatial duration of heatwaves between 2009 and 2022. 64

Figure S31: Annual spatial intensity between 1979 and 1993. 65

Figure S32: Annual spatial intensity between 1994 and 2008. 66

Figure S33: Annual spatial intensity between 2009 and 2022. 67

Figure S34: Annual spatial cumulative intensity between 1979 and 1993. 68

Figure S35: Annual spatial cumulative intensity between 1994 and 2008. 69

Figure S36: Annual spatial cumulative intensity between 2009 and 2022. 70

Figure S37: Annual spatial duration of droughts between 1979 and 1993. 71

Figure S38: Annual spatial duration of droughts between 1994 and 2008. 72

Figure S39: Annual spatial duration of droughts between 2009 and 2022. 73

Figure S40: Annual spatial magnitude of droughts between 1979 and 1993. 74

Figure S41: Annual spatial magnitude of droughts between 1994 and 2008. 75

Figure S42: Annual spatial magnitude of droughts between 2009 and 2022. 76

List of Tables

Table 1: Annual and monthly Pearson's correlation coefficients obtained between filtered time series of three indexes and WMF in Europe for the 1979 – 2022 period. In bold are shown the statistically significant correlation coefficients at a 5% significant level according to the Student's two-tailed t test. 22

Table S1: As in Table 1, but considering Iberia. 57

Table S2: As in Table 1, but considering France. 58

Chapter 1 – Introduction

1.1 Extreme events

According to the 6th Assessment Report of IPCC (IPCC, 2023), emissions of greenhouse gases from human activities are responsible for approximately 1.1 ºC of warming since 1850-1900. Furthermore, climatological global temperature is expected to reach or exceed 1.5 ºC of warming in the next 20 years.

Small changes in mean global temperature, particularly due to human influence, which have become more pronounced in the last decade, can have disproportionate consequences on the intensity and frequency of climate extremes (Perkins et al., 2015; IPCC, 2023). This can greatly impact society, the environment (Mueller et al., 2012; Kong et al., 2020), and ecosystems (Rilling et al., 2019). High temperatures can develop a state of dryness in vegetation, which can lead to drought events (Russo et al., 2018; Mueller and Seneviratne, 2012) and fires (Duff et al., 2018), depending on vegetation conditions (Olschewski et al., 2023).

Extremes of heat have a broader and far-reaching set of impacts than non-extreme temperatures, particularly when they occur for a prolonged period or suddenly (Wobus et al., 2018). When a prolonged period of excessive heat occurs, we are in the presence of an atmospheric heatwave (Perkins and Alexander, 2013). These events are characterized by having daily maximum temperatures greater than its climatological 90th percentile during a group of consecutive days (Nguyen et al., 2010). However, there is no universal definition for identifying these events (Zhang et al., 2011). It is estimated that the heatwaves of 2003 in Europe and 2010 in Russia were responsible for 70000 and 54000 deaths (Luterbacher et al., 2004; Coumou and Rahmostorf, 2012). It should be noted that it is difficult to correctly attribute the deaths associated with this type of event, and that these may be underestimated. Apart from the stated impacts, heatwaves can also increase the urban heat island effect (Leal-Filho et al., 2018), contribute to the rise of energy consumption (Santamouris et al., 2015) and have tremendous impacts in health (Geirinhas et al., 2019).

In addition to heatwaves, drought is another climate phenomenon, characterized by prolonged periods during which the amount of precipitation over a specific area is markedly less than normal in that same area and over a certain period (Allaby and Garratt, 2007). Drought events result in a negative impact on agricultural production, as happened during the 2010 event in Russia, causing a loss of around 30 percent in the harvest of cereals (Barriopedro et al., 2011), rice crops (Lanning et al., 2011) and milk production (Dunn et al., 2014). In addition to the consequences on agricultural production, droughts affect water resources (Peña-Guerrero et al., 2020) and natural ecosystems (Müller and Bahn, 2022), which has impacts on the environment and economic sectors, with billions of euros in direct and indirect damage (Vicente-Serrano et al., 2011; Turco et al., 2019).

Heatwaves and droughts are closely interconnected (Russo et al., 2018; Mueller and Seneviratne, 2012). Heatwaves dry out soils, leading to even higher temperatures (Geirinhas et al., 2022; Miralles et al., 2019; Hao et al., 2022). These elevated temperatures increase the evaporation of surface waters, like rivers and lakes, diminishing vital freshwater sources. Additionally, during a heatwave, the demand for water rises for drinking, cooling and crop irrigation, further aggravating water shortages caused by droughts (Figure 1).

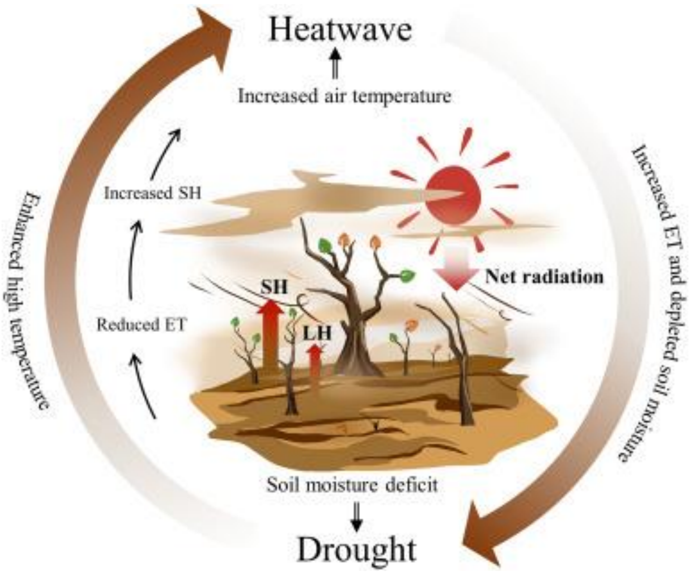

Figure 1: Schematic representation of the development of heatwaves, droughts, and CDHEs. SH represents sensible heat, LH represents latent heat and ET represents evapotranspiration (Hao et al., 2022).

The interplay between dry and hot events is commonly known as compound dry and hot events (CDHEs) (Leonard et al., 2014), defined as co-occurring or in sequence, in the same geographical location or multiple locations (Zscheischler et al., 2018; Raymond et al., 2020). In recent years, several studies have stressed the role played by the interplay between multiple climatic extremes, which may exacerbate the impacts of individual hazards (Zscheischler and Seneviratne, 2017; Ribeiro et al., 2020). Globally, an increase in CDHEs over a historical period as well as in future projections has been found (Manning et al., 2019; Feng et al., 2020) across multiple locations, pointed with high confidence by IPCC (2023), including USA (Alizadeh et al., 2020; Mazdiyasni and AghaHouchak, 2015), Europe (Russo et al., 2018; Hauser et al., 2015; Zscheischler et al., 2018), Australia (Seneviratne et al., 2012) and China (Lu et al., 2018). The progressive intensification of these compound extremes represents one of the largest challenges in climate change research (Dosio et al., 2018) and have strong impacts on ecosystems, vegetation reduction (Wu et al., 2022) and agricultural production (Hao et al., 2021), workplace productivity or wildfire frequency, more severe than single events of heatwaves or droughts (Sutanto et al., 2020). For example, in 2017 in Portugal, the previous conditions of low soil moisture in spring strongly amplified the magnitude of the devastating fires that occurred in the summer (Ramos et al., 2023). Similarly, the catastrophic fire seasons of 2019 in Greece (NASA Earth Observatory, 2024a) and 2019/2020 in Australia was also associated with a drought exacerbation due to hotter than usual conditions (NASA Earth Observatory, 2024b). These impacts will increase under enhanced global warming, where increasing heatwave trends will likely produce more severe and possibly irreversible impacts in some sectors (Beggs et al., 2019; King et al., 2018), possibly with higher costs.

In 2018, according to the insurance company Munich RE (2024), financial losses related to CDHE were estimated at around 3.3 billion euros, making it the costliest in Europe. Population exposure is also a consequence and is a commonly used metric to evaluate the impact of extreme events on human society, which is expected to be exacerbated with simultaneous increases in population and CDHEs in the future (Liu et al., 2021). Therefore, is vital to analyze the occurrence of CDHEs, particularly in sensitive areas as the Mediterranean.

When addressing heatwaves and droughts, key questions often intersect with the challenge of identifying their drivers, namely:

- What are the interactions and combined impacts of CDHEs, and how do they exacerbate individual hazards (Leonard et al., 2014; Zscheischler et al., 2018)?
- How do we identify and differentiate the drivers behind these compound events, particularly given the complexity of multiple interacting climatic and non-climatic factors (Zscheischler et al., 2018)?
- How do CDHEs impact regions differently, and what are the specific examples of their effects (Mazdiyasni and AghaKouchak, 2015; Hauser et al., 2015; Seneviratne et al., 2012; Lu et al., 2018)?

These questions highlight the difficulty in isolating and understanding the individual and combined drivers of heatwaves and droughts, which is essential for predicting future events and formulating effective mitigation and adaptation strategies. Given the complexity of these types of events and the multiple drivers that can be at their origins (Zscheischler et al., 2018), it is important to mention which mechanisms are known and used in the existing literature to study these types of extreme events, such as heat waves and droughts.

The driving mechanisms of heatwaves can be classified into two main categories: atmospheric (including moist and radiative processes) and surface, influencing each other (Jiménez-Esteve and Domeisen, 2022). Atmospheric circulation drivers of heatwaves include quasi-stationary upper-level ridges linked to surface high-pressure anticyclones and local amplification of Rossby waves (Wirth et al., 2018). High-pressure anticyclones can develop into atmospheric blocking due to wave breaking and can persist for several days (Jiménez-Esteve and Domeisen, 2022). Heatwaves have also been linked to surface drivers related to energy and momentum exchange at the interface between the atmosphere and the Earth's surface (ocean or land) (Jiménez-Esteve and Domeisen, 2022). Large-scale subsidence and increased solar radiation (Net Radiation in Figure 1) associated with clear-sky conditions within the anticyclone lead to strong near-surface warming, which in turn increases the likelihood of a heatwave (Xu et al., 2020) and weak pressure gradients cause a weak large-scale circulation (Spensberger et al., 2020).

The surface drivers are related to dry soil conditions and soil moisture can influence the persistence of heatwaves and droughts (Lorenz et al., 2010; Ribeiro et al., 2020). Higher levels of lower-tropospheric water vapor promoted by increasing temperatures, are linked to changes in the balance between evaporation and precipitation (E-P) that ultimately determines soil moisture, groundwater recharge and total water available for runoff (Zhou et al., 2021). In parallel, under a large atmospheric evaporative demand (ET in Figure 1), a strong soil moisture imbalance may also play a major role in the surface energy partitioning by constraining surface latent heat fluxes (LH in Figure 1), leading to an above normal accumulation of sensible heat (SH in Figure 1) in the atmosphere and to the escalation of temperatures (Geirinhas et al., 2022; Santanello et al., 2018; Miralles et al., 2019). This increase in SH flux is also caused by precipitation deficits, that leads to droughts. Precipitation recycling is the contribution of ET to precipitation regionally (Eltahir and Bras, 1996) and imply positive feedback where high ET increases atmospheric water vapor, generally leading to more precipitation, increasing soil moisture, and ET (Li et al., 2021). Long-term drying trends can influence the atmospheric water budget, particularly over drylands, by limiting ET and reducing moisture recycling for precipitation (Zhou et al., 2021). Moisture transport refers to moisture that originates as ET and is advected downwind, where it may eventually fall as precipitation (Roy et al., 2019). The role of moisture transport in drought development is poorly understood (Miralles et al., 2019). Recently, reduced moisture transport has been proposed as a mechanism (Herrera-Estrada et al., 2017; Roy et al., 2019). The hypothesis is that reduced moisture exports downwind, possibly amplifying drought conditions downwind (Herrera-Estrada et al., 2019). The positive feedback on the land-atmosphere coupling exacerbates the increase in vapor pressure deficit, and then transfer more moisture from the water bodies to the atmosphere by ET, thereby resulting in compound hot and dry extremes (Alizadeh et al., 2020). The interplay between soil moisture, atmospheric water budget and temperature is part of a large and complex framework of feedbacks that are modulated by climate change (i.e., increasing temperatures, changes in vegetation and in atmospherics dynamics), and that may also affect the climate trends themselves (Zhou et al., 2021; Miralles et al., 2019; Douville et al., 2013).

All these processes are modulated by a complex interplay between large-scale oceanic-atmospheric modes of variability, such as *North Atlantic Oscillation* (NAO), *El Niño-Southern Oscillation* (ENSO), *Atlantic Multidecadal Oscillation* (AMO), or *Eastern Atlantic* (EA). Typically, these teleconnections have been shown to be among the major driving factors that induce changes in the frequency and intensity of precipitation and temperature events in different regions (Wang et al., 2018; Zhou et al., 2020). The NAO is closely related to the formation of high-pressure systems and favor the concurrence of low precipitation and high temperatures at longer time scales (Hao et al., 2018) and has a significant impact on the atmospheric circulation and the European climate (Rodriguez-Puebla et al., 1998). The control exerted by NAO on the precipitation field over Europe is likely to be related to changes in the activity of North Atlantic storm tracks (Trigo et al., 2006) and have consequences on vegetation (Gouveia et al., 2008). The ENSO also has a strong influence on prevalence of anticyclonic and hot and dry conditions in China (Wu et al., 2021). Strong positive ENSO events produce high-pressure near western Europe, while moderate events produce low-pressure over this region in a pattern that projects negatively onto the NAO (Toniazzo et al., 2006). Typical modes of climate variability, include AMO, depending on regions and seasons. These climate variability modes influence semi-permanent and transient systems that play a key role for precipitation and evaporation in Europe. The EA is a complement of the NAO and also has an impact on atmospheric circulation over Europe, influencing its climate (Rodriguez-Puebla et al., 1998). Particularly, the EA is shown to modulate precipitation to the south-west off the UK and across the Iberia (Rodriguez-Puebla et al., 1998). In addition to circulation patterns, solar radiation, aerosols, clouds, water vapor transport and evaporation feedback also contribute to the occurrence and persistence of hot extremes (Tang et al., 2020).

1.2 Objectives and motivations

In recent decades, both heatwaves and droughts are increasing in number, duration, and intensity, leading to an increase in CDHEs (Tripathy and Mishra, 2023). For this reason and given their impact on various sectors of society and the environment, it is important to study these type of extreme events in more detail. This is particularly the case of the Mediterranean region.

The aims of this work are:

1. To provide a historical characterization of heatwaves and droughts, individually and simultaneously, in the recent past (1979-2022), in Europe focused in Mediterranean region. This characterization is based on an analysis of trends in temperature, precipitation and soil moisture and a probabilistic study of these variables.
2. Identify the mechanisms that drive the development of the three types of extreme events in the same period. This can be achieved by studying the atmospheric circulation for each event, identifying the centers of high-pressure and linking them to the rise in temperature and the moisture transport to analyze the drivers that potentiate the development of extreme events and to identify those regions most prone to these phenomena.

3. To analyze a case study: the year 2022. This year was extremely hot and dry, one of the most severe in recent history (Tripathy and Mishra, 2023) and characterized by the occurrence of a CDHE that affected most continents, especially Europe, in regions such as Iberia or France (Faranda et al., 2023), and various sectors of society (Tripathy and Mishra, 2023).

This study builds on the methodologies developed by Geirinhas et al. (2023), focused on South America, and Ionita et al. (2021), focused on Europe. This work aims at being an asset to the state of the art on CDHEs, focusing on the period spanning from January 1979 to December 2022.

This work is being carried out as part of project, DHEFEUS, which aims to study heatwaves, droughts and fires and their impact on air quality in Europe, and includes partners from the Dom Luiz Institute (*Instituto Dom Luiz*, IDL), the Portuguese Institute for the Sea and Atmosphere (*Instituto Português do Mar e da Atmosfera*, IPMA), the Environmental Physics Laboratory - Vigo University, and Oslo Metropolitan University – Norway.

Within the course of this work, the following questions are tackled:

- How did heatwaves, droughts and their drivers evolve during the recent past in Europe?
- Which type of extreme events – heatwaves or droughts – has a greater influence on the occurrence of CDHEs in Europe?
- How extreme was the year 2022 in Europe? And how is characterized regarding the drivers?
- How do atmospheric dynamics influence the development and extremeness of extreme events in Europe?

This document is organized into five main chapters, starting with the *Introduction*, which outlines the topics discussed in the following sections. The second section reports to *Data and Methodology* which introduces the data and the methodologies used. The third section is *Results* focuses on the analyses of the results obtained using the data and methodologies presented in the previous chapter and completes the tasks proposed in the introduction. The fourth chapter is *Discussion* and puts into perspective the results obtained based on the most recent literature. The final chapter is *Conclusions* and looks at what can be added in future work in the form of a continuation, summarizing the main points of the work.

Chapter 2 – Data and Methodology

This chapter describes the methodology and data used (1) to identify and characterize the heatwave and drought events; (2) to calculate the incidence of CDHEs in the study regions; (3) and to analyze the main driving mechanisms of the three types of extreme events.

2.1 Data

To study heatwaves and droughts in Europe, 2-meter temperature (in K), total precipitation (in m), soil moisture (*volumetric soil water layers 1, 2 and 3*, in $m^3\ m^{-3}$) and water vapor transport (*vertical integrate of eastward* and *northward water vapor flux*, in kg $m^{-1}\ s^{-1}$), geopotential at 500 hPa (in m^2/s^2), and temperature at 850 hPa (in K) data were used.

These datasets were retrieved from the Copernicus/ERA5 database. ERA5 is the 5th generation of the ECMWF (*European Centre for Medium-Range Weather Forecasts*) climate reanalysis (Hersbach et al., 2020). The reanalysis combines model data with observations from around the world into a globally complete and consistent dataset (Copernicus, 2023). The data was extracted in netCDF format and is arranged in a regular latitude and longitude grid of 0.25º x 0.25º and hourly time resolution spanning the period between 1979 January and 2022 December (44 years).

This study also used data from four teleconnections: the NAO (NOAAa, 2024), AMO (NCARa, 2024), EA (NOAAb, 2024), and Niño 3.4 (*N3.4*) (NCARb, 2024). These datasets are provided by NOAA and have a monthly time resolution. They were extracted between 1979 January and 2022 December.

Spyder software (version 5.4.3), with Python programming language, and *RStudio* (version 1.1.456) were used to process the data. The total study area extends from 32 to 60º N latitude and -13 to 32º E longitude, as shown in Figure 2. Although the study window shows North Africa, the calculations in this work are done with a mask for the ocean and also for this region. Furthermore, regional subdomains over Iberia and France are also selected to further analyze. Therefore, these results have been used in this work as a way to complete the presented study.

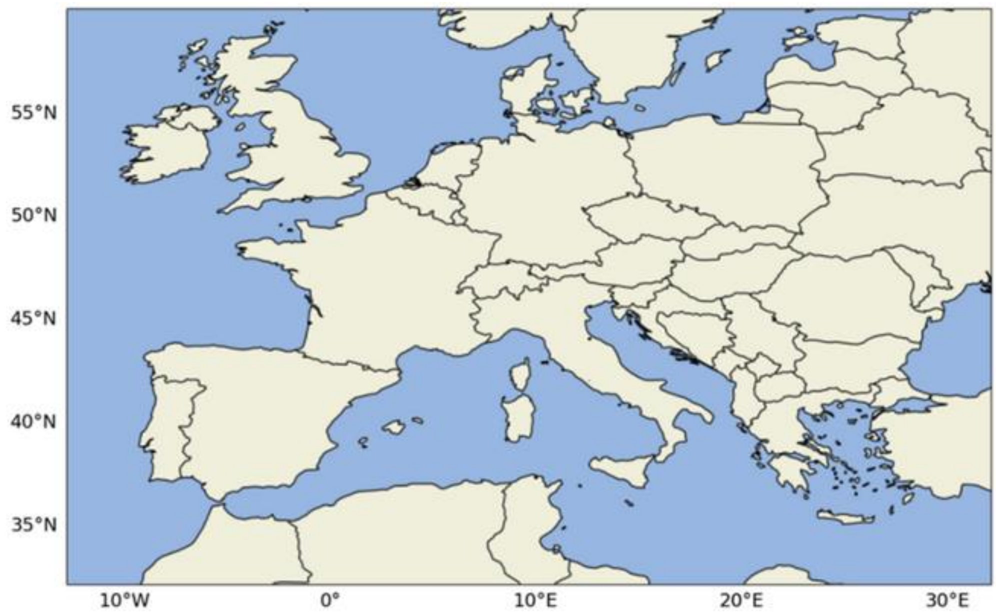

Figure 2: Study area representation, showing Central and Southern Europe.

2.2 Methodology

2.2.1 Heatwaves and droughts

Various studies have been conducted on extreme events in the atmosphere, and several definitions have been used to identify heatwaves. For instance, Perkins and Alexander (2013) defined a heatwave as prolonged periods of excessive heat. Heatwave events were identified using a relative threshold methodology that considers consecutive days with temperatures above a certain percentile. The lack of a universal definition of heatwaves complicates the identification and comparison of these events across different studies and regions. In this work, a heatwave is considered if the maximum temperature is higher than the 90th percentile of the maximum temperature (calculated on a 30-year basis between 1981 and 2010) for at least 5 consecutive days (Zhang et al., 2005). Heatwaves with an interval of less or equal to two days are also considered as the same event. The daily climatology was calculated from the average of the temperatures observed on the same day between 1981 and 2010, on a 30-year basis, as the 90th percentile.

Heatwaves were then identified and characterized between 1979 and 2022. Afterwards, the frequency, duration, and mean and cumulative intensity were computed for each grid point. The frequency of heatwaves is defined as the number of individual events that occur each year. The duration of heatwaves is defined as the period during which the observed temperatures exceed the daily variability threshold considered. To calculate the intensity, the 90th percentile of maximum temperature was used as the threshold, and the difference between the observed temperatures and the 90th percentile values was calculated. The mean and cumulative intensities of heatwaves are defined, respectively, as the average temperature anomaly in relation to the threshold during an event and the sum of the daily intensity anomalies over the duration of the event (Plecha and Soares, 2020; Hobday et al., 2016). A schematic representation of this method can be seen in Figure 3.

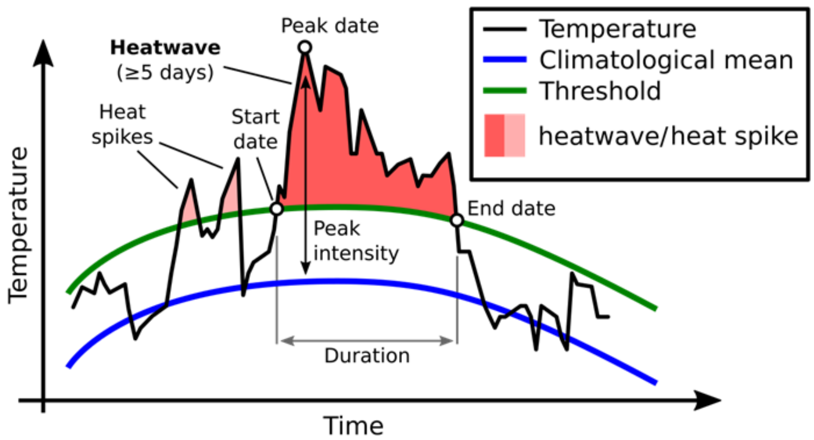

Figure 3: Schematic representation of the procedure applied to identify a heatwave (following Hobday et al., 2016). The blue line represents the climatology, the green represents the 90th percentile and the black represents the observed temperatures. Font: https://www.marineheatwaves.org/all-about-mhws.html.

Droughts are apparent after a long period without precipitation, but it is difficult to determine their onset, extent, and end (Vicente-Serrano et al., 2010). Thus, it is difficult to objectively quantify a drought event. To circumvent this caveat, drought indices such as the *Standardized Precipitation Index* (SPI) were developed (McKee et al., 1993).

The SPI is based on a probabilistic approach to precipitation (McKee et al., 1993) based only on precipitation data (Vicente-Serrano et al., 2010). SPI is a widely used index to characterize meteorological drought on a range of timescales.

SPI holds the advantage over other widely used drought indices such as the PDSI (*Palmer Drought Severity Index*), of having a temporal multi-scalar character (Vicente-Serrano et al., 2010; Russo et al., 2017). The application of multi-scalar indices to high spatial-resolution datasets allows associating a given temporal scale of drought to the occurrence of a given phenomenon or event (e.g. desertification or forest fires) (Russo et al., 2017).

In precipitation-based drought indices, as SPI, it is assumed that the variability of precipitation is much higher than that of other variables, such as temperature and potential evapotranspiration (PET), and the other variables are stationary (they have no temporal trend). In this scenario, the importance of these other variables is negligible, and droughts are controlled by the temporal variability in precipitation (Vicente-Serrano et al., 2010).

To calculate SPI, it was necessary to obtain monthly accumulated precipitation data (in mm). To do this, the data was processed to transform hourly data into monthly accumulated data. This process was repeated for all 44 years of the study on a grid basis. The positive values indicate wet conditions, and negative values indicate dry conditions.

SPI was calculated using a Gamma distribution to modulate precipitation, using the total period as reference period (Russo et al., 2018). This process is repeated for 1-, 3-, 6-, 12- and 24-month time scales. The SPI was chosen over the other widely used index – the *Standardized Precipitation-Evapotranspiration Index* (SPEI) – because the latter uses both accumulated precipitation and minimum and maximum temperature, as the former uses only accumulated precipitation. Therefore, considering that this work studies heatwaves and droughts, using the SPEI would give double importance to the temperature variable, which is present in the calculation of heatwaves but also in the calculation of droughts. It is these longer droughts that will have a more significant impact on the soil, leading to reductions in agricultural production and consequences for the economy and the landscape (Svoboda and Fuchs, 2016). However, in this work only SPI12 was used to study long-term droughts, considering 1-year composites, and was calculated in *RStudio* with a package developed by Santiago Beguería (CSIC, 2023).

Drought events were also characterized in terms of duration and magnitude (similar to cumulative intensity in case of heatwaves), where the duration is the number of months where SPI is below -1 and the magnitude is estimated as the sum of the difference between SPI and -1. By computing these characteristics (frequency, duration, and intensities) for heatwaves and (duration and magnitude) for droughts, it was possible to characterize the study area concerning these events and understand how these extreme events evolved over the study period.

For each month, the area affected by each type of drought was computed using the classification proposed by McKee et al. (1993), which considers mild drought as $0 \leq SPI < -1$, moderate drought as $-1 \leq SPI < -1.5$, severe drought as $-1.5 \leq SPI < -2$ and extreme drought as $SPI \leq -2$.

2.2.2 Identification of CDHEs

To identify and characterize the CDHEs, an Area Index was used representing the percentage of area under heatwaves, droughts and both, as shown in the Equation 1. To do this, a matrix was calculated, indicating at each grid point whether it was an extreme event (value 1) or not (value 0).

$$Area\ Index = \frac{Grid\ points\ under\ hazard}{All\ grid\ points \times Days\ of\ month} \quad (1)$$

The Area Index allows the percentage of area under each event to be accounted on a monthly basis over the 44 years of the study, aggregating spatial and temporal information. As with heatwave identification, CDHEs can be identified in a variety of ways and there is no universal formula. In this work, a methodology identical to that of Ridder et al. (2020) was used. Instead of using the probabilities of each hazard exceeding a threshold, the occurrence of events was used to determine the occurrence of CDHEs. This provides a characterization of when and where each CDHE occurs.

2.2.3 Analysis of driving mechanisms

To understand how events such as heatwaves and droughts occurred and what mechanisms were involved in their development, this subsection looks at temperature, precipitation, and soil moisture. For the soil moisture data, a preliminary analysis was carried out by calculating a time series of spatial means and also a spatial distribution of the respective trends, with statistical significance calculated at a 5% level according to the Mann-Kendall test between 1979 and 2022. The time series of spatial means of temperature and accumulated precipitation also were calculated for the same period.

To complement these preliminary results for soil moisture, bivariate distributions with kernel adjustment were also calculated for two time periods (1979-2000 and 2001-2022) in order to study the changes that occurred between the two time periods for temperature, daily accumulated precipitation and soil moisture, and to understand the compound effect of the two variables when analyzed together, with bivariate analysis. Furthermore, annual averages were calculated for the temperature, accumulated precipitation and soil moisture and the distributions were calculated in pairs: temperature – accumulated precipitation and temperature – soil moisture. The kernel fit was chosen because it does not assume a particular type of data distribution and is therefore more flexible (Chwialkowski et al., 2016). Unlike the normal (or Gaussian) fit, the kernel fit allows the data to be adjusted if it has a different type of distribution and is therefore not Gaussian. Although the kernel fit may not be as precise, its sensitivity makes it possible to examine in more detail what is happening probabilistically under more extreme conditions (Chwialkowski et al., 2016). These distributions were accompanied by PDFs (*Probability Density Function*), also with kernel fit, to maintain the same fit used in the distributions and divided for the same sub-periods of study. Hence, the PDFs allow to understand how each variable evolves independently over time (Chwialkowski et al., 2016).

The mean anomaly composites of temperature at 850 hPa level and geopotential height at 500 hPa level were calculated to study anticyclonic and cyclonic conditions over Europe. These calculations make it possible to identify anticyclonic (high pressure) and cyclonic (low pressure) zones, which are accompanied by positive and negative temperature anomalies, respectively. The 500 hPa level represents the top of the troposphere, which falls or rises depending on whether the anomaly value is negative or positive. The 850 hPa level represents the lower troposphere, where the temperature increase will be felt in the anticyclonic situation. To obtain the maps for the temperature and geopotential height composites, the 90th percentile of the Area Index for each type of event was calculated and, for each month value above this percentile, the anomaly of the two variables was calculated. The temperature and geopotential height composites were calculated for all months where the value of the index was above the 90th percentile to identify the most extreme events. To understand the existence of different atmospheric configurations during the winter and summer months, these average composites were divided into seasons encompassing the months from December to February (DJF) and June to August (JJA), respectively.

After obtaining the maps for each event and considering the three situations (all year, winter and summer months), it was possible to use them to classify the types of atmospheric circulation. The purpose of the summer/winter division, in addition to considering all months, is to identify possible variations in atmospheric patterns that might occur between the two seasons. In recent years, it has become important to develop classifications for different types of atmospheric configuration. This approach is often used to characterize the atmosphere during extreme events and to identify anticyclonic patterns as a mechanism for the development of these events.

Following the rationale presented in Figure 1, it is not only the moisture present in the soil that can determine the development of heatwaves and droughts, but also the moisture present in the atmosphere that can influence their development.

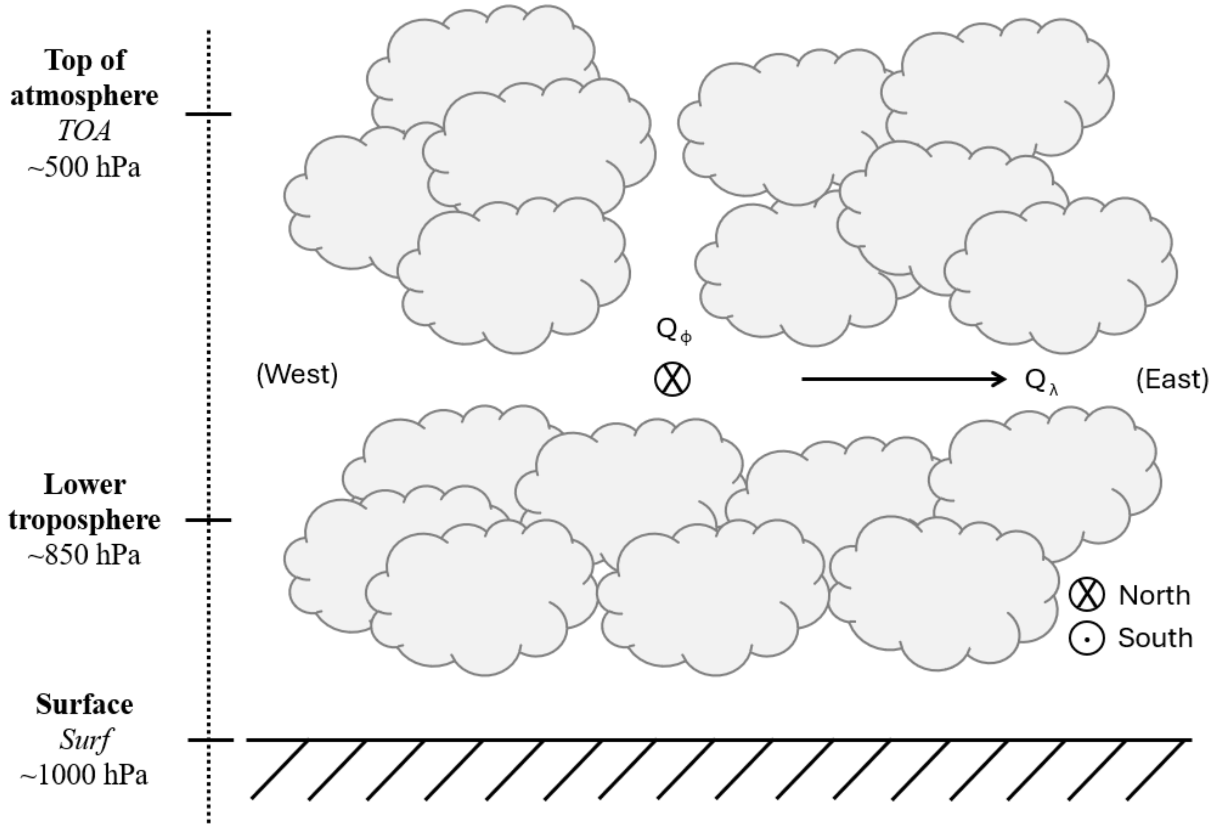

Figure 4: Schematic representation of zonal and meridional components of IVT.

The vertically *Integrated Water Vapor Transport* (IVT) quantifies the total horizontal moisture transport by integrating over the vertical column of the atmosphere, between the top of atmosphere (TOA) and the surface (surf), the zonal (Q_λ) and meridional (Q_ϕ) transport of specific humidity (q) (Equations 2, 3, and 4), defined as follows (Peixoto and Oort, 1943) (Figure 4):

$$IVT = \left[\left(\frac{1}{g}\int_{SURF}^{TOA} qudp\right)^2 + \left(\frac{1}{g}\int_{SURF}^{TOA} qvdp\right)^2\right]^{\frac{1}{2}} \quad (2)$$

$$com\ Q_{\lambda} = \frac{1}{g}\int_{SURF}^{TOA} qudp \qquad (3) \qquad\qquad Q_{\phi} = \frac{1}{g}\int_{SURF}^{TOA} qvdp \qquad (4)$$

Where g is the acceleration due to gravity and *qudp* and *qvdp* are the zonal and meridional components of moisture fluxes, respectively. The IVT anomalies were calculated with respect to the climatology (1981-2010) on a seasonal basis for winter (DJF), spring (MAM), summer (JJA) and autumn (SON). Anomalies in temperature, accumulated precipitation, soil moisture, geopotential height at 500 hPa level and temperature at 850 hPa level were also calculated for the same climatological period.

According to previous studies (Peixoto and Oort, 1943; Peixoto, 1973), the IVT that crosses a border can be obtained by the vertical integration of the convergence moisture. In this case, western boundary (F_W) was considered (Equation 5).

$$F_W = \int_{\phi_i}^{\phi_f} Q_{\lambda_i} d\phi \qquad (5)$$

Where λ_i represents the first value of longitude (-13º E) and ϕ_i and ϕ_f represent the initial and final value of latitude (32º and 60º N), respectively. To complement the results obtained for the variations of the water vapor balance in the study areas, the vertical integration of the water vapor data was processed in order to study in which areas water vapor is less present compared to the climatology. The types of movement that water vapor undergoes in the atmosphere is also important to understand. The divergence of the vertical integration of water vapor was calculated for the same year in relation to the same climatology (Equation 6). These analyses were seasonally divided.

$$\nabla \cdot \vec{Q} = \frac{\partial Q_{\lambda}}{\partial x} + \frac{\partial Q_{\phi}}{\partial y} \qquad (6)$$

To understand how the teleconnections, influence the moisture supply to Europe, and consequently to Iberia and France, the monthly data for each teleconnection were transformed into annual data and the moisture flux anomalies across the western boundary were calculated (using Equation 5), known as the *Western Moisture Flux* (WMF) (Figure 5).

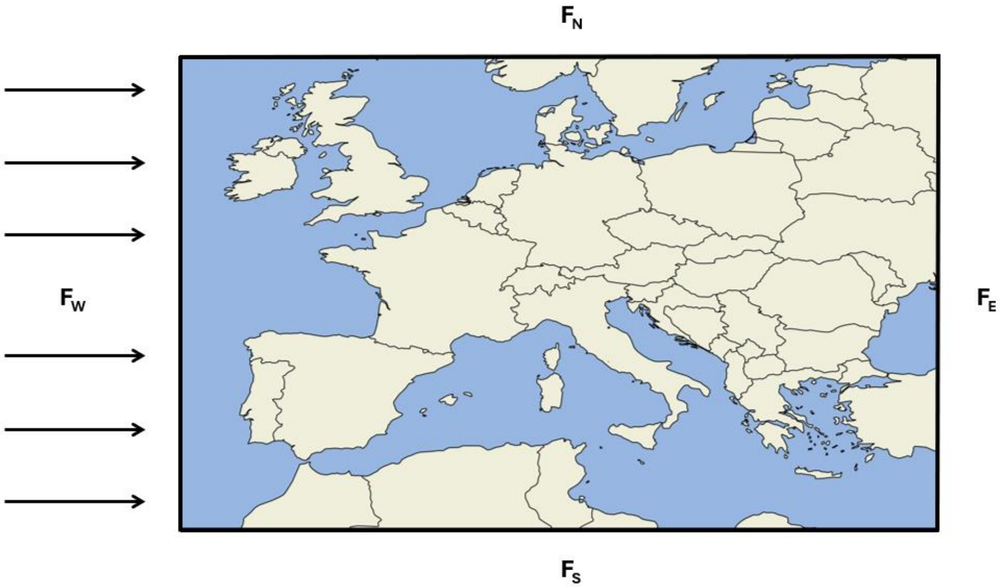

Figure 5: Schematic representation of the boundaries. F_W represents western boundary, F_N represents northern boundary, F_E represents eastern boundary, and F_S represents southern boundary.

In this work, only the western boundary was considered because it is the boundary where there are the greatest variations in water vapor flow. The atmospheric movements that occur in the North Atlantic towards Europe are mostly in an east-west direction, and therefore only this boundary was considered as the main boundary. Pearson's correlations were then calculated between the WMF and each teleconnection on a monthly, seasonal, annual and Lanczos low-pass filtered annual basis using the *pearsonr* function from the *scipy.stats* library. Pearson's correlation takes into account the original values of the variables and does not rely, for example, on ranking, and the square of Pearson's coefficient provides a proportion of the variance of one variable explained by the other, making interpretation in cause-and-effect analyses easier (Shiekh and El-Hashash, 2022). The Lanczos filter is widely used in this type of work due to its ability to smooth signals by removing high frequency components and reducing the amplitude of distributions. It has important advantages related to the good preservation of the characteristics of the original signal, as well as its effectiveness with high-frequency noise (Duchon, 1979).

Teleconnections, which can have an atmospheric or oceanic influence, affect the variability of the climate system over a wide range of spatial and temporal scales (Kucharski et al., 2010). For example, teleconnections can affect the spatial distribution of precipitation and temperature. There are several teleconnections that affect different regions in different ways. In this work, we have used the positive phase of the NAO (NAO+), AMO, EA and N3.4, which are the teleconnections that mostly influence Europe and especially the Mediterranean region. The specification of the NAO phase is due to the fact that the positive phase causes a colder and drier climate in the Mediterranean region, which is conducive to the development of dry events (NOAA, 2024). Most of these teleconnections have a wide application, either as a mechanism for the development of extreme events, or as an influence on vegetation dynamics or even precipitation variation. Therefore, the purpose of studying them in this work is to relate them to the water vapor entering Europe through the western border and to understand which teleconnection is the most correlated and which phase of the supply is the greatest.

The year 2022 has been identified in the literature as a very hot and dry year characterized by the occurrence of a CDHE. In comparison with previous mega events (as in 2003, 2015, and 2018), the 2022 CDHE was substantially more severe. According to Tripathy and Mishra (2023), 3/4 of European land areas were affected by drought, with around 55% experiencing severe droughts in the summer, and experienced temperature high-temperature anomalies, nearly 50 and 20% experiencing temperature anomalies over 2 and 3 ºC, respectively. Therefore, the specific development mechanisms for this year were analyzed. Starting from winter 2021/22, there was a persistent deficit of precipitation, resulting in pronounced negative anomalies in soil moisture and streamflow over a large area of the continent (Copernicus, 2024). This drying trend has been linked mainly to increases in temperature and record-breaking heatwaves associated with climate change (Seneviratne et al., 2021). This section therefore aims to analyze the dynamics between atmospheric circulation and soil and atmospheric moisture, taking into account temperature and precipitation.

Chapter 3 – Results

3.1 Historical characterization of extreme events

This section presents the results of the historical characterization of heatwaves and droughts in the study area and its respective sub-areas, Iberia and France. Time series of annual spatial means of temperature, daily accumulated precipitation, and soil moisture were calculated, which allowed a historical and preliminary analysis of the atmospheric and soil conditions (Figure 6).

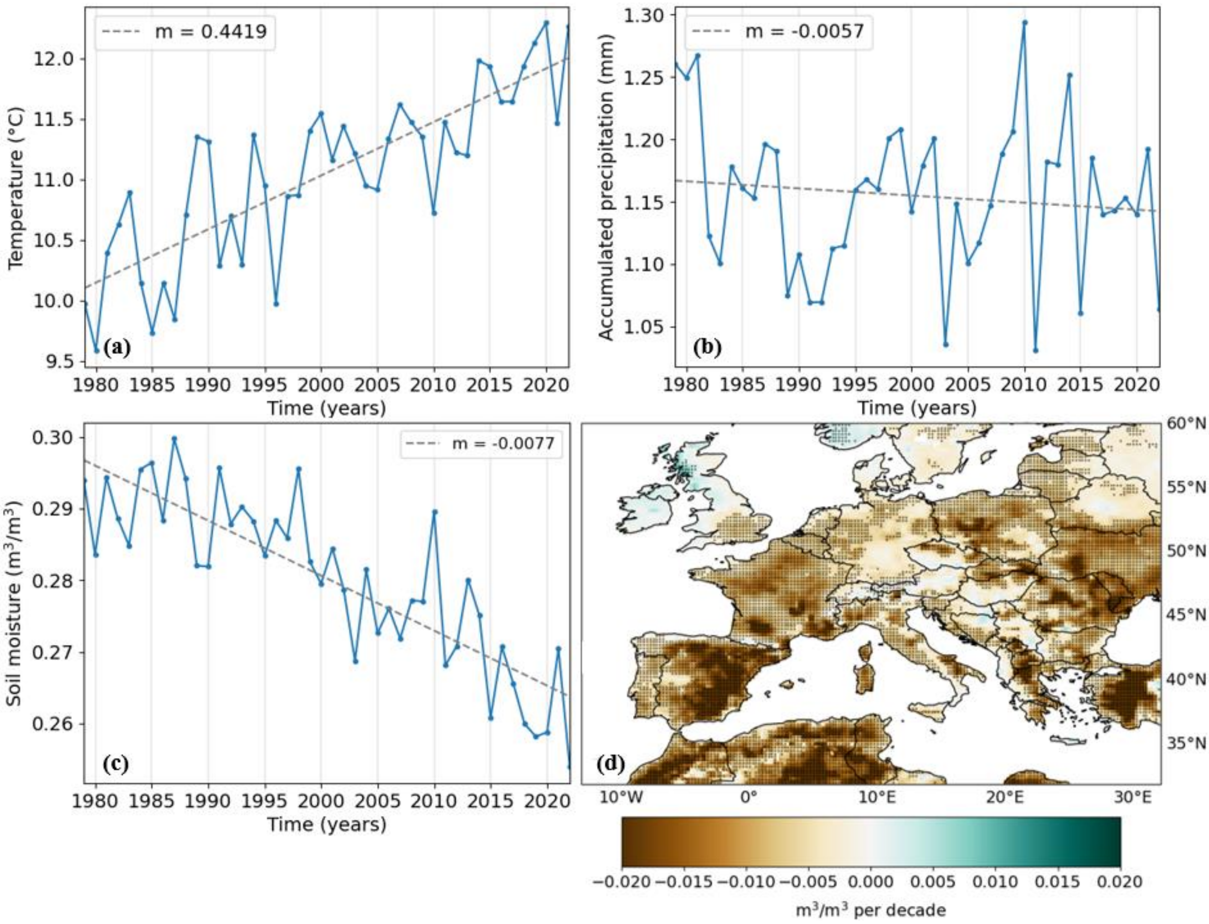

Figure 6: Time series of annual spatial means of temperature (a), daily accumulated precipitation (b) and soil moisture (c) accompanied by decadal trend values, in the study area, with the value of the respective trends labelled "m". Trends of soil moisture (dots depict statically significant trends at a 5% level) (d).

There is a positive trend for temperature, with around 0.44 ºC per decade (Figure 6a), and a negative trend for the daily accumulated precipitation series, with approximately -0.006 mm per decade (Figure 6b), and for soil moisture, with circa -0.008 m^3/m^3 per decade (Figure 6c). The results show an increase of temperature of about 2 ºC and a decrease of accumulated precipitation and soil moisture of 0.2 mm and 0.04 m^3/m^3, respectively, over the studied period. The maximum temperature value occurs in 2020 with ~12.4 ºC, the minimum accumulated precipitation in 2011 with ~1.03 mm and the minimum soil moisture in 2022 with ~0.255 m^3/m^3.

Most of Europe shows negative soil moisture trends, with smaller areas of positive trends in the north (Figure 6d). The most negative trends are found in eastern Iberia, southern France, the Balkans, western Turkey, and some parts of eastern Europe, with values reaching ~-0.020 m^3/m^3. This shows that a large part of Europe is moving towards drier conditions, in some areas at a very high rate.

As expected, the plots for Iberia and France (Figure S1 in the Supplementary Material) show almost identical situations. Temperatures show positive trends, with slopes of ~0.33 ºC and ~0.42 ºC respectively, and accumulated precipitation and soil moisture show negative trends, with slopes of ~-0.007 mm and ~-0.035 mm and ~-0.011 m^3/m^3 and ~-0.009 m^3/m^3 respectively. Soil moisture minima and temperature maxima have been reached in recent years. It should be noted that the trend in accumulated precipitation is much larger in France than in Iberia and Europe.

Seasonally, positive decadal trends are observed for temperature. Accumulated precipitation shows negative decadal trends, except for DJF, and soil moisture shows negative decadal trends for all seasons. The season with the strongest trends is JJA, considering all three variables (Figure S2, S3, and S4 in Supplementary Material). The same is true for Iberia and France. In the case of temperature, both subregions show positive downward trends, with the JJA season being the most intense. Soil moisture shows negative decreasing trends, with SON for Iberia and JJA for France being the most intense seasons. For Iberia, accumulated precipitation, except for MAM, shows negative decadal trends, with JJA being the most intense season. In France, all seasons show negative trends, with SON being the most intense season (Figures S5 to S10 in Supplementary Material).

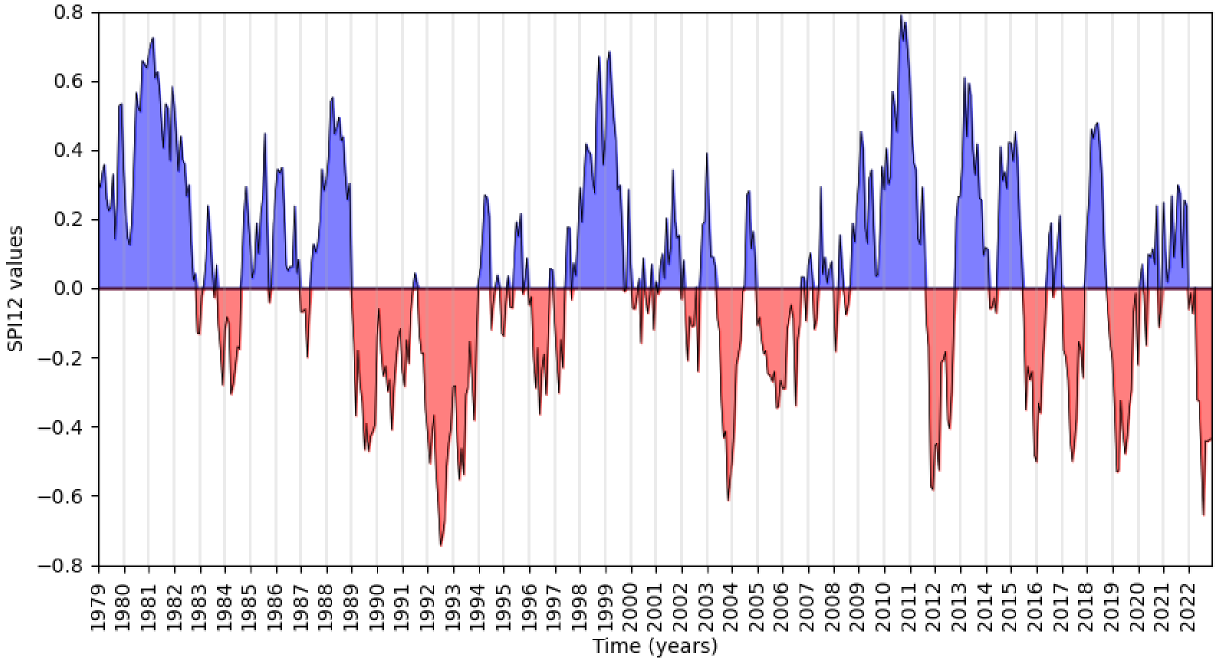

Figure 7: SPI time series for Europe. Positive SPI values are shown in blue, representing months with wet conditions. Negative SPI values are shown in red, representing months with dry conditions.

There is a large inter-annual variability, with dry and wet periods well marked, as depicted by the interlace of negative and positive SPI values (Figure 7). The early years of the study, the last years of the last millennium and some years towards the end of the study period are characterized by positive SPI values, reaching maximum values of ~0.8 in 2010. While the 1990s and some years from the new millennium onwards show negative SPI, reaching minimum values of ~-0.7. The most recent years show a greater variability between positive and negative values. Looking at the negative values, the main drought periods in Europe were 1989 - 94, 2003 - 06, 2011/12, 2015 - 17, 2019 and 2022, with 1992 being the most intense.

In the time series for Iberia, we can see that the maximum and minimum values are much sharper, reaching values around 1.4 and -2 respectively (Figure S11 in the Supplementary Material). There is a large inter-annual variability, and the main drought periods are 1991 - 96, 1999 - 2000, 2004 - 07, 2011/12, 2015 - 17, 2019 and 2022, with 2005 being the most intense. Of the two sub-domains studied – Iberia and France –, the latter has the most similar time series to Europe (Figure S12 in the Supplementary Material). The most intense year was 1989, with the main drought periods coinciding with those in Europe. The minimum and maximum values are around -1.8 and 1.8, respectively.

To complement and better understand the results, Figure 8 also shows the same characteristics spatially, divided into two sub-periods (1979-2000 and 2001-2022).

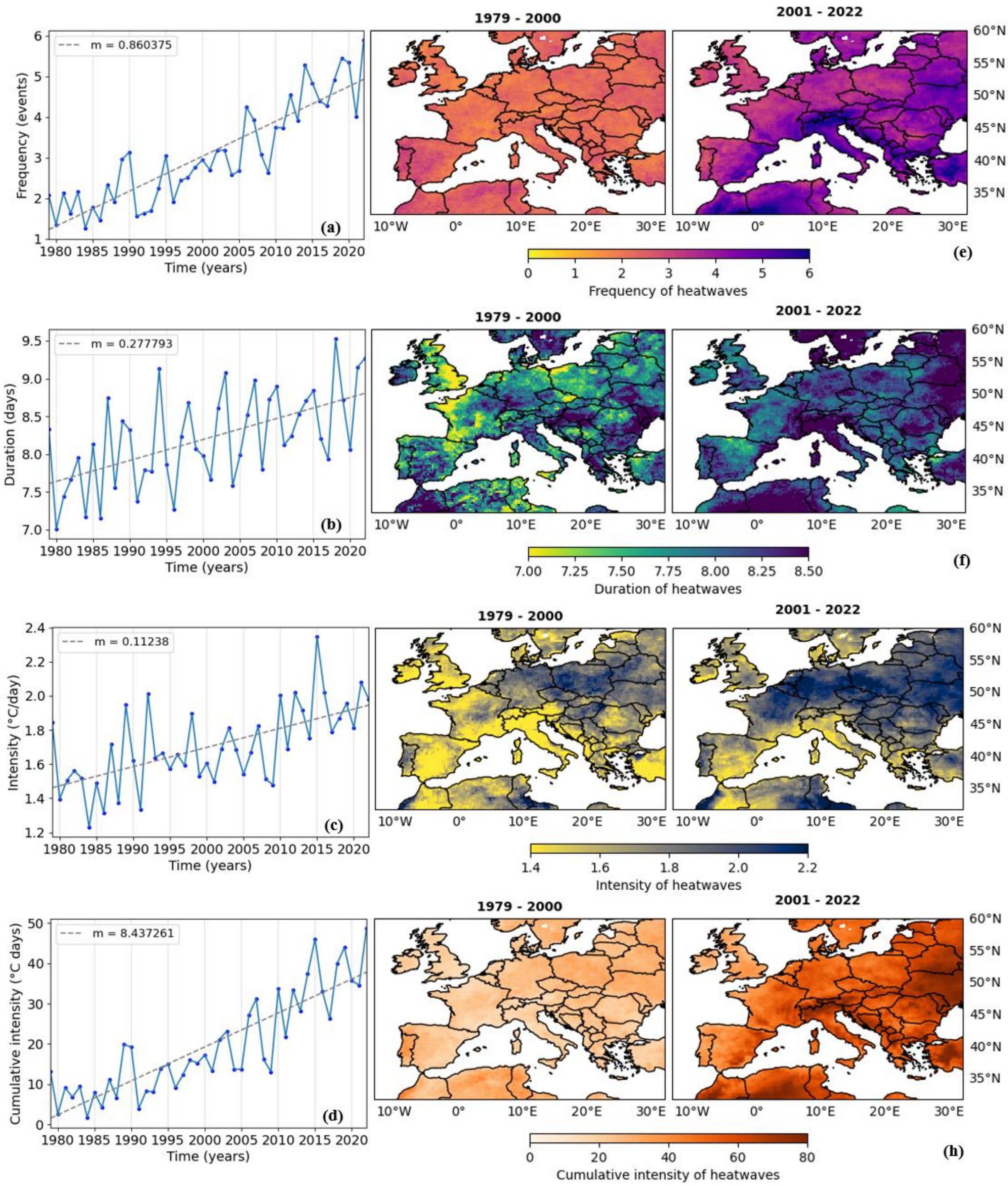

Figure 8: Frequency (a and e), duration (b and f), intensity (c and g) and cumulative intensity (d and h) of heatwaves with decadal trends and divided in two subperiods, 1979-2000 and 2001-2022, considering the whole domain.

Figure 8 (left panel) shows that all characteristics present large inter-annual variability and positive decadal trends. The number of heatwaves per year increased over time, reaching a maximum in 2022 with ~6 events/year. The decadal trend line shows a positive slope of ~0.86 events/year, with an increase of ~4 events between 1979 and 2022 (Figure 8a). The duration also shows an increase in the number of days reaching a maximum in 2018, with ~9.5 days. The decadal trend line shows a positive slope of ~0.28 days/year. Between 1979 and 2022 there was an increase of 0.8 days (Figure 8b). The intensities show an increase in their values, reaching maxima in 2015 and 2022, respectively, with ~2.4 ºC/day, ~50 ºC days. The decadal trend line shows a positive slope of ~0.11 ºC/day and ~8.44 ºC days, and there was an increase of ~0.1 ºC/day and ~35 ºC days (Figures 8c and 8d).

In general, the results for the 2001-2022 subperiod show higher values for all the characteristics compared to the 1979-2000 subperiod (Figure 8e, 8f, 8g, and 8h). Particularly noteworthy are those for frequency and cumulative intensity, which show strong increases in the Mediterranean region and Eastern Europe, reaching more than 5 events and 80 ºC day on average respectively.

The same procedure was carried out for drought events. In this case, the characteristics studied were the months of drought in each year and their magnitude. The results are shown in Figure 9.

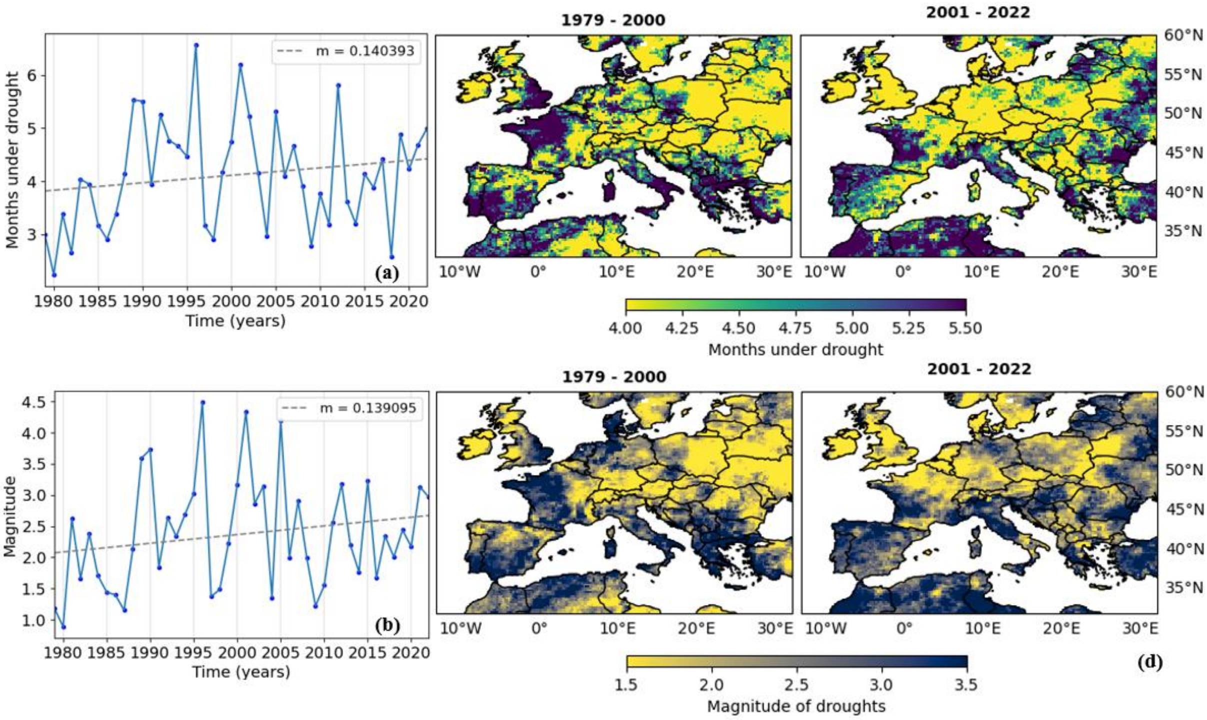

Figure 9: Months under drought (a and c), and magnitude (b and d) of droughts with decadal trends and divided in two subperiods, 1979-2000 and 2001-2022, considering the whole domain.

Figure 9 presents large inter-annual variability and positive decadal trends. The months under drought show an increase in the number of days reaching a maximum in 1996, with ~6.8 months/year. The decadal trend line shows a positive slope of ~0.14 months/year. Between 1979 and 2022 there was an increase of ~2 months (Figure 9a). The magnitude of droughts also shows an increase in their values, reaching maxima in 1996, with ~4.5. The decadal trend line shows a positive slope of ~0.14 and there was an increase of ~2.8 (Figure 9b).

In contrast to heatwaves, it is not so easy to observe an increase in the values of the characteristics studied in the case of droughts (Figure 9c and 9d). The trends of the two characteristics are low, which means that the values in the two sub-periods are similar and there is also little spatial variation. The maximum values reached for months under drought and magnitude are 8 months and 4, respectively.

In the results for the Iberia, the characteristics of heatwaves and droughts are increasing and show trend lines with positive slopes, except for the duration of droughts, which has a very slight negative slope. Like the results for Europe as a whole, the results for the Iberia show a high inter-annual variability, more pronounced in the early years and peaking in the later years (Figure S13 in the Supplementary Material). The results for France for both events are similar to those for Europe and the Iberia, with a significantly negative slope and high inter-annual variability (Figure S14 in the supplementary material).

After characterizing the four types of droughts, Figure 10 shows a monthly time series with a Lanczos low pass filter on the percentage of Europe's area under four types of droughts: mild, moderate, severe, and extreme drought.

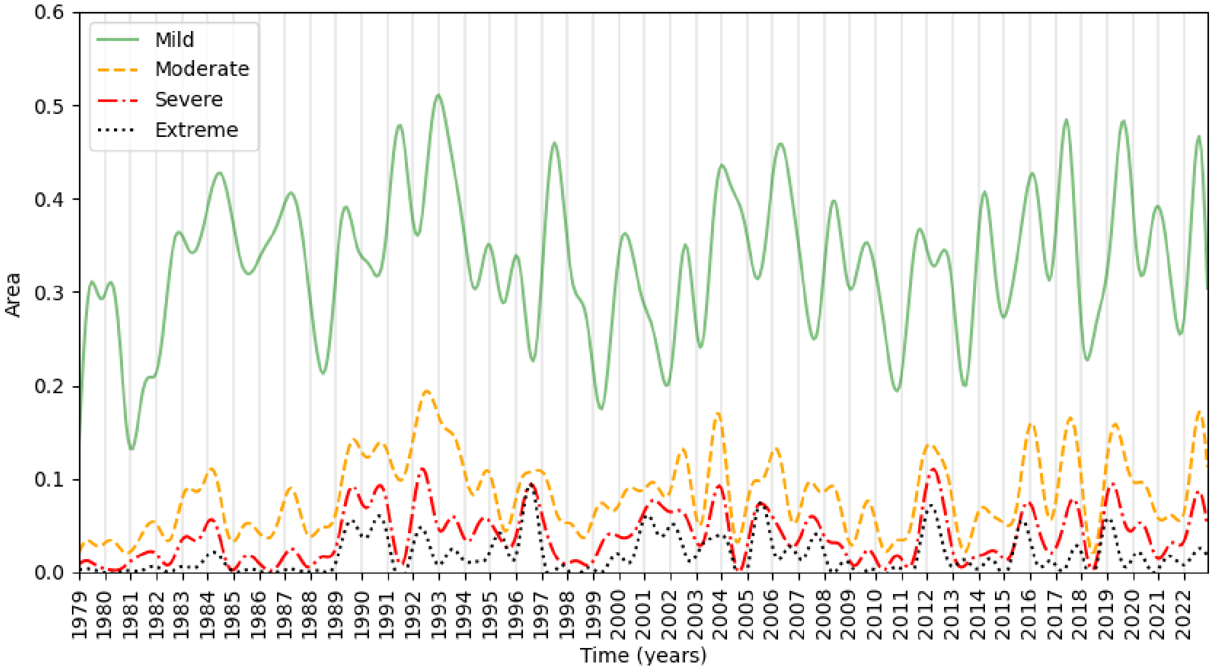

Figure 10: Europe's area affected by each type of drought. Continuous (green) line indicates mild drought, long dashed (orange) line indicates moderate drought, dot dashed (red) line indicates severe drought and dotted (black) line indicates extreme events.

The highest value occurs at the beginning of 1993 with about 50% for mild drought, in the middle of 1992 and 1993 with about 20% and 10% respectively for moderate and severe drought and in the middle of 1996 with about 10% for extreme drought, where it approaches the values for moderate and severe drought in the same year. These results are in line with the SPI peaks seen in Figure 7.

In the case of the subregions, identical distributions are observed for the four types of droughts. In Iberia, 1995 and 2005 were years of extreme drought, with almost 50% of Iberia experiencing very extreme hot conditions. The year 2012 was characterized by moderate and severe drought (Figure S15 in Supplementary Material). In France, at the end of 1989, the area affected by extreme drought was greater than that affected by moderate and severe drought, and at the beginning of 1992, the area affected by moderate and severe drought was greater than that affected by mild drought (Figure S16 in Supplementary Material).

To understand how each variable varies in conjunction with the other variables and individually, the bivariate distributions and univariate PDFs with kernel adjustment were calculated (Figure 11).

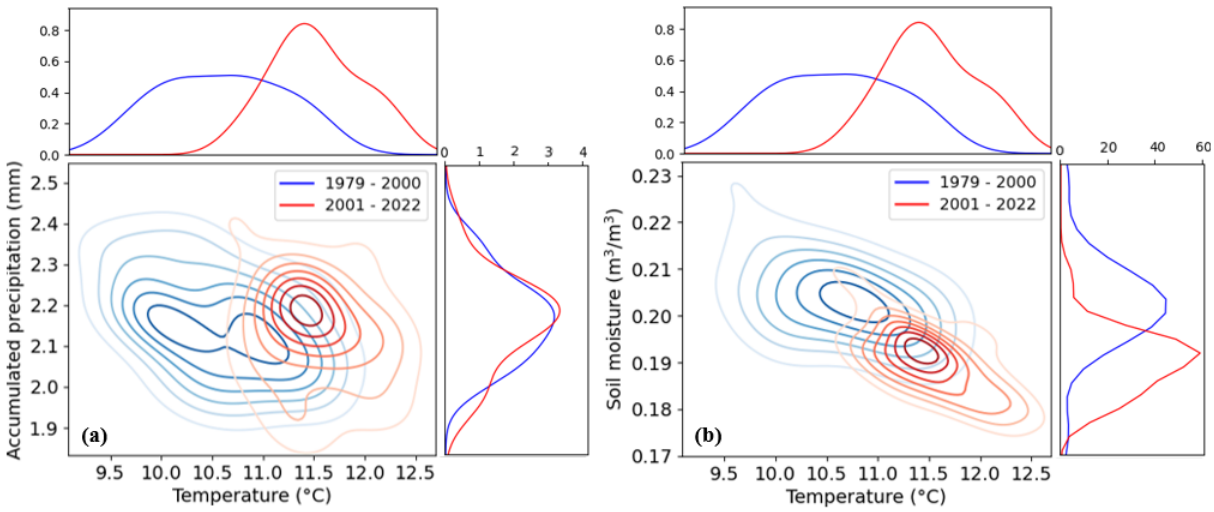

Figure 11: Plots of the bivariate distributions with kernel fit plots accompanied by univariate PDFs with kernel fit of each variable: temperature and accumulated precipitation (a) and temperature and soil moisture (b), considering whole domain.

Figure 11 shows that in the second sub-period (2001-2022) the ellipses of the bivariate distributions shift towards more extreme temperature and soil moisture conditions, showing the effect of the coupling of higher temperature with roughly invariant accumulated precipitation (Figure 11a) and the coupling of temperature with soil moisture (Figure 11b). The temperature and soil moisture PDFs show a shift to the right, with an increase in frequencies for high values of the variables, as show the right tail of the 2001-2022 distribution. The PDF for accumulated precipitation shows a similar distribution in the two periods, but we can see that the frequency of high accumulated precipitation is lower, and the frequency of low accumulated precipitation is higher when comparing the 2001-2022 sub-period with 1979-2000.

The bivariate distributions for both Iberia and France show very similar characteristics to those for Europe, as do the univariate PDFs (Figures S17 and S18 in the Supplementary Material). It is possible to observe shifts towards higher values of temperature and towards lower values of soil moisture, while accumulated precipitation remains largely unchanged. For the latter variable, the frequency of precipitation deficit extremes increases in the most recent subperiod decrease in the more distant subperiod.

Monthly occurrence of individual heatwaves or droughts, or by CDHEs and the respective percentage of area affected by them for the whole domain was calculated (Figure 12).

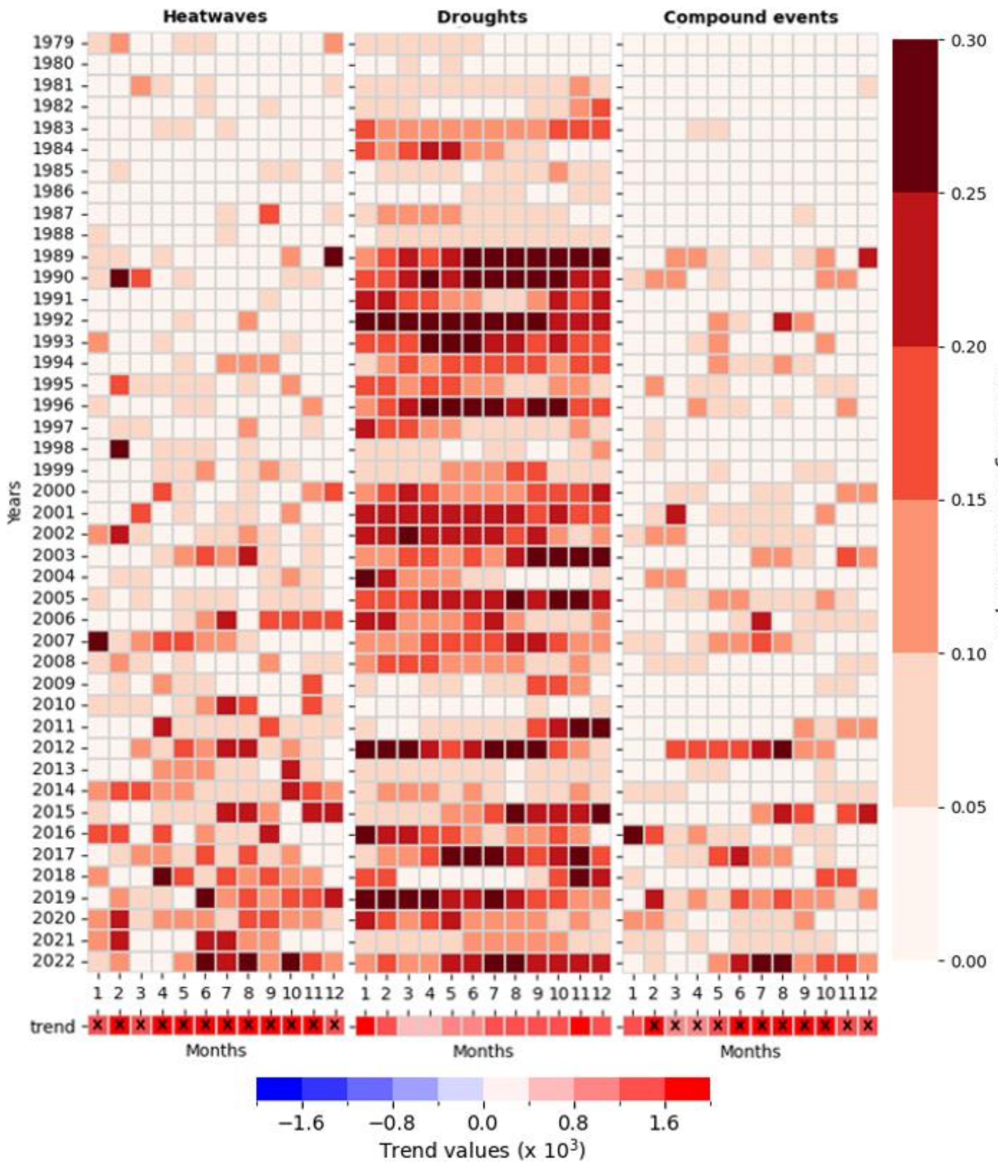

Figure 12: Incidence (%) of heatwaves, droughts and CDHEs occurrences in Europe (vertical colorbar), with trends for each month between 1979 and 2022 ('X' marking statically significant trends at a 5% level; horizontal colorbar).

The area occupied by heatwave events is much larger in recent years, as shown by the statistically significant positive monthly trends in the last row. The trend line of droughts shows positive monthly trends, but they are not statistically significant. In general, droughts tend to cover a larger area than heatwaves. On the other hand, there are some similarities between the distributions of CDHEs and heatwave events. They also show a positive trend in maximum values, with positive and statistically significant monthly trends. It can also be seen that the occurrence of CDHEs is strongly dependent on the occurrence of heatwaves. The most intense periods were 2012, 2015-17, 2019 and 2022, affecting about 30% of Europe for CDHEs.

The results for Iberia show similar trends, again with most months showing statistically significant trends for heatwaves and CDHEs. The most intense periods for CDHEs were 1994/95, 2005, 2012, 2019 and 2022, affecting at least 25% of the region. For heatwaves, there are also more months with high percentages in the last years of the study (Figure S19 in Supplementary Material). The results for France again show positive and statistically significant trends, as in Europe and Iberia. In the case of droughts, specific periods of drought can be observed: 1989-92, 1996-99, 2002-07, 2011/12, 2017, 2019 and 2022. The most intense years of CDHEs were 1989/90, 2005, 2017, 2019 and 2022, affecting at least 20% of French territory (Figure S20 in Supplementary Material).

To identify the atmospheric configuration during each type of event, the average composites of the temperature anomalies at 850 hPa and the geopotential height at 500 hPa were calculated (Figure 13).

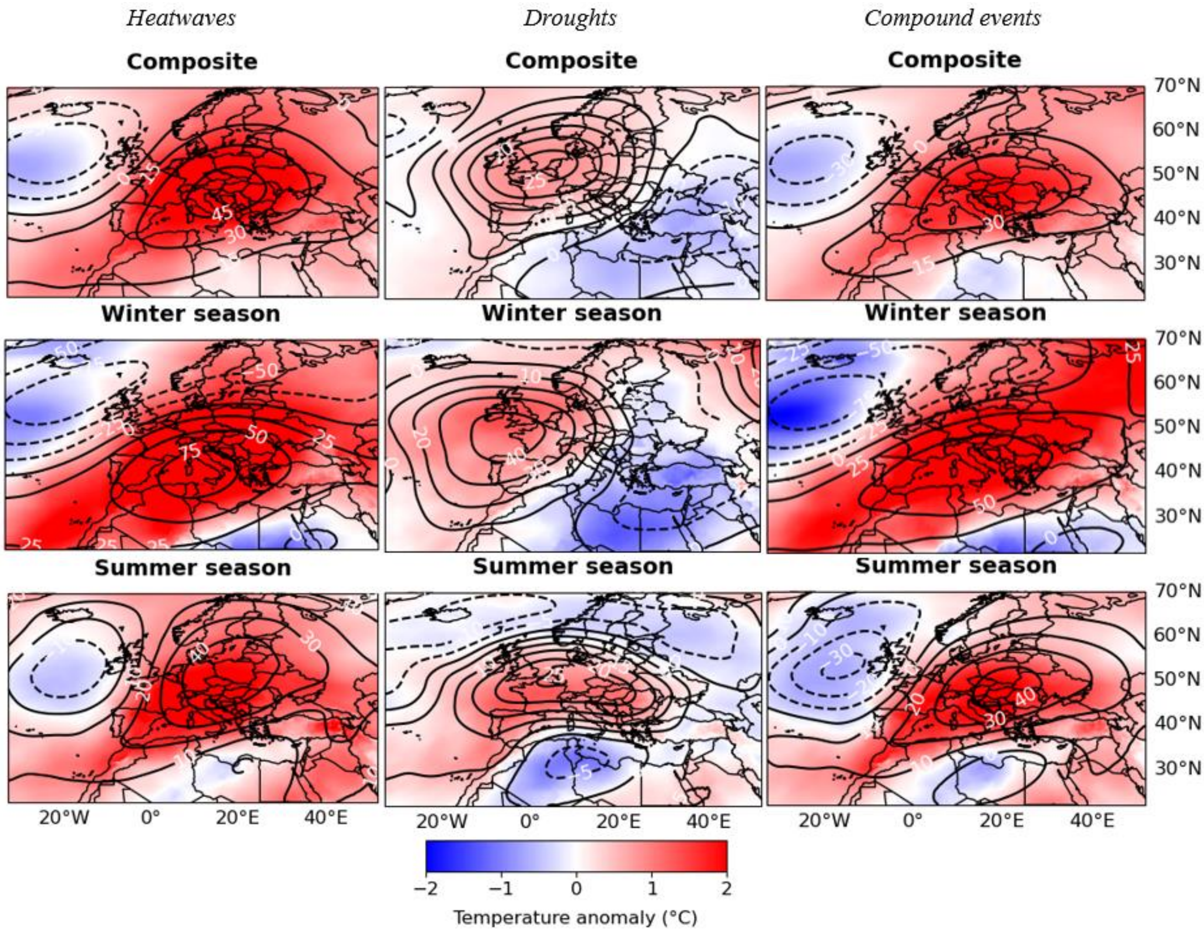

Figure 13: Mean composite of temperature anomalies at 850 hPa level (color shading) and geopotential height at 500 hPa level (m) (contours). The red zones and continuous lines indicate positive anomalies and blue zones and discontinuous lines indicate negative anomalies. “Composite” indicates an annual composite, “Winter season” indicates a composite of the DJF months, and “Summer season” indicates a composite of the JJA months.

Figure 13 shows the atmospheric configurations for the most extreme heatwaves, droughts and CDHEs, for winter and summer. The atmospheric configurations of heatwaves and CDHEs are very similar, due to the similarity observed in the monthly distributions of the Area Index shown in Figure 12. Both types of events are characterized by a high-pressure centre located in the centre of Europe, accompanied by positive temperature anomalies, while the low-pressure centre is associated with negative temperature anomalies and is located north of the Azores. This configuration does not change whether all the months are considered or only the summer and winter months. As for the drought maps, they show identical configurations in all three situations, with the high-pressure centre mostly located over Western Europe, with a vertical flattening in the summer months. Low-pressure centres over the south-eastern region of the study area in all months and in winter, and to the north in summer.

As in the study region, the heatwave and CDHE maps for both Iberia and France show a similar distribution with the prevalence of the high-pressure centre over Europe, accompanied by positive temperature anomalies (Figs. S21 and S22 in the Supplementary Material). The drought maps for Iberia show a large variation. Considering all months, the high-pressure centre is located northwest of Iberia and over Russia, while in winter it is between the Azores and Iceland and again over Europe. The summer months show the opposite of the winter maps, with the anticyclone over Iceland and Eastern Europe. It should be noted that in this case the positive temperature anomalies do not coincide with the positive geopotential anomalies. As for France, the drought maps show a greater similarity between the three situations, with the high-pressure centre located to the north-west of Iberia and the low-pressure centre to the south-east of the study area and, in the case of summer, also over Iceland.

In this study, teleconnections have been used to relate to water vapor flux from west and to investigate how each teleconnection contributes to that flux in each sub-domain and which of them is the most important influence (Figure 14). Figure 14 shows time series of absolute values of the NAO, AMO, N3.4, EA, and anomalies of WMF, filtered with 10-year low pass Lanczos filter.

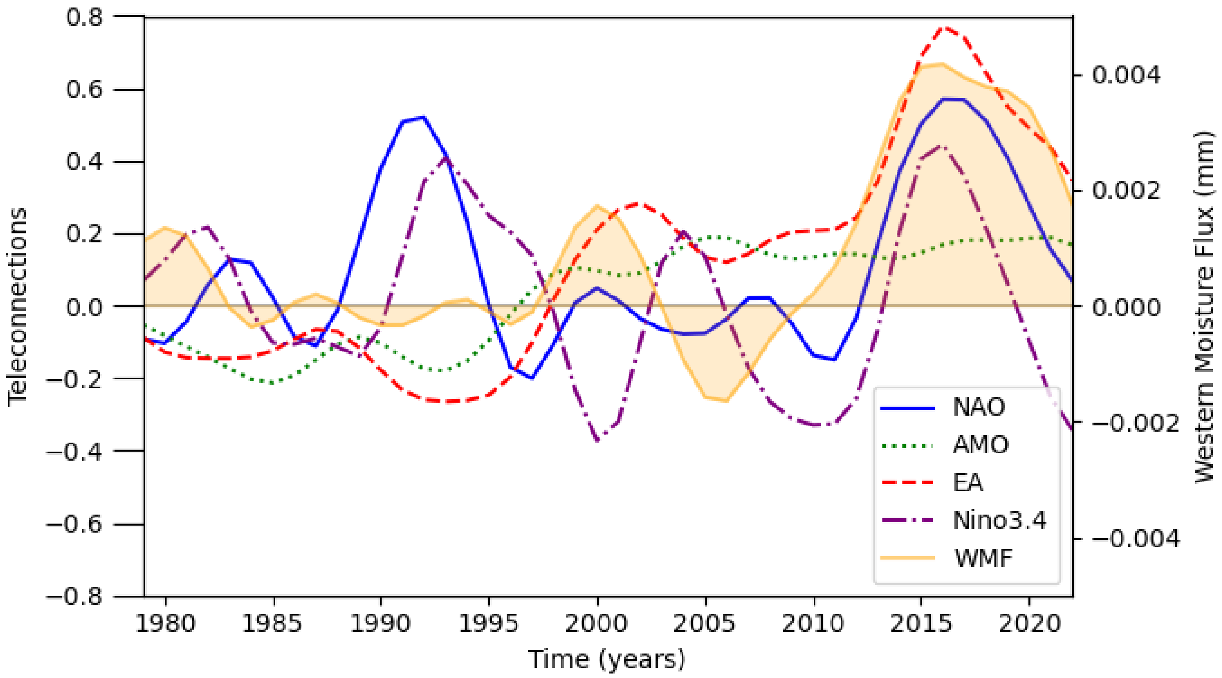

Figure 1: Time series from 1979 to 2022 of the NAO (blue and continuous line), the AMO (green and dot line), the EA (red and long dash line), and the N3.4 (purple and dot dash line) and of the anomalies of western moisture flux in Europe (yellow and shaded line) filtered by a 10-year low pass Lanczos filter.

While the NAO+ peaked in the early 1990s and in 2016/17, showing markedly five phases in study period. The EA peaked in 2016 and the AMO peaked in 2005, maintaining values close to this maximum in the following years. The N3.4 has been on an upward trend since 1993, after reaching a low of around -0.4. It peaked at around 0.7 in 2010. The WMF anomalies show similar interannual variability to the teleconnections studied, with similar distributions in certain periods. It reaches its minimum peak in 2006, with a distribution opposite to that of the NAO+. It reaches its maximum peaks in 2000 and 2016, coinciding with the EA and NAO+ distribution in the last years. Both Iberia and France show a similar distribution of WMF anomalies to Europe (Figures S22 and S23 in the Supplementary Material).

To quantify this similarity, Table 1 shows the monthly and annual Pearson correlations with and without Lanczos filter, showing that individual teleconnections have an influence on the moisture flux that occurs in each subdomain of the study.

Table 1: Annual and monthly Pearson's correlation coefficients obtained between filtered time series of three indexes and WMF in Europe for the 1979 – 2022 period. In bold are shown the statistically significant correlation coefficients at a 5% significant level according to the Student's two-tailed t test.

	NAO+	*AMO*	*N3.4*	*EA*		*NAO+*	*AMO*	*N3.4*	*EA*
January	**0.52**	0.09	0.11	**0.62**	July	0.02	0.27	-0.06	**0.40**
February	**0.77**	0.13	0.03	**0.79**	August	**0.43**	0	0.04	**0.61**
March	**0.70**	-0.16	0.07	0.20	September	**0.42**	0.05	-0.22	**0.68**
April	**-0.27**	-0.10	0.13	**0.62**	October	0.22	0.12	-0.05	**0.69**
May	0.14	0.06	-0.15	**0.76**	November	**0.34**	-0.15	**0.51**	**0.88**
June	**0.82**	0.10	0.19	**0.53**	December	**0.34**	-0.16	0.27	**0.59**
Annual (filt.)	**0.42**	0.06	0.20	**0.59**	Annual	**0.49**	**0.42**	0.17	**0.77**
DJF	**0.54**	0.02	0.13	**0.65**	JJA	**0.39**	0.13	0.04	**0.50**
MAM	**0.37**	-0.08	0.02	**0.47**	SON	**0.29**	-0.01	0.16	**0.72**

Most of the correlations between WMF and positive phase of NAO are positive. The minimum occurs in April and reaches -0.27. The period with the highest correlation between these two variables is winter with 0.54. On the other hand, autumn has the lowest correlation with 0.29. However, the month with the highest correlation is summer, June, with 0.82. The same applies to EA, which shows very high correlations throughout the year. Together with the NAO+, it is the most influential teleconnection with the flow of moisture reaching Europe via the western border, considering the autumn months. The maximum value is 0.88 in November, with all correlations being positive. Considering the annual values, it is the most influential teleconnection. The AMO and N3.4 teleconnections both show very low correlations, alternating between positive and negative values. The AMO reaches its maximum in July with 0.27 and its minimum in March and December with -0.16, while the N3.4 reaches its maximum in November with 0.51 and its minimum in September with -0.22. When analyzing the filtered annual values, AMO increase its correlations, with 0.42.

The results obtained for Iberia are similar, but the correlations for NAO+ are weaker and there are more months with negative correlations, with EA being the most influential teleconnection (Table S1 in the Supplementary Material). For France, the results are very similar to those for Europe (Table S2 in the Supplementary Material).

3.2 Study case: 2022 CDHE

This subsection analysis the driving mechanisms of the CDHE that occurred in 2022 in Europe, namely regarding the anomalies in temperature, accumulated precipitation and soil moisture against the climatological conditions (1981-2010) (Figure 15).

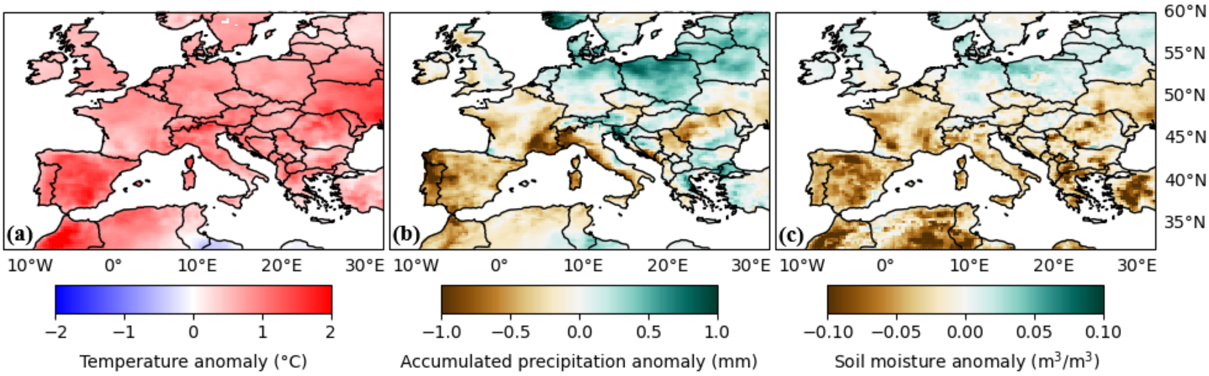

Figure 15: Spatial anomalies of temperature (a), accumulated precipitation (b), and soil moisture (c) for 2022, regarding 1981-2010 climatological period.

The positive temperature anomalies cover the whole of Europe and reach 1 ºC above average (Figure 15a). The distributions of accumulated precipitation and soil moisture anomalies are similar. For accumulated precipitation, the minima are in the northwest of the Iberia, the south-east of France and the west coast of Italy (Figure 15b). For soil moisture, the minima are in the center of Iberia and the Mediterranean region, especially in the Balkan region (Figure 15c). The strongest minima are found in western Iberia and the southeastern border of France, with about -1 mm for accumulated precipitation, and in central Iberia and the Balkan region, with about -0.1 m^3/m^3 for soil moisture.

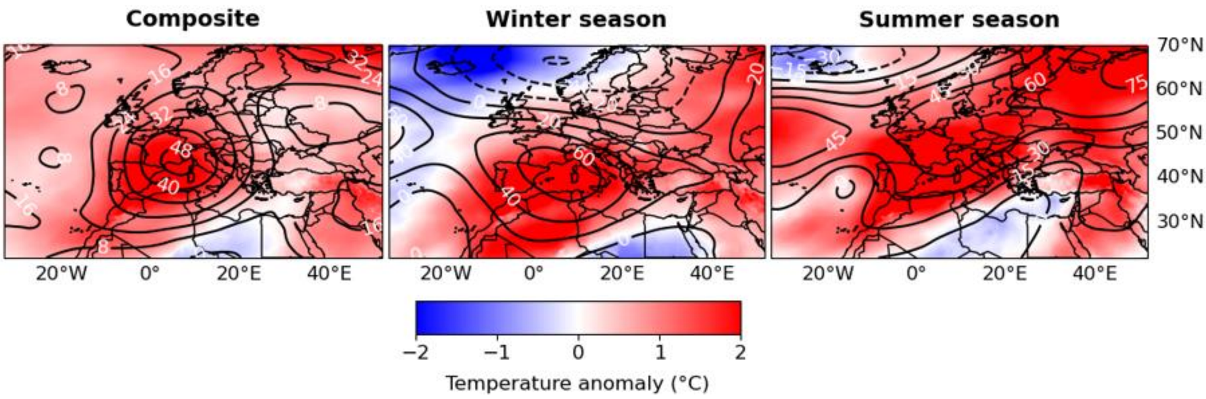

Figure 16: Composite of temperature anomalies at 850 hPa level (color shading) and geopotential height at 500 hPa level (m) (contours), considering all months, winter and summer of 2022, regarding 1981-2010 climatological period.

During 2022, the average atmospheric configuration is characterized by a high-pressure center over France accompanied by positive anomalies of temperature, considering all months ("Composite" in Figure 16). In winter, there is a high-pressure centre in the same location, but also the appearance of a low-pressure centre with negative temperature anomalies to the north of the study area. In the summer months, there is a weakening of the anticyclone in the region of France, with a shift to the region of Russia and north of the Azores.

Complementing the results obtained and presented above, it is also important to analyze the availability of moisture in the atmosphere to understand its influence on this type of event (Figure 17).

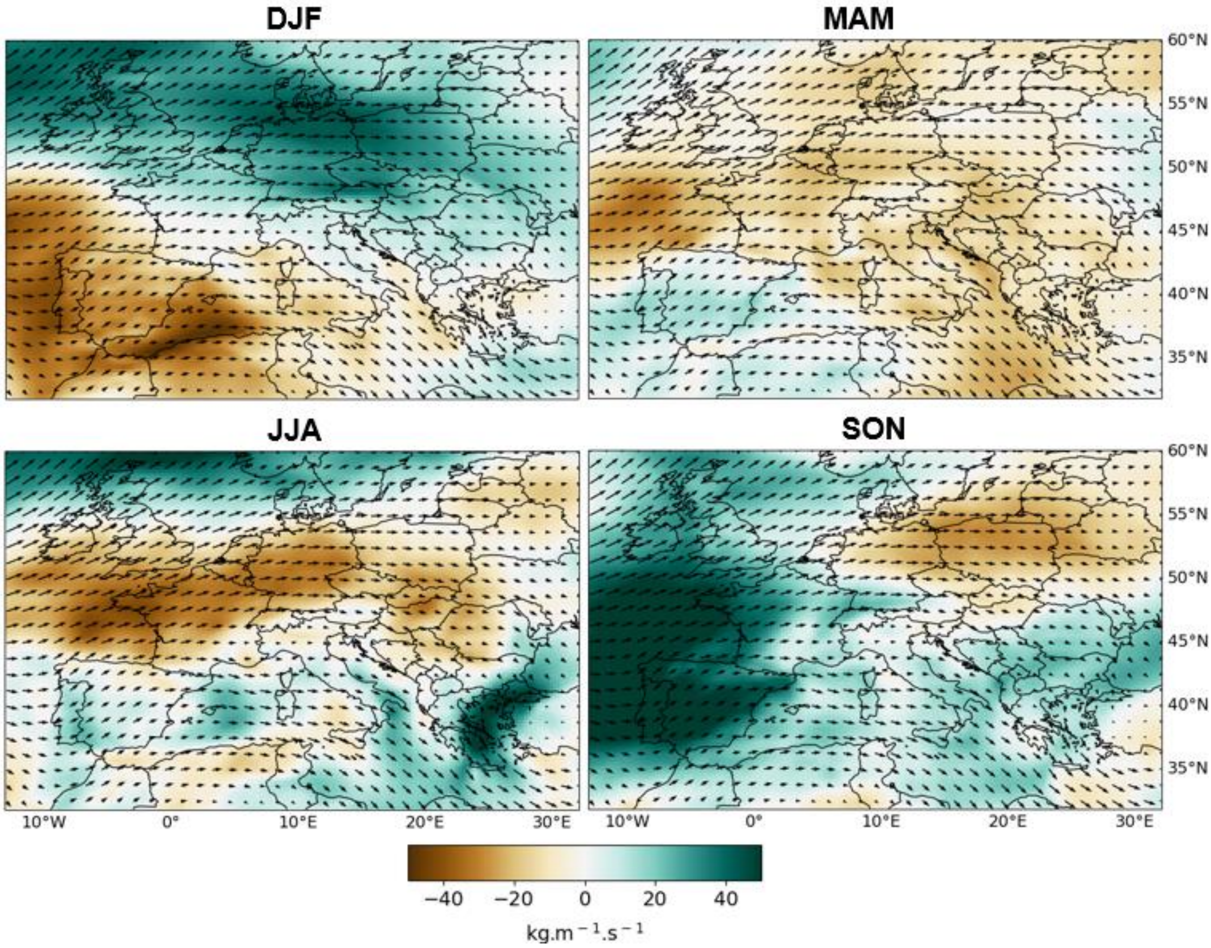

Figure 17: Seasonal IVT anomaly (regarding the 1981 - 2010 climatology) during 2022 (absolute field – color shading; direction – vectors).

Between December 2021 and November 2022, we see that during the winter there is a prevalence of negative IVT anomalies over Iberia, reaching values around -50 kg/m/s, and that in the following months there is a migration of these negative anomalies towards the center of Europe (Figure 17). The transition from winter to spring is characterised by a migration of negative IVT anomalies from Iberia to central Europe, which remain localised in this region until the end of the year. At the same time as the negative IVT anomalies migrate towards the centre of Europe, positive IVT anomalies become established on the western side. It should be noted that in spring the negative anomalies are distributed uniformly over the whole of Europe with the exception of Iberia, while in summer the minima are latitudinal distributed, specifically affecting central Europe, and in autumn they are located in eastern Europe, while the positive IVT anomalies begin to occupy the western region of Europe.

As a complement to the results in Figure 16, in addition to identifying the regions where the presence of moisture is lower than the climatological average, it is also important to identify the movements that this moisture undergoes, in other words, to identify the regions that act as sources and sinks of moisture (Figure 18).

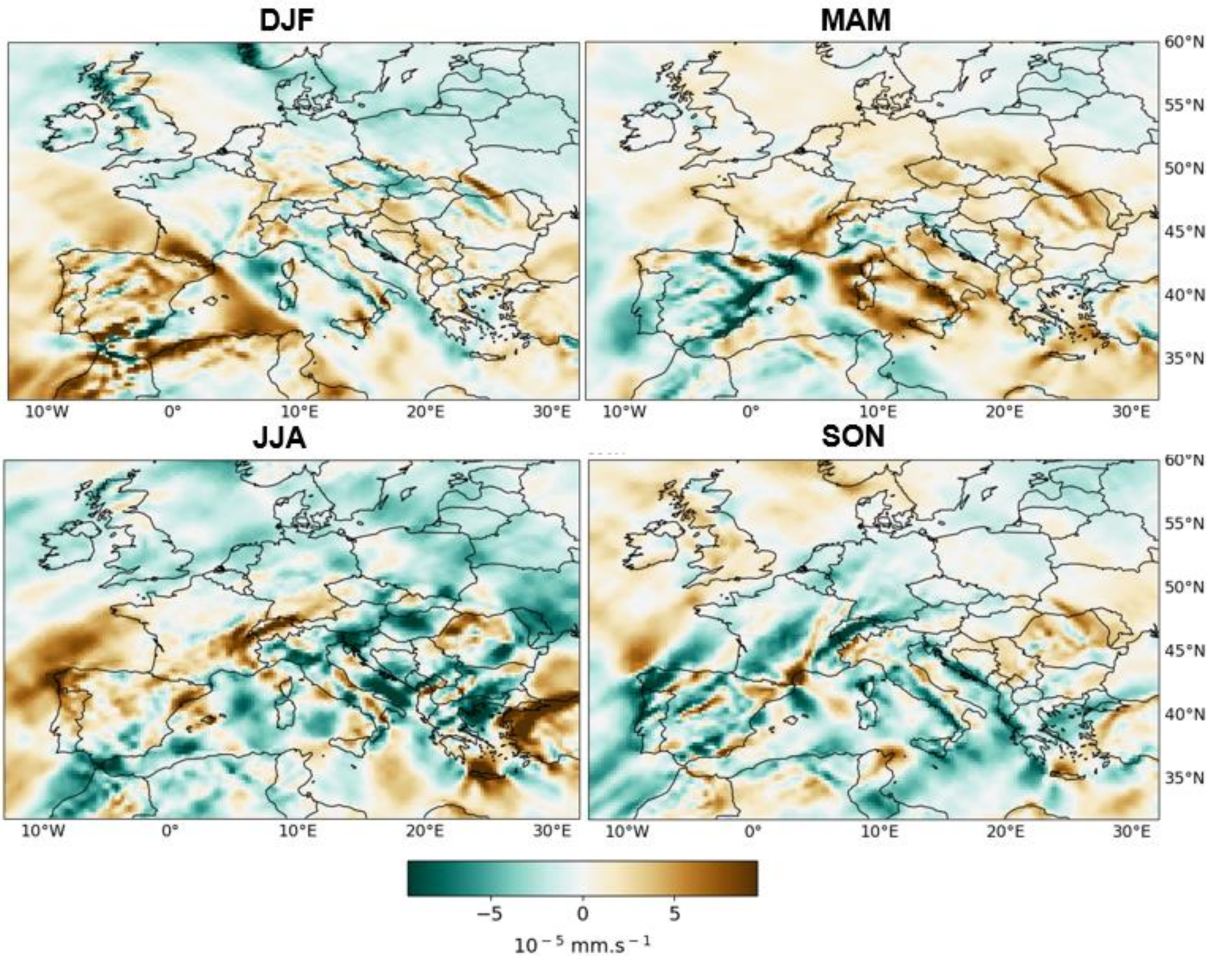

Figure 18: Seasonal anomalies of moisture divergence (regarding the 1981 - 2010 climatology) during 2022.

During the winter months, over Iberia and surrounding regions, the positive anomalies are very intense, ~$9x10^{-5}$ mm/s, leading to water vapor divergence. This divergence motion is associated with the negative anomalies seen in Figure 17, i.e., enhanced divergence motions associated with anomalous sinking in the atmosphere led to water vapor dissipation over Iberia. In spring, it can be seen that the centre of Europe has positive moisture divergence anomalies, with southern France and Italy standing out. In the following months, these anomalies become negative. In summer, the Galicia region shows high divergence anomalies, as do the Turkey-Greece region and the Alps. The autumn, which was characterised by very positive IVT anomalies, now shows negative divergence anomalies, which means that there is an above normal convergence of water vapour during this period. The same happens in more southern European regions.

In the remaining months, it is not so easy to see a direct relationship between the negative IVT anomalies and the moisture divergence. However, in spring and autumn, Iberia mostly experiences moisture convergence. In summer, on the other hand, the divergence is high in Galicia and the surrounding regions, suggesting that this moisture is displaced southwards and converges in Andalusia.

Chapter 4 – Discussion

The trends show positive values for temperature and negative values for accumulated precipitation and soil moisture. The study area, the Mediterranean region, is located in mid-latitudes, where solar radiation is relatively high (Pyrina et al., 2015), and therefore this characteristic favors an increase in evaporation, thus contributing to a decrease in soil moisture. However, this decrease in soil moisture can lead to an increase in temperature due to the increase in sensible heat emitted to the atmosphere. Precipitation deficits are associated with low soil moisture, causing a reduction in evaporation, but also a reduction in the transport of moisture in the atmosphere (van den Hurk et al., 2010). These characteristics have increased over the years due to internal variability and anthropogenic activities.

The trends of temperature, accumulated precipitation and soil moisture, analyzed individually or together, show a tendency towards dry and hot conditions, favorable to the development of these types of events and are accompanied by an increase in the frequency, duration and magnitude of heatwaves, droughts and CDHEs. These results are in line with previous studies by Guerreiro et al. (2018), which also show an increase in the number of days as well as the amplitude, especially in southern Europe. The study by Perkins-Kirkpatrick and Lewis (2020) also shows consistent trends for heatwaves between 1950 and 2017 for different regions, especially the Mediterranean. The trends presented confirm the results obtained in this work, with values that are as close as could be expected due to the use of different study periods. Although in this study duration and cumulative intensity are replaced by maximum duration and cumulative heat, the decadal trends are also consistent. According to the results obtained, in addition to a significant increase in the decadal trends of the features, there is also an acceleration in the presence of anthropogenic climate change (Mukherjee and Mishra et al., 2020), especially over Europe (Fischer et al., 2015). Heatwaves are also highly sensitive to internal climate variability (Perkins-Kirkpatrick et al., 2017). The study by Mukherjee et al. (2022) shows that the warming process is accelerated and intensified by increased emissions of heat-trapping gases due to anthropogenic activities (Samset et al., 2018) and conditions favored by large-scale teleconnections (Mukherjee et al., 2021), which reinforce the effects of increased anthropogenic warming. In the Mediterranean region, the occurrence of dry and/or hot events can be strongly attributed to anthropogenic forcing, while natural variability is very weak or absent (Mukherjee et al., 2021). On the other hand, the study by Perkins-Kirkpatrick et al. (2017) showed the significant influence of internal climate variability on trends in the frequency of heatwaves. Short-term trends are more variable in magnitude and direction than long-term trends, and short periods of decreasing heat wave frequency are possible under anthropogenic influence. However, anthropogenic influence is forcing heatwave trends, especially over the long-term, towards unprecedented rates of increase.

As for droughts, they are accompanied by decadal trends that are also positive, with months below this event (~0.14 months) and magnitude (~0.14) (Figure 9). These results are confirmed by Trnka et al. (2016) and Páscoa et al. (2021), who show positive trends for Central Europe and the Iberia, respectively. The first study also shows an increase in characteristics for the period 1991 - 2014 compared to the period 1960 - 1990. These increases are associated with rising temperatures, a decrease in long-term precipitation, and an increase in evapotranspiration. However, the study by Vicente-Serrano et al. (2021) shows different results, indicating that from a long-term perspective (1851 - 2018) there are no generally consistent trends in droughts across Western Europe. These results may be due to the fact that the study period is too long, the study region is not exactly the same as the one used in this work, or even to the fact that the precipitation data used are from meteorological agencies, whereas in this work we used ERA5 reanalysis data.

The results show that droughts affect large areas over several months, while heatwaves are more localized and less widespread, considering both Europe and the two sub-regions (Figure 12). The boundaries used in this work to define heatwave and drought events may influence this distribution, i.e. by being different they may lead to different results. The use of other time scales in the calculation of the SPI, 3 or 6 months, will consider a smaller composite of months and therefore it is very likely that the maximum values will not occur in the same months and that there will be a smoothing (intensification) when the observed conditions are less (more) extreme. On the other hand, the number of days used in this work may also influence the distribution of heatwaves, i.e. using fewer days would result in more heatwave events being identified. However, it should be stressed that this work aims to study the most extreme individual and simultaneous drought and heatwave events. Therefore, the limits used to obtain the results are justified. Heatwaves ultimately have a strong atmospheric influence, while droughts have a strong soil moisture influence in addition to the atmospheric one. The atmospheric reaction time is faster than that of the soil, which can influence the duration associated with each event, making heatwaves more intermittent and localized events, while droughts are more prolonged, even if there are improvements in dry conditions. Thus, CDHEs are mostly influenced by heatwaves because their occurrence is more punctual than that of droughts.

Atmospheric dynamics have an important influence on the development of extreme phenomena. In this work, as in Herrera-Lormendez et al. (2021), a distinction was made between winter (DJF) and summer (JJA) months in Central Europe due to differences in the pressure gradient. They observed more intense (weaker) meridional gradients during winter (summer), as expected from the associated meridional temperature gradients over the mid-latitudes. Heatwaves and CDHEs are strongly influenced by an anticyclone over central Europe. This pattern causes a flow of warm air from the east in the lower troposphere, and in addition to the horizontal advection present in both the lower and upper troposphere, the downward motion of air and adiabatic subsidence in anticyclones can contribute to an increase in air temperature at the surface (Tomczyk and Bednorz, 2015). Although droughts show greater variability in the location of the high-pressure center, the high-pressure center over western Europe promotes west/southwest flow of moist tropical air masses in the lower troposphere and southerly circulation in the mid-troposphere (Kingston et al., 2015).

Depending on the region, the moisture fluxes may also depend on one or more teleconnections. The westerly flow, which transports moisture through the atmosphere to Europe, is strongly related to NAO+ and EA when Europe and France are considered, but only to EA when Iberia is considered (Table 1). These two teleconnections are closely linked to the formation of high-pressure systems and favor the coincidence of low precipitation and high temperatures (or droughts and hot extremes) on longer time scales (Wu et al., 2021). This is in agreement with the results of Lemus-Canovas et al. (2022), who also identified the influence of the positive EA phase and, to a lesser extent, the negative NAO phase in the Mediterranean region. The positive EA phase promotes an increase in surface temperatures, while the negative NAO phase is associated with lower temperatures but a drier climate, associated with precipitation deficits. Both characteristics favor conditions for the development of CDHEs in the region studied. The intensity/magnitude of individual events is also influenced by teleconnections, and the corresponding correlation was calculated, which also showed a stronger influence of NAO+ and EA.

Unlike temperature-related extremes such as heatwaves and droughts, precipitation variability is more influenced by internal climate variability, especially at the regional scale (Dai et al., 2018). The increasing trend in the occurrence of CDHEs on a global scale due to anthropogenic forcing is likely dominated by the strong signal of increasing temperature (Zhang et al., 2022). The influence of internal variability and/or anthropogenic forcing (or other external forcing, such as solar activity) remains questionable (Egorova et al., 2018). The combination of precipitation deficit and high temperatures contributed to the persistence and severity of the drought, which in turn reduced soil moisture (Figures 15 and 16). This situation created positive feedback in which dry soils led to even more severe droughts. The regions of the Iberia and France were severely affected by forest fires and water shortages (Tripathy and Mishra, 2023).

In 2022, Europe was strongly affected by a CDHE. Europe experienced an increase in temperature, but also a deficit in precipitation and soil moisture. This was due to the high-pressure center positioned over Europe, which promoted the descent of warmer air caused by adiabatic subsidence processes (Tripathy and Mishra, 2023). On the other hand, and as a consequence of the establishment of the anticyclone over Europe, the deficit in precipitation and subsequently in soil moisture was associated with the negative IVT anomalies and also with the regions of moisture divergence in the atmosphere, as can be seen in Iberia in DJF and in Central Europe in the remaining seasons. Even if the respective maps don't show this association so strongly, due to the characteristic orography of Europe, they represent a vertical descent of warmer air associated with a horizontal lack of clouds and, consequently, precipitation in the regions during these periods. It should be remembered that 2021/22 was a period strongly characterized by drought conditions, and most of the region was affected by moderate drought conditions and only a few areas experienced extreme and severe drought levels, to which we can compare the hydrological year 2004/05 in Iberia (García-Herrera et al., 2007) or the hot and dry year 2015 in Europe (Ionita et al., 2017). The persistence of these events for several months could have led to successive productivity deficits in vegetation (Ermitão et al., 2021) and increased the number of emergency cases, putting pressure on hospitals (Yao et al., 2024). Conditions of high temperatures and low rainfall (or soil moisture deficit) with low relative humidity favor the occurrence of wildfires, especially in the Mediterranean region (Ruffault et al., 2020). The co-occurrence of heatwaves and droughts also causes an increase in population exposure, and in cases where heatwaves and extreme precipitation coincide and a sequential episode of droughts or heatwaves and extreme precipitation emerges as more important in explaining this change in population exposure to these types of events (Das et al., 2022). Tripathy et al. (2023) projected future shifts in heatwaves, droughts, and CDHEs, accompanied by increases in temperature, decreases in soil moisture, and variations in precipitation.

Mediterranean countries are considered a hotspot of climate change (Giorgi and Lionello, 2008), where larger precipitation losses and increases of heavy precipitation events are expected in the future climate (Gao et al., 2006). In the future, projections show a significant decrease in the number of wet days (above 1 mm), from -15% in the northwest to -30% in the south of Portugal, with decline mostly in spring, summer, and autumn (Soares et al., 2016). The same results are obtained for the Mediterranean region with small decrease in summer and autumn in east and southeast regions, when analyzed with RCP8.5 (Marras et al., 2021). Nguyen et al. (2016) have pointed out the climate change in the Mediterranean region will endure faster and intense soil dissection enhancing droughts and water scarcity. This soil moisture depletion promotes the occurrence of land-atmosphere feedback and mutual intensification of heatwaves and droughts. In Soares and Lima (2022), RCP2.6, RCP4.5, and RCP8.5 scenarios present soil moisture depletion with concerns to extreme total soil moisture values there is a pronounced shift for much negative values and as well a flattening of the distributions much like what is projected for temperature in many regions of the world, accompanied by projections of precipitation reductions, regional warming and the subsequent large increase of potential evapotranspiration, which may lead to an intensification of heatwaves and droughts.

There are some inherent uncertainties in the datasets used in this thesis. Nevertheless, results obtained for the troposphere and in different areas of the planet when studying different climatic variables have been considered robust (Hersbach et al., 2020). The use of the SPI is limited because only uses a single meteorological element for describing a complex event (Caparrini and Manzella, 2009). On the other hand, the SPEI takes into account potential evapotranspiration and could have been used instead of the SPI. Heatwaves are on a daily scale, while droughts are on a monthly scale. The fact that these scales are not the same means that the time scale for identifying CDHEs is monthly, which reduces the accuracy of the characterization. Hypothetically, if different scales were used for both type of events, a daily analysis of CDHEs could be made and related to other parameters, such as mortality, in future work. A major advantage of this method is that it identifies the occurrence of CDHEs at each grid point and that this identification is done in absolute form, i.e. through matrices of the occurrence of individual heatwave and drought events. These results can be complemented in the future by calculating their characteristics (frequency, duration and intensity).

The questions that this work set out to answer were successfully answered. Throughout the study period, there was a co-occurrence of heatwaves and droughts that led to the development of CDHEs. The increase in temperature and the decrease in precipitation and soil moisture, as well as the anticyclonic conditions observed in the recent past, contributed positively to triggering this type of event. The year 2022 was very extreme and the CDHE that occurred was enhanced by positive temperature anomalies and negative accumulated precipitation and soil moisture anomalies, the persistence of anticyclonic conditions and negative IVT anomalies accompanied by positive water vapour divergence anomalies, creating conditions for the development of extremely hot and dry events. These features contributed to 2022 being a very extreme year.

Chapter 5 – Conclusions

Taking into account the main results obtained in this work, we can conclude the following:

- Evolution of climatic conditions towards more extreme conditions, characterized by positive decadal trends in temperature and negative in accumulated precipitation and soil moisture (spatially with statistically significant negative values, especially in the Mediterranean region). The seasonal analysis is also similar for the three variables studied.
- The frequency, duration, intensity and cumulative intensity of heatwaves show positive trends, with peaks in the last years of the study. Droughts, on the other hand, show smooth positive decadal trends and high inter-annual variability.
- The second subperiod, 2001-2022, compared to 1979-2000, shows high values in the characteristics of heatwaves, as well as a gradual evolution of conditions towards warmer and drier conditions, with a high frequency of accumulated precipitation deficit, through bivariate analysis with kernel adjustment.
- The maximum areas occupied by droughts last longer than heat waves and CDHEs, which is related to the faster response times of the atmosphere in relation to the soil. In this way, the areas occupied by CDHEs are strongly influenced by heat waves, due to the punctuality of the distribution of their maxima.
- High pressure centers positioned over central Europe are identified as the predominant atmospheric configuration during the most extreme heat wave events and CDHEs. Droughts show a greater variation in the location of anticyclones, which occur mainly in western Europe. The variation in these results between summer and winter months is not apparent, except for the drought results.
- The NAO and EA have a strong influence on the WMF variation and also on the intensity/magnitude of heatwave and drought events, in contrast to the AMO and N3.4.
- The case study, the 2022 CDHE, was characterized by unusually very hot and very dry conditions due to the prevalence of anticyclonic conditions in central Europe and negative IVT anomalies accompanied by positive water vapor divergence anomalies, which caused a moisture deficit in the region.

The driving mechanisms behind heatwaves, droughts or even their co-occurrence are vast and their possible simultaneity should be highlighted. A positive trend was identified in the evolution of climatic conditions towards more extreme conditions, with an increase in temperature and a decrease in precipitation and soil moisture. This evidence may be a first trigger and may be associated with other driving mechanisms. Atmospheric configurations play an important role in the climatic conditions felt at the Earth's surface. Teleconnections can also have an important influence on the temperature and precipitation regime of a given region, with the NAO and EA being the most important in the case of Europe. These atmospheric conditions were observed during the 2022 CDHE, making it an important recent case study in the literature.

This work has contributed to understanding the mechanisms behind events such as heatwaves and droughts and how they have changed in the recent past, i.e., what atmospheric dynamics have influenced the development and extreme nature of extreme events, what type of event has the greatest influence on the occurrence of CDHEs, how extreme the 2022 CDHE was and how it was characterized. The future work could be complemented by future projections with ensembles as in Meng et al. (2022). Meng et al. (2022) indicate that the single and co-occurrence of heatwaves and droughts will increase. The analysis of population exposure is also a parameter that can complement this work in the future. This was analyzed by Wu et al. (2022) for China, which found an increase in population exposure with two temperature increase scenarios, 1.5 and 2 ºC, which also led to an increase in the risk of mortality due to excessive heat. About 106% of the total change in exposure to extreme combined dry and hot events can be attributed to the climate effect, and 0.5°C less warming, particularly in eastern China, would provide useful insights for advancing climate change adaptation. Another parameter that could be addressed in the future is the quantification of the anthropogenic component of climate change, something identical to what was done in Meng et al. (2023). In this study, they used an approach that considers the likelihood of extremes occurring under climate conditions with anthropogenic influence and the likelihood of extremes occurring in a counterfactual world with little or no human influence (Philip et al., 2022). They showed that the 2022 CDHEs area in the Northern Hemisphere would have been virtually impossible without anthropogenic climate change. The methodology of ranking of events over a pre-selected period, discussed in Geirinhas et al. (2023), could also be used in this work by calculating the *Rindex*, which quantifies and ranks the magnitude of soil moisture anomalies on a daily basis. In this way, each event could be individualized and classified according to its magnitude.

References

Alizadeh, M. R., Adamowski, J., Nikoo, M. R., AghaKouchak, A., Dennison, P., & Sadegh, M. (2020). A century of observations reveals increasing likelihood of continental-scale compound dry-hot extremes. Science Advances, 6, eaaz4571.

Allaby, M., Garratt, R., 2007. Encyclopedia of Weather and Climate, Revised edition. Facts on File, New York.

Barriopedro, D., Fischer, E.M., Luterbacher, J., Trigo, R.M., García-Herrera, R., 2011. The hot summer of 2010: redrawing the temperature record map of Europe. Science 332 (6026), 220–224.

Beggs, P. J. et al. The 2019 report of the MJA-Lancet Countdown on health and climate change: a turbulent year with mixed progress. Med. J. Aust. https://doi.org/10.5694/mja2.50405 (2019).

Bowman, D. M. J. S., Balch J. K., Artaxo P., Bond W. J., Carlson J. M., Cochrane M. A. M., DeFries R. S., Doyle J. C., Harrison S. P., Johnston F. H., Keeley J. E., Krawchuk M. A., Kull C. A., Marston J. B., Moritz M. A., Prentice I. C., Roos C. I., Scott A. C., Swetnam T. W., Van Der Werf G. R., Pyne S. J.. Science 324, 481 (2009). doi: 10.1126/science.1163886.

Caparrini F, Manzella F. 2009. Hydrometeorological and vegetation indices for the drought monitoring system in Tuscany Region, Italy. Advances in Geosciences 17, 105-110.

Cheval, S., Busuioc, A., Dumitrescu, A., & Birsan, M. V. (2014). Spatiotemporal variability of meteorological drought in Romania using the standardized precipitation index (SPI). Climate Research, 60(3), 235-248.

Chwialkowski, K., Strathmann, H. and Gretton, A.. (2016). A Kernel Test of Goodness of Fit. Proceedings of The 33rd International Conference on Machine Learning, in Proceedings of Machine Learning Research 48:2606-2615 Available from https://proceedings.mlr.press/v48/chwialkowski16.html.

Copernicus, 2023. The Europen State of the Climate 2022. Accessed at 29/05/2024.

Coumou, D., Rahmstorf, S., 2012. A decade of weather extremes. Nat. Clim. Chang. 2 (7), 491–496.

Dai, A., Zhao, T., & Chen, J. (2018). Climate change and drought: a precipitation and evaporation perspective. Current Climate Change Reports, 4, 301-312.

Das, J., Manikanta, V., & Umamahesh, N. V. (2022). Population exposure to compound extreme events in India under different emission and population scenarios. Science of The Total Environment, 806, 150424.

Dosio A, Mentaschi L, Fischer E M and Wyser K 2018 Extreme heat waves under 1.5 °C and 2 °C global warming Environ. Res. Lett. 13 0540046.

Douville, H., Ribes, A., Decharme, B., Alkama, R. & Sheffield, J. (2013). Anthropogenic influence on multidecadal changes in reconstructed global evapotranspiration. Nat. Clim. Chang. 3, 59–62.

Duchon, C. E. (1979). Lanczos filtering in one and two dimensions. *Journal of Applied Meteorology and Climatology*, *18*(8), 1016-1022.

Duff, T.J., Cawson, J.G. & Harris, S. Dryness thresholds for fire occurrence vary by forest type along an aridity gradient: evidence from Southern Australia. Landscape Ecol 33, 1369–1383 (2018). https://doi.org/10.1007/s10980-018-0655-7.

Dunn, R.J., Mead, N.E., Willett, K.M., Parker, D.E., 2014. Analysis of heat stress in UK dairy cattle and impact on milk yields. Environ. Res. Lett. 9 (6), 064006. http://dx.doi.org/10.1007/s00382-012-1415-z.

Egorova, T., Rozanov, E., Arsenovic, P., Peter, T., & Schmutz, W. (2018). Contributions of natural and anthropogenic forcing agents to the early 20th century warming. Frontiers in Earth Science, 6, 206.

Ermitão, T., Gouveia, C. M., Bastos, A., & Russo, A. C. (2021). Vegetation productivity losses linked to mediterranean hot and dry events. Remote Sensing, 13(19), 4010.

European Commission, 2022. Crop monitoring in Europe July 2022. JRC MARS Bull. 30.

Faranda, D., Pascale, S., & Bulut, B. (2023). Persistent anticyclonic conditions and climate change exacerbated the exceptional 2022 European-Mediterranean drought. Environmental Research Letters.

Fischer, E. M., & Knutti, R. (2015). Anthropogenic contribution to global occurrence of heavy-precipitation and high-temperature extremes. Nature climate change, 5(6), 560-564.

Gao X, Pal JS, Giorgi F (2006) Projected changes in mean and extreme precipitation over the Mediterranean region from a high resolution double nested RCM simulation. Geophys Res Lett 33:L03706. doi:10.1029/2005GL024954.

García-Herrera, R., Hernández, E., Barriopedro, D., Paredes, D., Trigo, R. M., Trigo, I. F., & Mendes, M. A. (2007). The outstanding 2004/05 drought in the Iberian Peninsula: associated atmospheric circulation. Journal of Hydrometeorology, 8(3), 483-498.

Geirinhas, J. L., Trigo, R. M., Libonati, R., Castro, L. C., Sousa, P. M., Coelho, C. A., ... & Mônica de Avelar, F. M. (2019). Characterizing the atmospheric conditions during the 2010 heatwave in Rio de Janeiro marked by excessive mortality rates. Science of The Total Environment, 650, 796-808.

Geirinhas, J. L. et al. The influence of soil dry-out on the record-breaking hot 2013/2014 summer in Southeast Brazil. Sci. Rep. 12, 5836 (2022).

Geirinhas, J.L., Russo, A.C., Libonati, R. et al. Combined large-scale tropical and subtropical forcing on the severe 2019–2022 drought in South America. npj Clim Atmos Sci 6, 185 (2023). https://doi.org/10.1038/s41612-023-00510-3.

Giorgi, F., & Lionello, P. (2008). Climate change projections for the Mediterranean region. Global and planetary change, 63(2-3), 90-104.

Gouveia, C., Trigo, R. M., DaCamara, C. C., Libonati, R., & Pereira, J. M. (2008). The North Atlantic oscillation and European vegetation dynamics. International Journal of Climatology: A Journal of the Royal Meteorological Society, 28(14), 1835-1847.

Guerreiro, S. B., Dawson, R. J., Kilsby, C., Lewis, E., & Ford, A. (2018). Future heat-waves, droughts and floods in 571 European cities. Environmental Research Letters, 13(3), 034009.

Hao Y, Hao Z, Fu Y, Feng S, Zhang X, Wu X and Hao F 2021 Probabilistic assessments of the impacts of compound dry and hot events on global vegetation during growing seasons Environ. Res. Lett. 16 074055.

Hao, Z., Hao, F., Xia, Y., Feng, S., Sun, C., Zhang, X., ... & Meng, Y. (2022). Compound droughts and hot extremes: Characteristics, drivers, changes, and impacts. Earth-Science Reviews, 235, 104241.

Hauser, M., Gudmundsson, L., Orth, R., Jézéquel, A., Haustein, K., Vautard, R., ... & Seneviratne, S. I. (2017). Methods and model dependency of extreme event attribution: the 2015 European drought. Earth's Future, 5(10), 1034-1043.

Herrera-Estrada, J. E., Satoh, Y., & Sheffield, J. (2017). Spatiotemporal dynamics of global drought. Geophysical Research Letters, 44, 1–25. https://doi.org/10.1002/2016GL071768.

Herrera-Lormendez, P., Mastrantonas, N., Douville, H., Hoy, A., & Matschullat, J. (2022). Synoptic circulation changes over central Europe from 1900 to 2100: Reanalyses and coupled model intercomparison project phase 6. International Journal of Climatology, 42(7), 4062-4077.

Hersbach, H., Bell, B., Berrisford, P., Hirahara, S., Horányi, A., Muñoz-Sabater, J., ... & Thépaut, J. N. (2020). The ERA5 global reanalysis. *Quarterly Journal of the Royal Meteorological Society*, *146*(730), 1999-2049.

Ionita, M., Tallaksen, L. M., Kingston, D. G., Stagge, J. H., Laaha, G., Van Lanen, H. A., ... & Haslinger, K. (2017). The European 2015 drought from a climatological perspective. Hydrology and Earth System Sciences, 21(3), 1397-1419.

IPCC, 2022. Summary for Policymakers [H.-O. Portner, D.C. Roberts, E.S. Poloczanska, K. Mintenbeck, M. Tignor, A. Alegría, M. Craig, S. Langsdorf, S. Loschke, V. Moller, A. Okem (eds.)]. In: Portner, ¨ H.-O., Roberts, D.C., Tignor, M., Poloczanska, E.S., Mintenbeck, K., Alegría, A., Craig, M., Langsdorf, S., Loschke, S., Moller, V., Okem, A., Rama, B. (Eds.), Climate Change 2022: Impacts, Adaptation and Vulnerability. Contribution of Working Group II to the Sixth Assessment Report of the Intergovernmental Panel on Climate Change. Cambridge University Press Cambridge, UK and New York, NY, USA, pp. 3–33.

Jiménez-Esteve, B., & Domeisen, D. I. (2022). The role of atmospheric dynamics and large-scale topography in driving heatwaves. Quarterly Journal of the Royal Meteorological Society, 148(746), 2344-2367.

Keyantash, John & National Center for Atmospheric Research Staff (Eds). Last modified 2023-08-19 "The Climate Data Guide: Standardized Precipitation Index (SPI)." Retrieved from https://climatedataguide.ucar.edu/climate-data/standardized-precipitation-index-spi on 2024-05-19.

King, A. D. & Harrington, J. The inequality of climate change from 1.5 °C to 2 °C of global warming. Geophys. Res. Lett. 45, 5030–5033 (2018).

Kingston, D. G., Stagge, J. H., Tallaksen, L. M., & Hannah, D. M. (2015). European-scale drought: understanding connections between atmospheric circulation and meteorological drought indices. Journal of Climate, 28(2), 505-516.

Kong, Q., Guerreiro, S. B., Blenkinsop, S., Li, X.-F., and Fowler, H. J. (2020). Increases in summertime concurrent drought and heatwave in Eastern China. Weather Clim. Extrem. 28:100242. doi: 10.1016/j.wace.2019.10024.

Kucharski, F., Kang, I.-S., Straus, D., & King, M. P. (2010). TELECONNECTIONS IN THE ATMOSPHERE AND OCEANS. *Bulletin of the American Meteorological Society*, *91*(3), 381–383. http://www.jstor.org/stable/26232892

Lanning, S.B., Siebenmorgen, T.J., Counce, P.A., Ambardekar, A.A., Mauromoustakos, A., 2011. Extreme nighttime air temperatures in 2010 impact rice chalkiness and milling quality. Field Crop Res. 124 (1), 132–136.

Leal Filho, W., Echevarria Icaza, L., Neht, A., Klavins, M., & Morgan, E. A. (2018). Coping with the impacts of urban heat islands. A literature based study on understanding urban heat vulnerability and the need for resilience in cities in a global climate change context. Journal of Cleaner Production, 171. https://doi.org/10.1016/j.jclepro.2017.10.086.

Lemus-Canovas, M. (2022). Changes in compound monthly precipitation and temperature extremes and their relationship with teleconnection patterns in the Mediterranean. Journal of Hydrology, 608, 127580.

Leonard, M., Westra, S., Phatak, A., Lambert, M., van den Hurk, B., McInnes, K., et al. (2014). A compound event framework for understanding extreme impacts. WIREs Clim. Change 5, 113–128. doi: 10.1002/wcc.252.

Li, J., Wang, Z., Wu, X., Wu, X., Zscheischler, J., Guo, S., & Chen, X. (2021). A standardized index for assessing sub-monthly compound dry and hot conditions with application in China. Hydrology and Earth System Sciences, 25(3), 1587–1601. https://doi.org/10.5194/hess-25-1587-2021.

Libonati, R., Geirinhas, J. L., Silva, P. S., Russo, A., Rodrigues, J. A., Belém, L. B., ... & Trigo, R. M. (2022). Assessing the role of compound drought and heatwave events on unprecedented 2020 wildfires in the Pantanal. Environmental Research Letters, 17(1), 015005.

Lima DC, Lemos G, Bento VA, Nogueira M, Soares PM (2023) A multi-variable constrained ensemble of regional climate projections under multi-scenarios for Portugal-Part I: An overview of impacts on means and extremes. Clim Service 30:100351.

Lionello P, Scarascia L (2018) The relation between climate change in the Mediterranean region and global warming. Reg Environ Change 18:1481–1493. https://doi.org/10.1007/s10113-018-1290-1.

Liu, W., Sun, F., Feng, Y., Li, C., Chen, J., Sang, Y. F., & Zhang, Q. (2021). Increasing population exposure to global warm-season concurrent dry and hot extremes under different warming levels. Environmental Research Letters, 16(9), 094002. https://doi.org/10.1088/17489326/ac188f.

Lorenz, R., Jaeger, E.B. and Seneviratne, S.I. (2010) Persistence of heat waves and its link to soil moisture memory. Geophysical Research Letters, 37(9), L09703. https://doi.org/10.1029/2010GL042764.

Lu Y, Hu H, Li C and Tian F 2018 Increasing compound events of extreme hot and dry days during growing seasons of wheat and maize in China Sci. Rep. 8 16700.

Luterbacher, J., Dietrich, D., Xoplaki, E., Grosjean, M., Wanner, H., 2004. European seasonal and annual temperature variability, trends, and extremes since 1500. Science 303 (5663), 1499–1503.

Manning, C., Widmann, M., Bevacqua, E., Van Loon, A. F., Maraun, D., & Vrac, M. (2019). Increased probability of compound long-duration dry and hot events in Europe during summer (1950–2013). Environmental Research Letters, 14(9), 094006.

Marras, P. A., Lima, D. C., Soares, P. M., Cardoso, R. M., Medas, D., Dore, E., & De Giudici, G. (2021). Future precipitation in a Mediterranean island and streamflow changes for a small basin using EURO-CORDEX regional climate simulations and the SWAT model. Journal of Hydrology, 603, 127025.

Mazdiyasni, O., & AghaKouchak, A. (2015). Substantial increase in concurrent droughts and heatwaves in the United States. Proceedings of the National Academy of Sciences of the United States of America, 112, 11484–11489.

Meng, Y., Hao, Z., Feng, S., Zhang, X., & Hao, F. (2022). Increase in compound dry-warm and wet-warm events under global warming in CMIP6 models. Global and Planetary Change, 210, 103773.

Meng, Y., Hao, Z., Zhang, Y., & Feng, S. (2023). The 2022-like compound dry and hot extreme in the Northern Hemisphere: Extremeness, attribution, and projection. Atmospheric Research, 295, 107009.

Miralles, D. G., Gentine, P., Seneviratne, S. I. & Teuling, A. J. Land–atmospheric feedbacks during droughts and heatwaves: state of the science and current challenges. Ann. N. Y. Acad. Sci. 1436, 19–35 (2019).

Molina, M. O., Sánchez, E., & Gutiérrez, C. (2020). Future heat waves over the Mediterranean from an Euro-CORDEX regional climate model ensemble. Scientific reports, 10(1), 8801.

Mukherjee, S., Mishra, A. K., Mann, M. E., & Raymond, C. (2021). Anthropogenic warming and population growth may double US heat stress by the late 21st century. Earth's Future, 9(5), e2020EF001886.

Mukherjee, I., & Singh, U. K. (2022). Environmental fate and health exposures of the geogenic and anthropogenic contaminants in potable groundwater of Lower Ganga Basin, India. Geoscience Frontiers, 13(3), 101365.

Mueller, B., and Seneviratne, S. I. (2012). Hot days induced by precipitation deficits at the global scale. Proc. Natl. Acad. Sci. U.S.A. 109, 12398–12403. doi: 10.1073/pnas.1204330109.

Müller, L.M., Bahn, M., 2022. Drought legacies and ecosystem responses to subsequent drought. Glob. Chang. Biol. 28, 5086–5103. https://doi.org/10.1111/GCB.16270.

Munich RE (2024). Heatwaves, Drought, and Forest Fires in Europe: Billions of Dollars in Losses for Agricultural Sector. Munich: Munich Re. Accessed on 28 May 2024

NASA Earth Observatory, 2024a. Fires in Greece. https://earthobservatory.nasa.gov/images/39913/fires-in-greece.

NASA Earth Observatory, 2024b. Drought exacerbates Australian fires. https://earthobservatory.nasa.gov/images/145599/drought-exacerbates-australian-fires.

Nguyen, M., Wang, X., & Chen, D. (2010). An investigation of extreme heatwave events and their effects on building & infrastructure. National Research Flagships Climate Adaptation.

Nguyen, T. P. L., Mula, L., Cortignani, R., Seddaiu, G., Dono, G., Virdis, S. G., ... & Roggero, P. P. (2016). Perceptions of present and future climate change impacts on water availability for agricultural systems in the western Mediterranean region. Water, 8(11), 523.

NOAAa – National Oceanic and Atmospheric Administration. North Atlantic Oscillation (NAO). https://www.ncei.noaa.gov/access/monitoring/nao/. Last access at 26/07/2024.

NOAAb – National Oceanic and Atmospheric Administration. Eastern Atlantic (EA). https://www.cpc.ncep.noaa.gov/data/teledoc/ea.shtml. Last access at 26/07/2024.

Olschewski, P., Dieng, M. D. B., Moutahir, H., Böker, B., Haas, E., Kunstmann, H., & Laux, P. (2024). Amplified potential for vegetation stress under climate-change-induced intensifying compound extreme events in the Greater Mediterranean Region. Natural Hazards and Earth System Sciences, 24(4), 1099-1134.

Pascoa, P., Russo, A., Gouveia, C. M., Soares, P. M., Cardoso, R. M., Careto, J. A., & Ribeiro, A. F. (2021). A high-resolution view of the recent drought trends over the Iberian Peninsula. Weather and Climate Extremes, 32, 100320.

Peña-Guerrero, M.D., Nauditt, A., Munoz-Robles, C., Ribbe, L., Meza, F., 2020. Drought impacts on water quality and potential implications for agricultural production in the Maipo River Basin, Central Chile. Hydrol. Sci. J. 65, 1005–1021. https://doi.org/10.1080/02626667.2020.1711911.

Perkins, S. E. & Alexander, L. V. On the measurement of heat waves. J. Clim. 26, 4500–4517 (2013).

Perkins, S. E. (2015). A review on the scientific understanding of heatwaves-Their measurement, driving mechanisms, and changes at the global scale. In Atmospheric Research (Vols. 164–165). https://doi.org/10.1016/j.atmosres.2015.05.014.

Perkins-Kirkpatrick, S. E., Fischer, E. M., Angélil, O., & Gibson, P. B. (2017). The influence of internal climate variability on heatwave frequency trends. Environmental Research Letters, 12(4), 044005.

Perkins-Kirkpatrick, S.E., Lewis, S.C. Increasing trends in regional heatwaves. Nat Commun 11, 3357 (2020). https://doi.org/10.1038/s41467-020-16970-7.

Pyrina, M., Hatzianastassiou, N., Matsoukas, C., Fotiadi, A., Papadimas, C. D., Pavlakis, K. G., & Vardavas, I. (2015). Cloud effects on the solar and thermal radiation budgets of the Mediterranean basin. *Atmospheric Research*, *152*, 14-28.

Philip, S. Y., Kew, S. F., Van Oldenborgh, G. J., Anslow, F. S., Seneviratne, S. I., Vautard, R., ... & Otto, F. E. (2022). Rapid attribution analysis of the extraordinary heat wave on the Pacific coast of the US and Canada in June 2021. Earth System Dynamics, 13(4), 1689-1713.

Ribeiro, A. F. S., Russo, A., Gouveia, C. M., Páscoa, P., & Zscheischler, J. (2020). Risk of crop failure due to compound dry and hot extremes estimated with nested copulas. Biogeosciences, 17(19), 4815–4830. https://doi.org/10.5194/bg-17-4815-2020.

Rillig, M. C., Ryo, M., Lehmann, A., Aguilar-Trigueros, C. A., Buchert, S., Wulf, A., ... & Yang, G. (2019). The role of multiple global change factors in driving soil functions and microbial biodiversity. Science, 366(6467), 886-890.

Roy, T., Martinez, J. A., Herrera-Estrada, J. E., Zhang, Y., Dominguez, F., Berg, A., et al. (2019). Role of moisture transport and recycling incharacterizing droughts: Perspectives from two recent US droughts and the CFSv2 system. Journal of Hydrometeorology, 20, 139–154. https://doi.org/10.1175/JHM-D-18-0159.1.

Ruffault, J., Curt, T., Moron, V., Trigo, R. M., Mouillot, F., Koutsias, N., ... & Belhadj-Khedher, C. (2020). Increased likelihood of heat-induced large wildfires in the Mediterranean Basin. Scientific reports, 10(1), 13790.

Seneviratne, S. I., Nicholls, N., Easterling, D., Goodess, C. M., Kanae, S., Kossin, J., et al. (2012). “Changes in climate extremes and their impacts on the natural physical environment,” in Managing the Risks of Extreme Events and Disasters.

Ramos, A. M., Russo, A., DaCamara, C. C., Nunes, S., Sousa, P., Soares, P. M. M., ... & Trigo, R. M. (2023). The compound event that triggered the destructive fires of October 2017 in Portugal. IScience, 26(3).

Rodriguez-Puebla, C., Encinas, A.H. & Nieto, S. [et al], 1998, “Spatial and temporal patterns of annual precipitation variability over the Iberian Peninsula”, Int. J. Clim., no. 18, pp. 299-316.

Russo A, Gouveia C M, Dutra E, Soares P M M and Trigo R M 2018 The synergy between drought and extremely hot summers in the Mediterranean Environ. Res. Lett. 14 014011.

Russo, S., Sillmann, J., & Fischer, E. M. (2015). Top ten European heatwaves since 1950 and their occurrence in the coming decades. Environmental Research Letters, 10(12), 124003.

Russo, S. & Sterl, A. Global changes in indices describing moderate temperature extremes from the daily output of a climate model. J. Geophys. Res. 116, D03104 (2011).

Samset, B. H., Sand, M., Smith, C. J., Bauer, S. E., Forster, P. M., Fuglestvedt, J. S., ... & Schleussner, C. F. (2018). Climate impacts from a removal of anthropogenic aerosol emissions. Geophysical Research Letters, 45(2), 1020-1029.

Santamouris, M., Cartalis, C., Synnefa, A., & Kolokotsa, D. (2015). On the impact of urban heat island and global warming on the power demand and electricity consumption of buildings—A review. Energy and buildings, 98, 119-124.

Santanello, J. A. et al. Land–Atmosphere Interactions: The LoCo Perspective. Bull. Am. Meteorol. Soc. 99, 1253–1272 (2018). 20.

Seneviratne SI, Lüthi D, Litschi M, Schär C. 22. 2006. Land-atmosphere coupling and climate change in Europe. Nature 443:205–9.

Shiekh, R. H. A., & El-Hashash, E. F. (2022). A comparison of the pearson, spearman rank and kendall tau correlation coefficients using quantitative variables. *Asian Journal of Probability and Statistics*, 36-48.

Spensberger, C., Madonna, E., Boettcher, M., Grams, C.M., Papritz, L., Quinting, J.F., Röthlisberger, M., Sprenger, M. and Zschenderlein, P. (2020) Dynamics of concurrent and sequential Central European and Scandinavian heatwaves. Quarterly Journal of the Royal Meteorological Society, 146(732), 2998–3013. https://doi.org/10.1002/qj.3822.

Soares, P. M., Cardoso, R. M., Lima, D. C., & Miranda, P. M. (2017). Future precipitation in Portugal: high-resolution projections using WRF model and EURO-CORDEX multi-model ensembles. Climate Dynamics, 49, 2503-2530.

Soares, P. M., & Lima, D. C. (2022). Water scarcity down to earth surface in a Mediterranean climate: The extreme future of soil moisture in Portugal. Journal of Hydrology, 615, 128731.

Sutanto, S. J., Vitolo, C., Di Napoli, C., D'Andrea, M., & Van Lanen, H. A. (2020). Heatwaves, droughts, and fires: Exploring compound and cascading dry hazards at the pan-European scale. Environment international, 134, 105276.

Svoboda, M. D., & Fuchs, B. A. (2016). Handbook of drought indicators and indices (Vol. 2). Geneva, Switzerland: World Meteorological Organization.

Tang, T., Shindell, D., Zhang, Y., Voulgarakis, A., Lamarque, J. F., Myhre, G., ... & Samset, B. H. (2020). Response of surface shortwave cloud radiative effect to greenhouse gases and aerosols and its impact on summer maximum temperature. Atmospheric Chemistry and Physics, 20(13), 8251-8266.

Teuling, A. J. (2018). A hot future for European droughts. Nature Climate Change, 8(5), 364-365.

Tomczyk, A. M., & Bednorz, E. (2016). Heat waves in Central Europe and their circulation conditions. International Journal of Climatology, 36(2), 770-782.

Toniazzo, T., & Scaife, A. A. (2006). The influence of ENSO on winter North Atlantic climate. *Geophysical Research Letters*, *33*(24).

Trigo IF. 2006. Climatology and Interannual Variability of StormTracks in the Euro-Atlantic sector: a comparison between ERA-40 and NCEP/NCAR Reanalyses. Climate Dynamics 26: 127–143.

Tripathy, K. P., & Mishra, A. K. (2023). How unusual is the 2022 European compound drought and heatwave event? Geophysical Research Letters, 50, e2023GL105453. https://doi.org/10.1029/2023GL105453.

Tripathy, K. P., Mukherjee, S., Mishra, A. K., Mann, M. E., & Williams, A. P. (2023). Climate change will accelerate the high-end risk of compound drought and heatwave events. Proceedings of the National Academy of Sciences, 120(28), e2219825120.

Trnka, M., Balek, J., Zahradníček, P., Eitzinger, J., Formayer, H., Turňa, M., ... & Brázdil, R. (2016). Drought trends over part of Central Europe between 1961 and 2014. Climate Research, 70(2-3), 143-160.

Turco, M., Jerez, S., Augusto, S., Tarín-Carrasco, P., Ratola, N., Jiménez-Guerrero, P., Trigo, R.M., 2019. Climate drivers of the 2017 devastating fires in Portugal. https://doi.org/10.1038/s41598-019-50281-2.

NCARa – National Center for Atmospheric Research. Atlantic Multidecadal Oscillation (AMO). https://climatedataguide.ucar.edu/climate-data/atlantic-multi-decadal-oscillation-amo. Last access at 26/07/2024.

NCARb – National Center for Atmospheric Research. Niño 3.4 Index (N3.4). https://climatedataguide.ucar.edu/climate-data/nino-sst-indices-nino-12-3-34-4-oni-and-tni. Last access at 26/07/2024.

van den Hurk, B., Doblas-Reyes, F., Balsamo, G., Koster, R. D., Seneviratne, S. I., & Camargo, H. (2012). Soil moisture effects on seasonal temperature and precipitation forecast scores in Europe. Climate dynamics, 38, 349-362.

Vicente-Serrano, S. M., Beguería, S. & López-Moreno, J. I. A multiscalar drought index sensitive to global warming: the standardized precipitation evapotranspiration index. J. Clim. 23, 1696–1718 (2010).

Vicente-Serrano, S.M., Lopez-Moreno, J.I., Gimeno, L., Nieto, R., Morán-Tejeda, E., Lorenzo-Lacruz, J., Beguería, S., Azorin-Molina, C., 2011. A multiscalar global evaluation of the impact of ENSO on droughts. J. Geophys. Res.-Atmos. 116 https://doi.org/10.1029/2011JD016039.

Vicente-Serrano, S. M., Domínguez-Castro, F., Murphy, C., Hannaford, J., Reig, F., Peña-Angulo, D., ... & El Kenawy, A. (2021). Long-term variability and trends in meteorological droughts in Western Europe (1851–2018). International journal of climatology, 41, E690-E717.

Wang, Z., Yang, S., Lau, N. C., & Duan, A. (2018). Teleconnection between summer NAO and East China rainfall variations: A bridge effect of the Tibetan Plateau. Journal of Climate, 31(16), 6433-6444.

Wang, R., Lü, G., Ning, L., Yuan, L., & Li, L. (2021). Likelihood of compound dry and hot extremes increased with stronger dependence during warm seasons. Atmospheric Research, 260, 105692.

Wirth, V., Riemer, M., Chang, E.K.M. and Martius, O. (2018) Rossby-wave packets on the midlatitude waveguide – a review. Monthly Weather Review, 146(7), 1965–2001. https://doi.org/10.1175/MWR-D-16-0483.1.

Wobus, C., Zarakas, C., Malek, P., Sanderson, B., Crimmins, A., Kolian, M., ... & Weaver, C. P. (2018). Reframing future risks of extreme heat in the United States. Earth's future, 6(9), 1323-1335.

Wu, X., Hao, Z., Tang, Q., Zhang, X., Feng, S., & Hao, F. (2021). Population exposure to compound dry and hot events in China under 1.5 and 2°C global warming. International Journal of Climatology, 41(12), 5766–5775. https://doi.org/10.1002/joc.7152.

Wu, X., Hao, Z., Hao, F., Zhang, X., Singh, V. P., & Sun, C. (2021). Influence of large-scale circulation patterns on compound dry and hot events in China. Journal of Geophysical Research: Atmospheres, 126(4), e2020JD033918.

Wu, X., & Jiang, D. (2022). Probabilistic impacts of compound dry and hot events on global gross primary production. Environmental Research Letters, 17(3), 034049.

Xu, P., Wang, L., Liu, Y., Chen, W. and Huang, P. (2020) The record-breaking heat wave of June 2019 in Central Europe. Atmospheric Science Letters, 21(4), e964. https://doi.org/10.1002/asl.964.

Zhang X, Hegerl G, Zwiers FW, Kenyon J (2005) Avoiding Inhomogeneity in Percentile-Based Indices of Temperature Extremes. Journal of Climate 18(11), 1641–1651. doi:10.1175/jcli3366.1

Zhang X, Alexander L, Hegerl G C, Jones P, Tank A K, Peterson T C, Trewin B and Zwiers F W 2011 Indices for monitoring changes in extremes based on daily temperature and precipitation data Wires Clim. Change 2 851–70.

Zhang, Y., Hao, Z., Zhang, X., & Hao, F. (2022). Anthropogenically forced increases in compound dry and hot events at the global and continental scales. Environmental Research Letters, 17(2), 024018.

Zhou, P., Liu, Z., & Cheng, L. (2020). An alternative approach for quantitatively estimating climate variability over China under the effects of ENSO events. Atmospheric research, 238, 104897.

Zhou, S. et al. Soil moisture–atmosphere feedbacks mitigate declining water availability in drylands. Nat. Clim. Chang. 11, 38–44 (2021).

Zscheischler, J. & Seneviratne, S. I. Dependence of drivers affects risks associated with compound events. Sci. Adv. 3, e1700263 (2017).

Zscheischler, J., Westra, S., van den Hurk, B. J. J. M., Seneviratne, S. I., Ward, P. J., Pitman, A., et al. (2018). Future climate risk from compound events. Nat. Clim. Change 8, 469–477. doi: 10.1038/s41558-018-0156-3.

Supplementary material

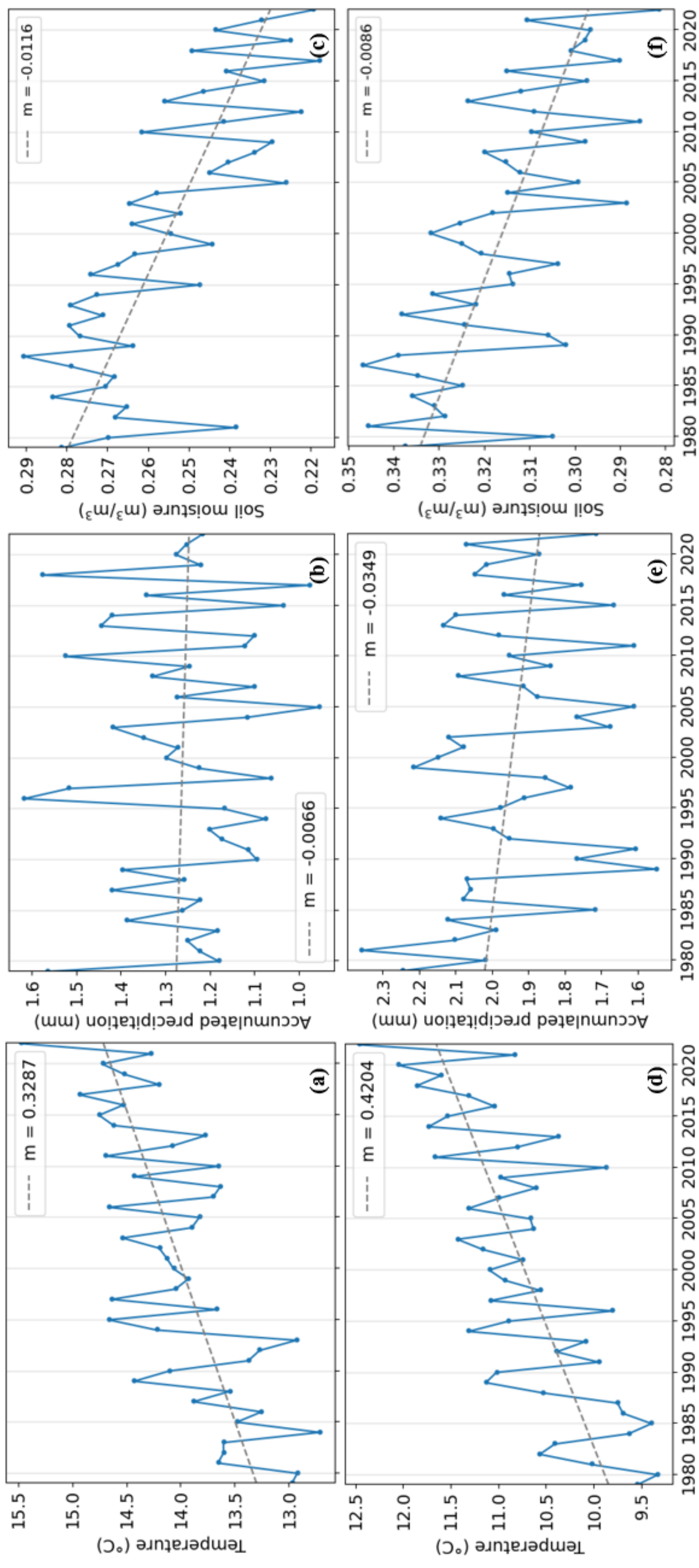

Figure S1: Time series of mean temperature (a and d), accumulated precipitation (b and e) and soil moisture (c and f) accompanied by decadal trend values, The first line corresponds to Iberia and the second line correspond to France.

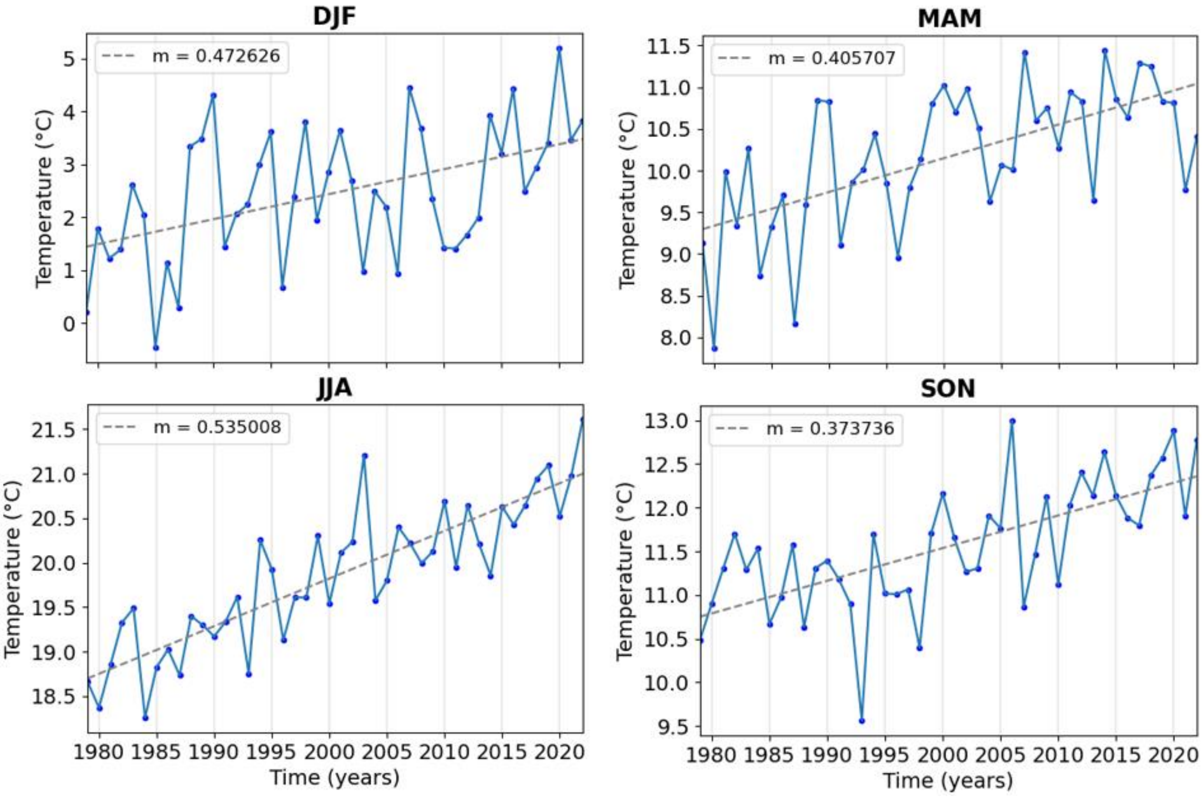

Figure S2: Seasonal mean temperature with decadal trend, considering Europe.

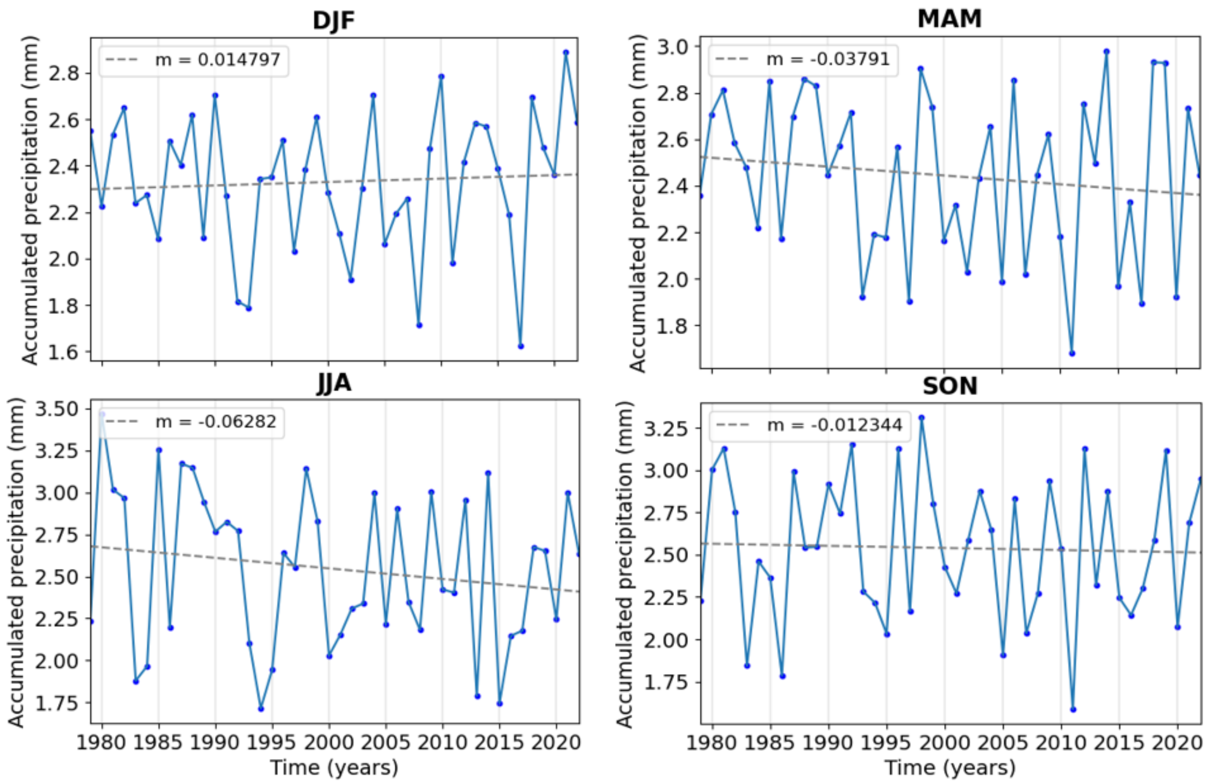

Figure S3: Seasonal mean accumulated precipitation with decadal trend, considering Europe.

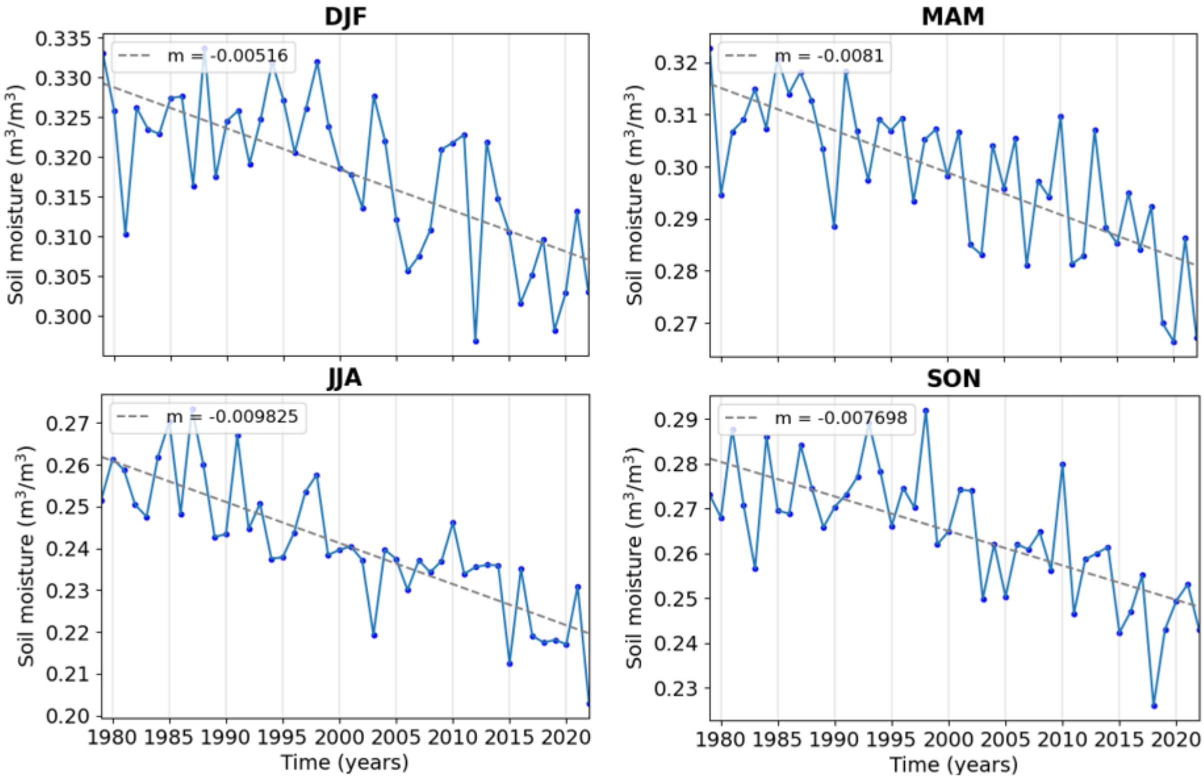

Figure S4: Seasonal mean soil moisture with decadal trend, considering Europe.

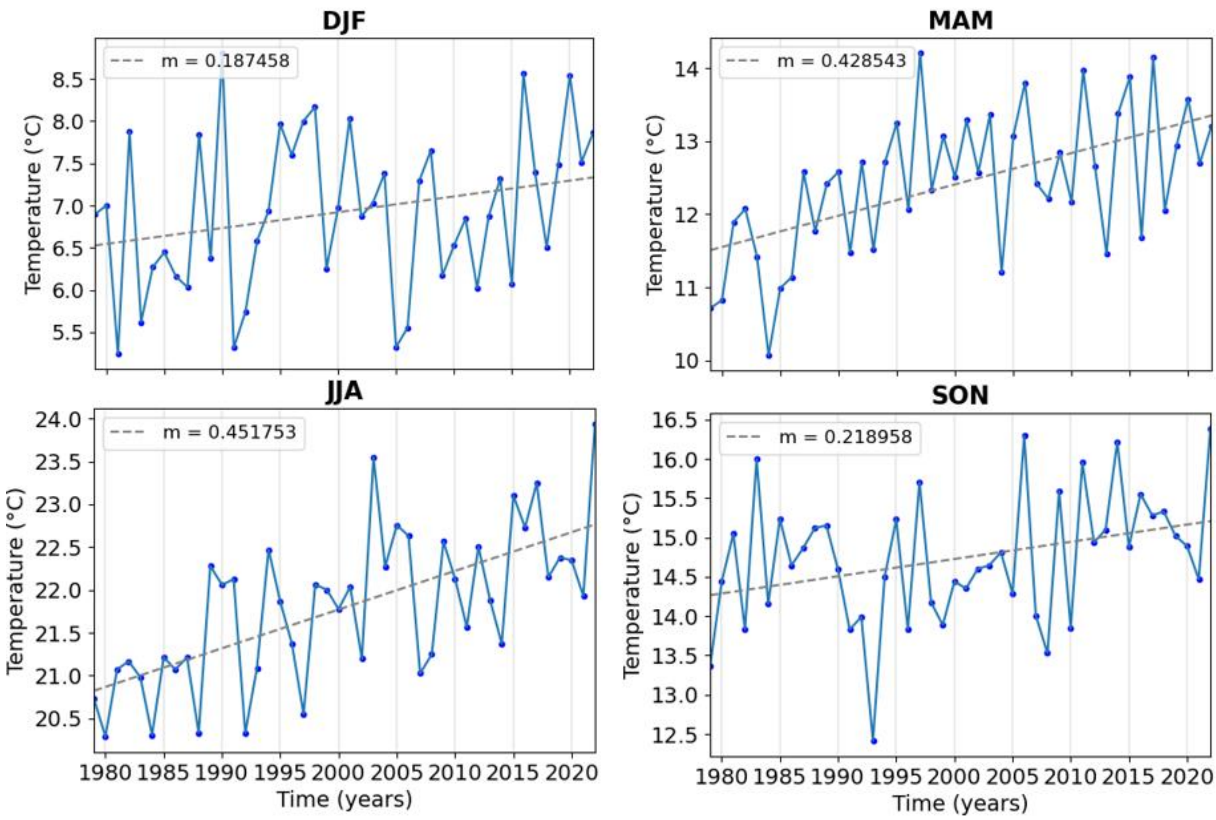

Figure S5: As in Fig. S2, but considering Iberia.

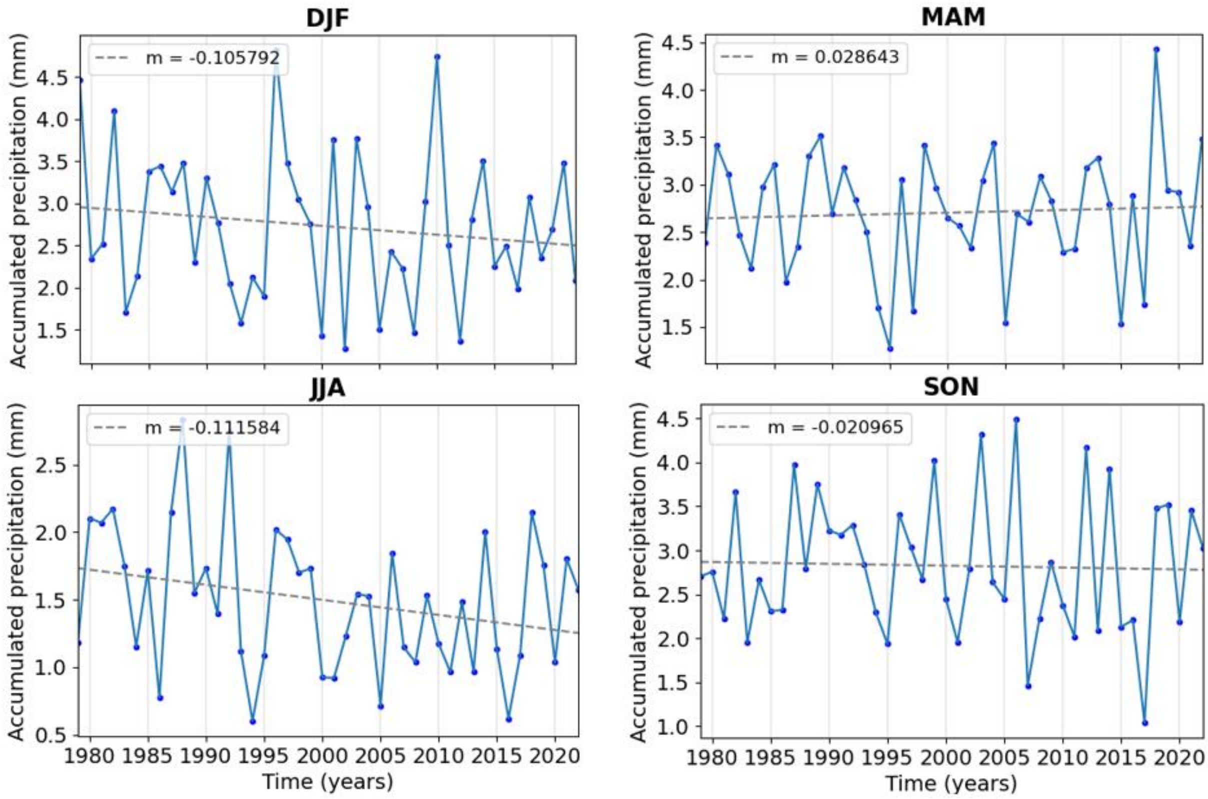

Figure S6: As in Fig. S3, but considering Iberia.

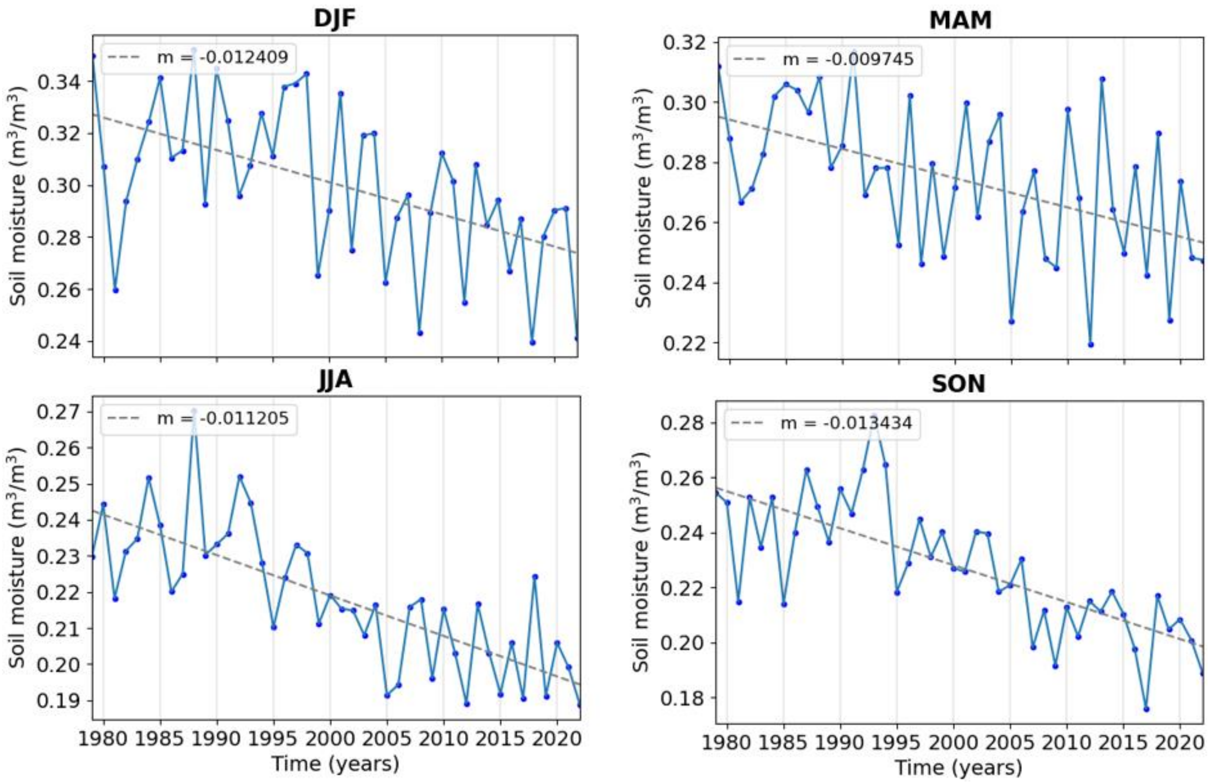

Figure S7: As in Fig. S4, but considering Iberia.

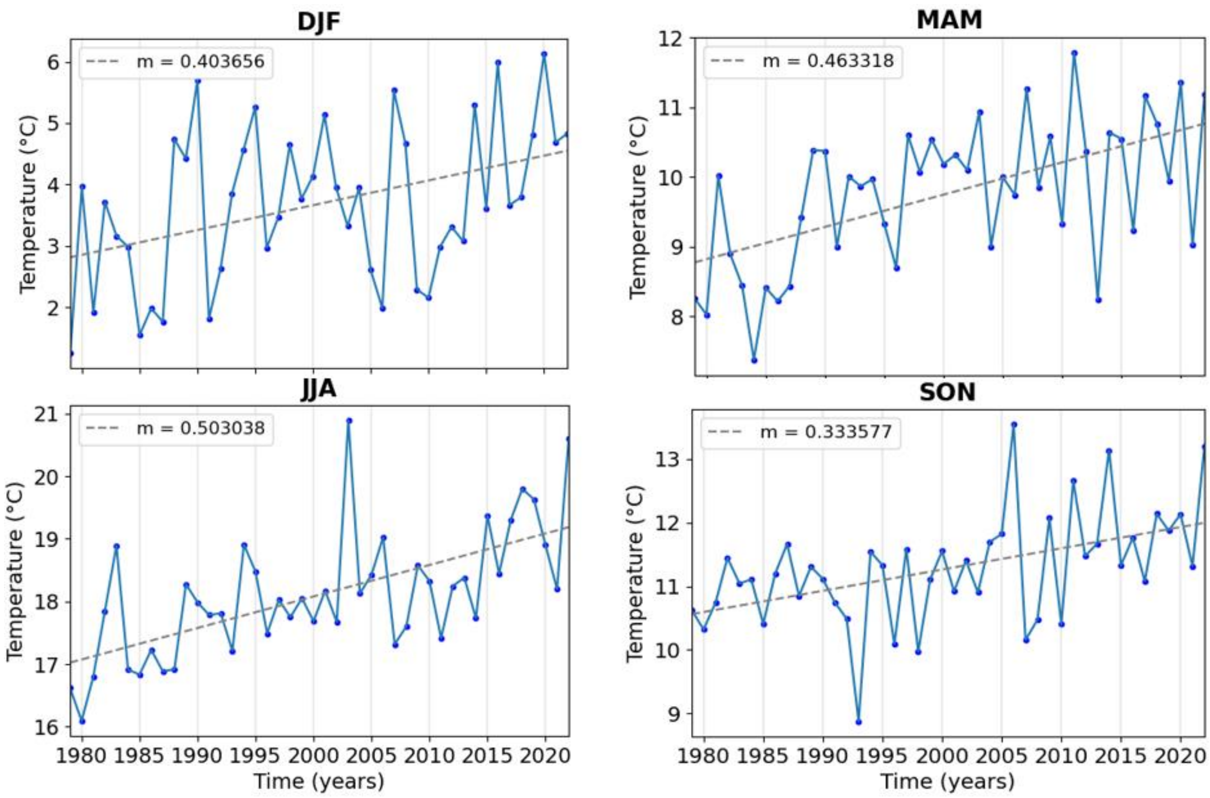

Figure S8: As in Fig. S2, but considering France.

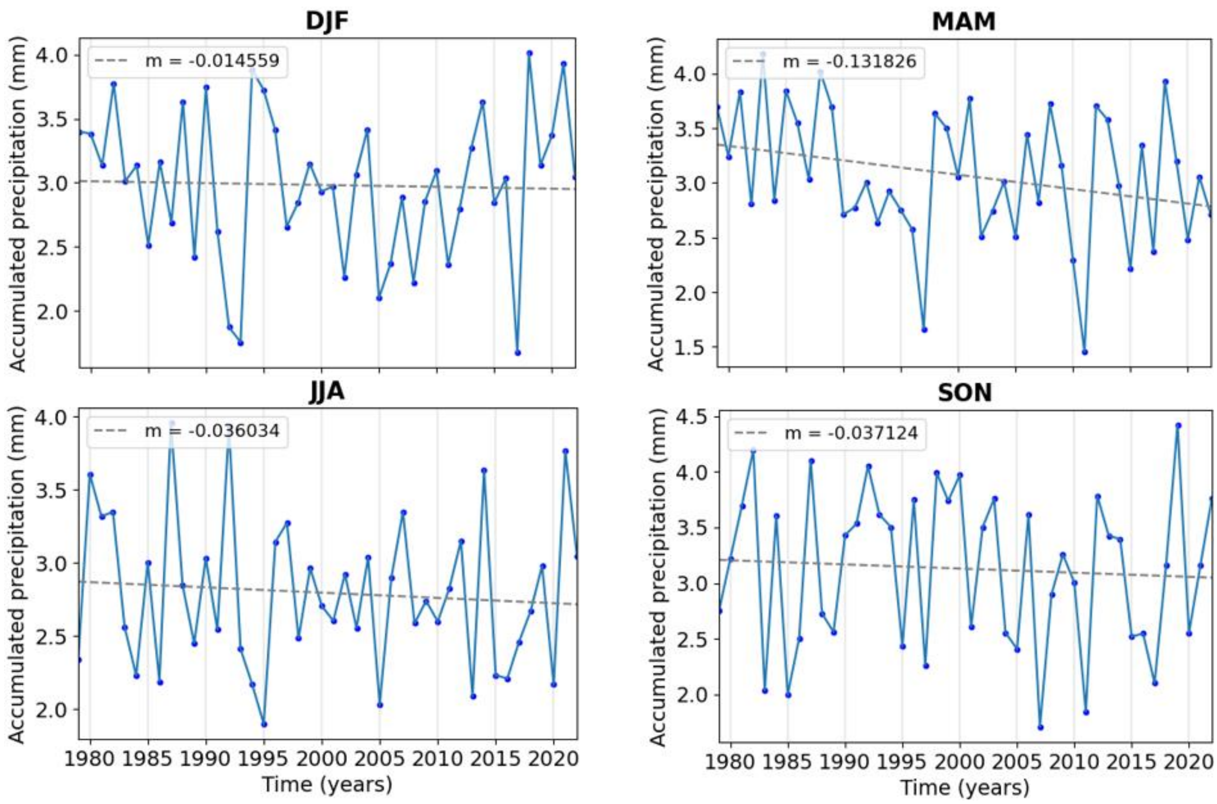

Figure S9: As in Fig. S3, but considering France.

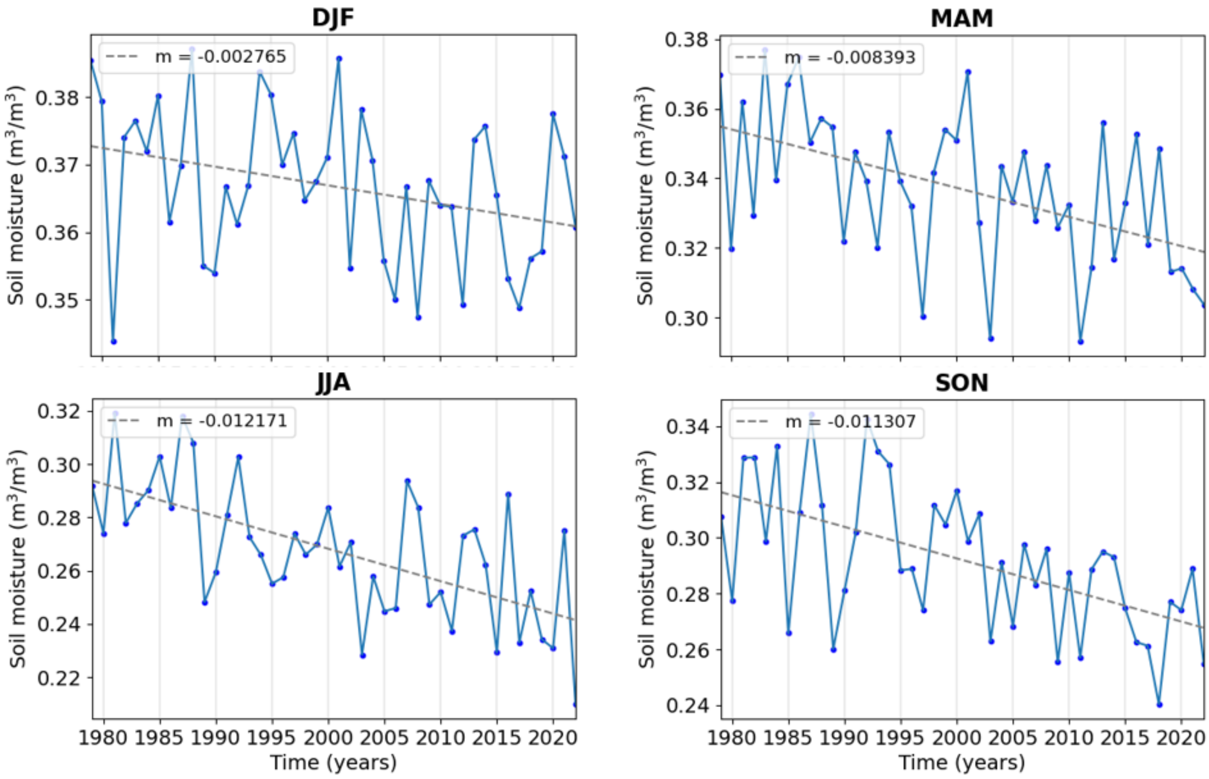

Figure S10: As in Fig. S4, but considering France.

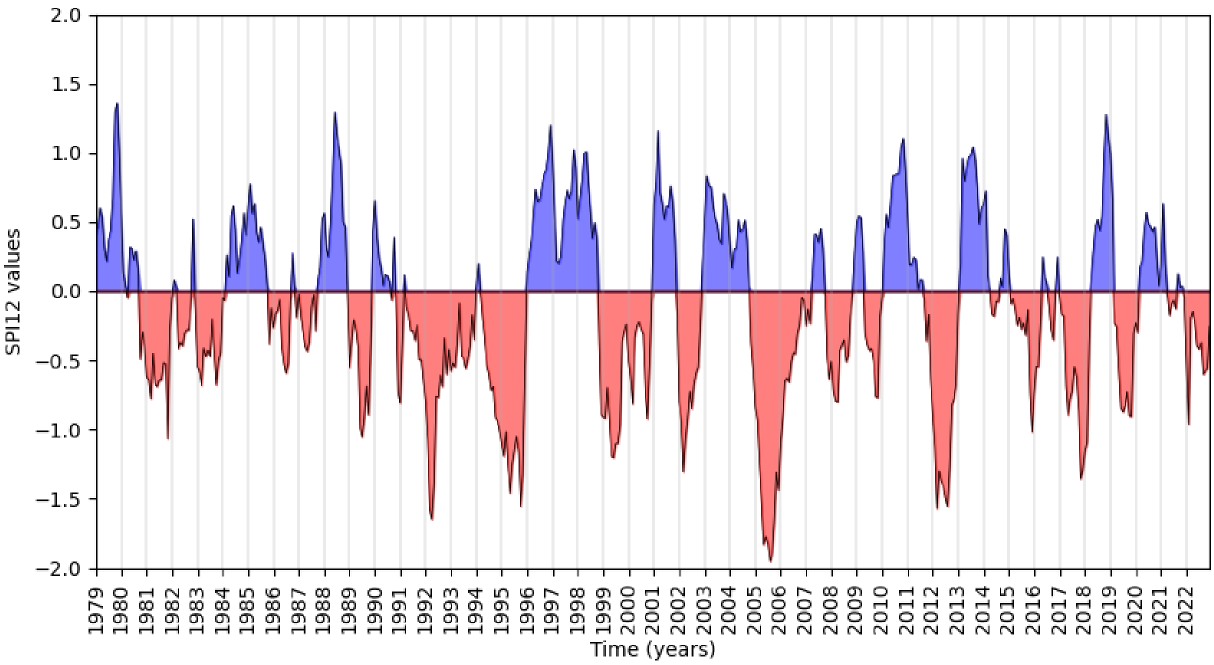

Figure S11: As in Fig. 7, but considering Iberia.

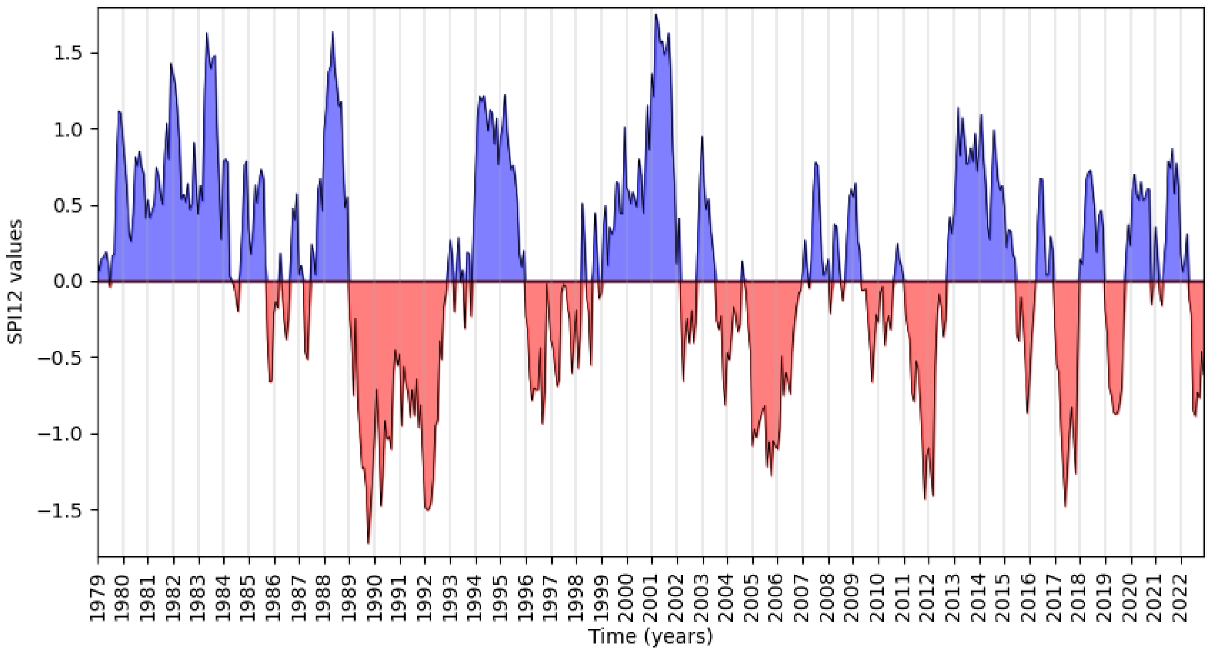

Figure S12: As in Fig. 7, but considering France.

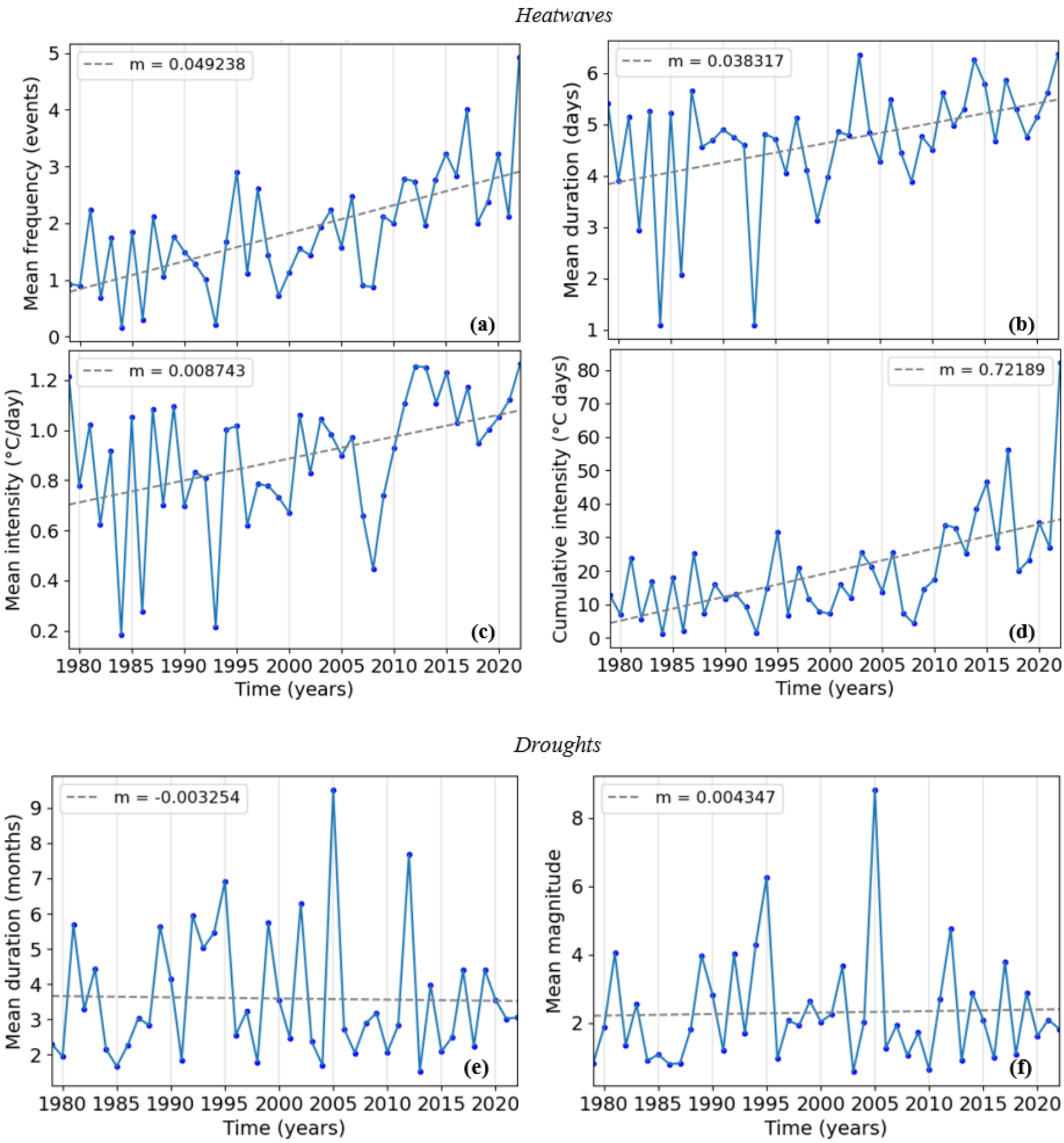

Figure S13: As in Figs. 8 and 9, but considering Iberia.

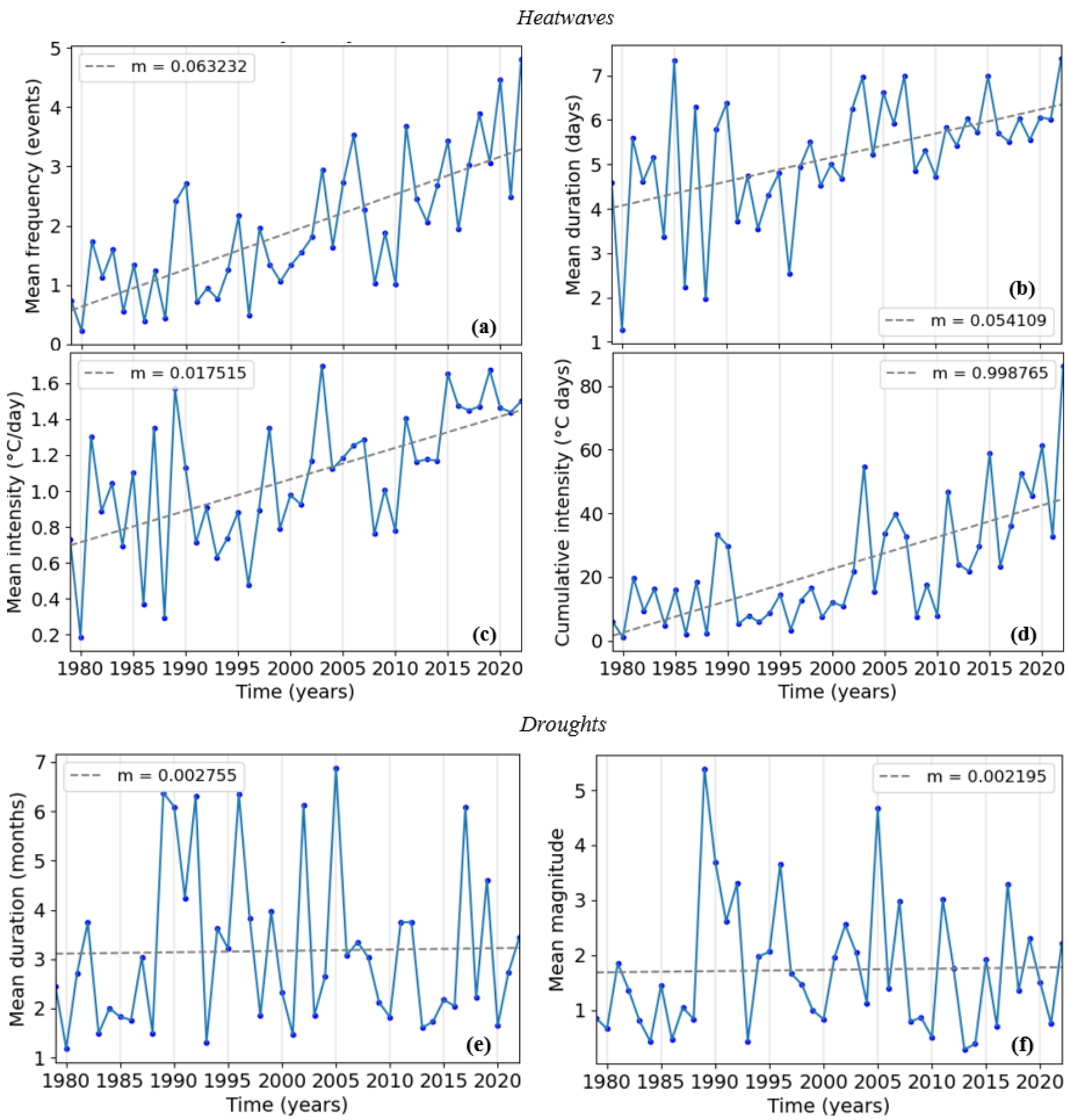

Figure S14: As in Figs. 8 and 9, but considering France.

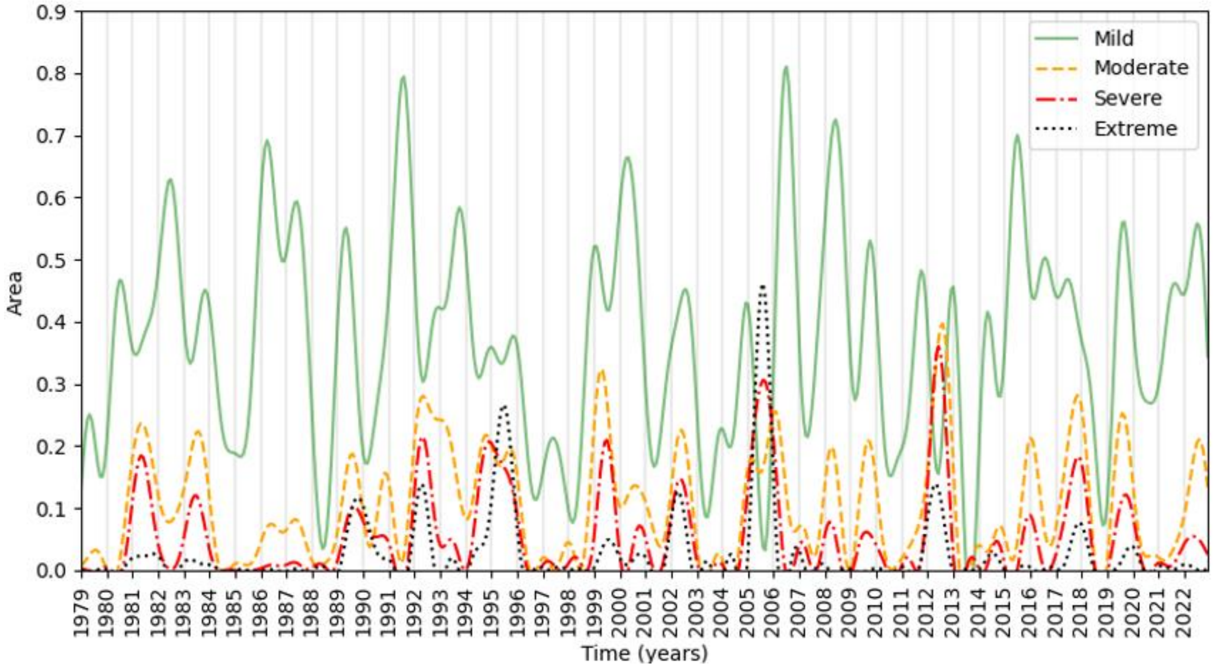

Figure S15: As in Fig. 10, but considering Iberia.

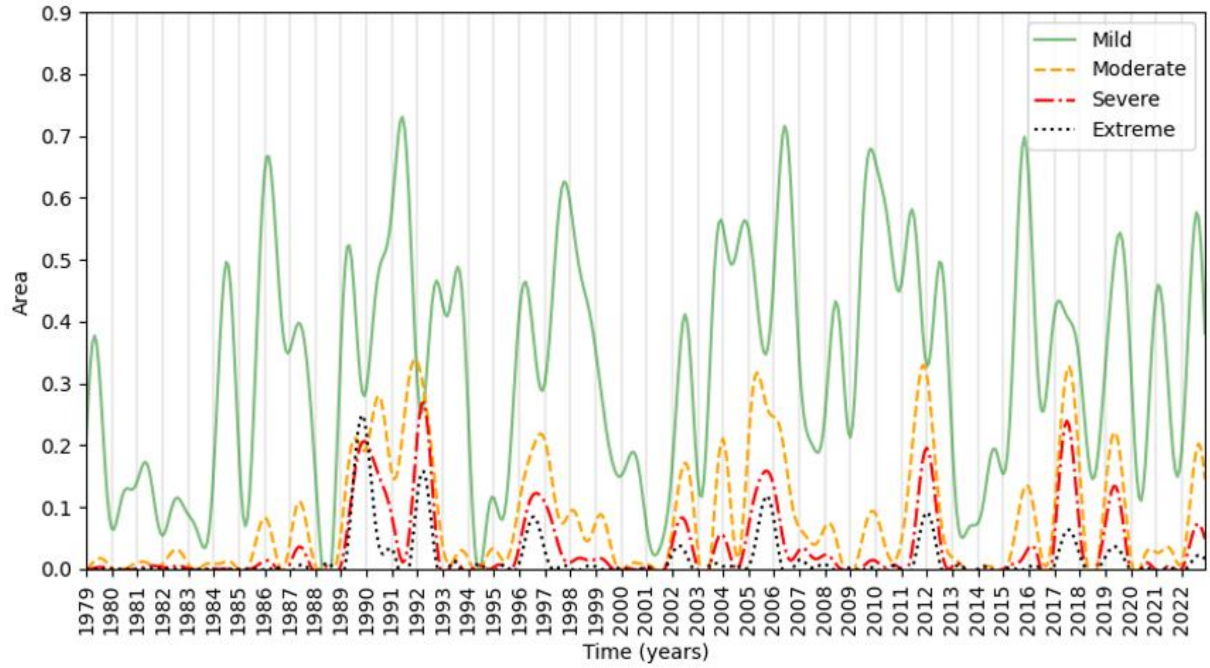

Figure S16: As in Fig. 10, but considering France.

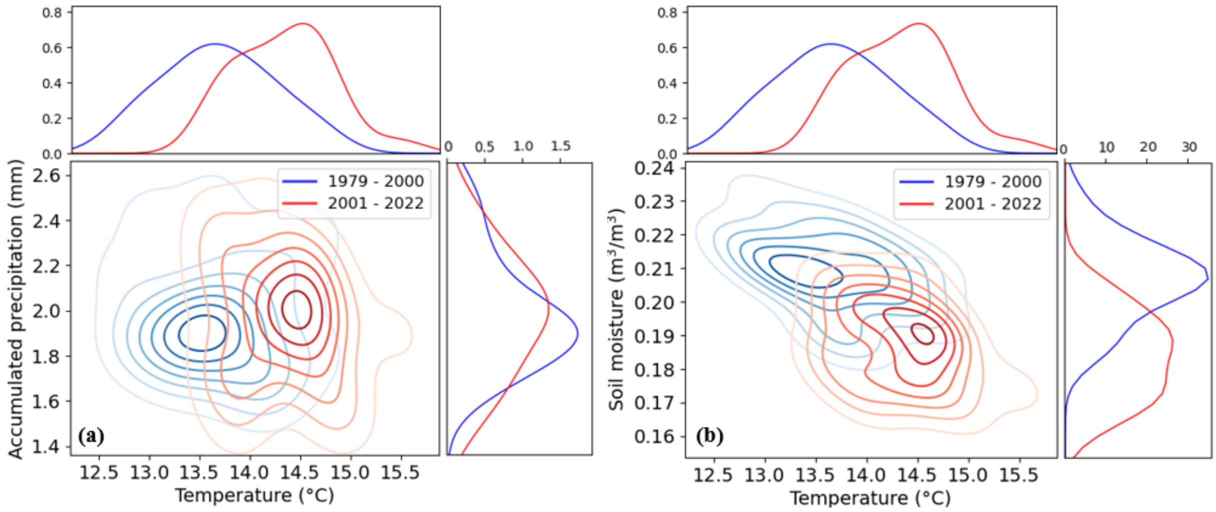

Figure S17: As in Fig. 11, but considering Iberia.

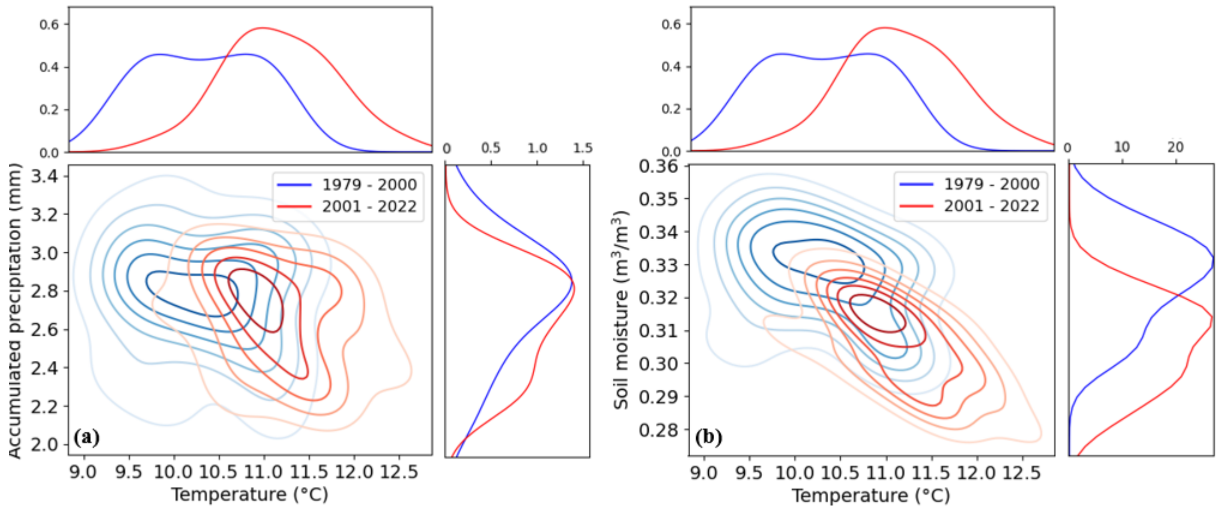

Figure S18: As in Fig. 11, but considering France.

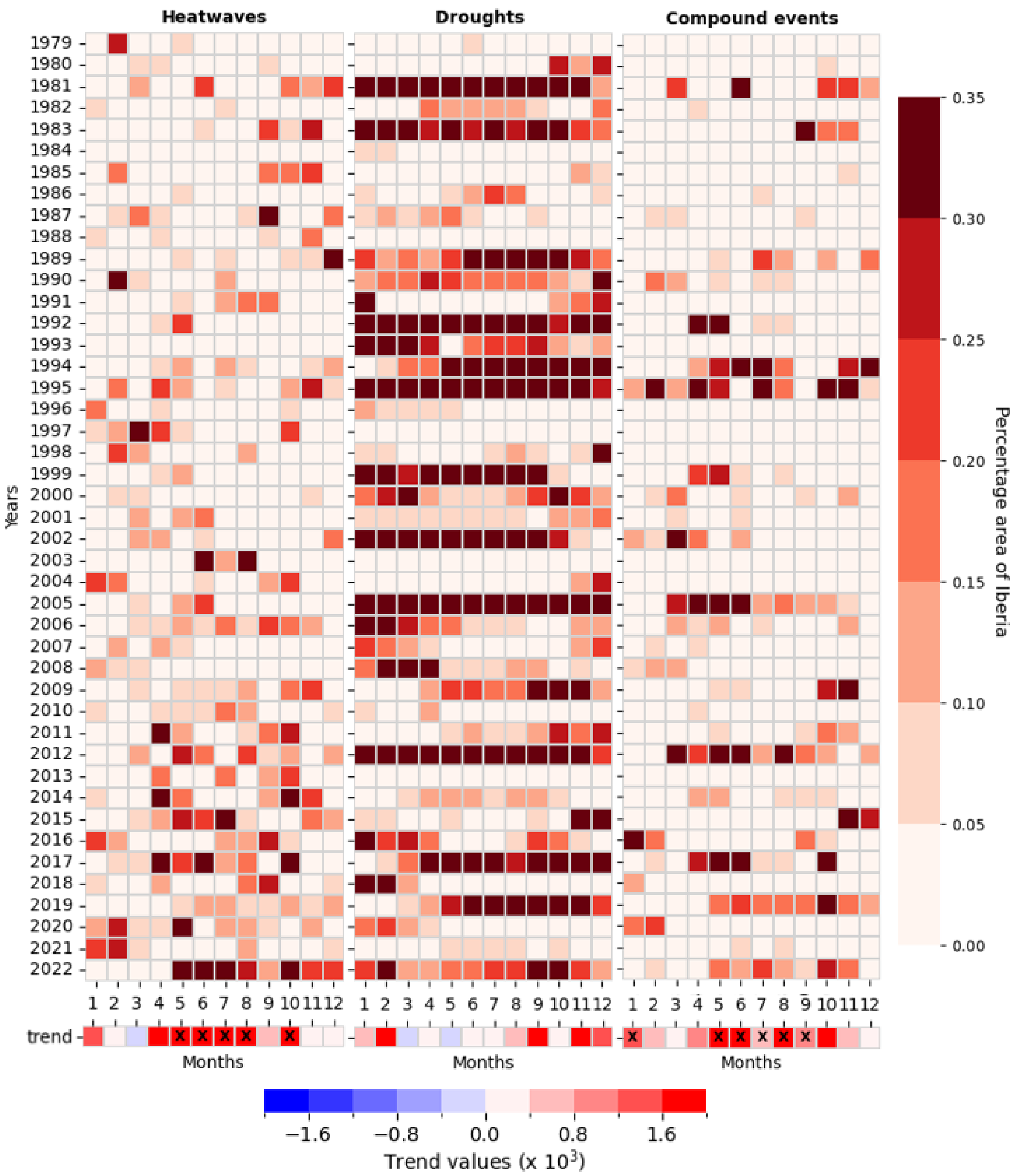

Figure S19: As in Fig. 12, but considering Iberia.

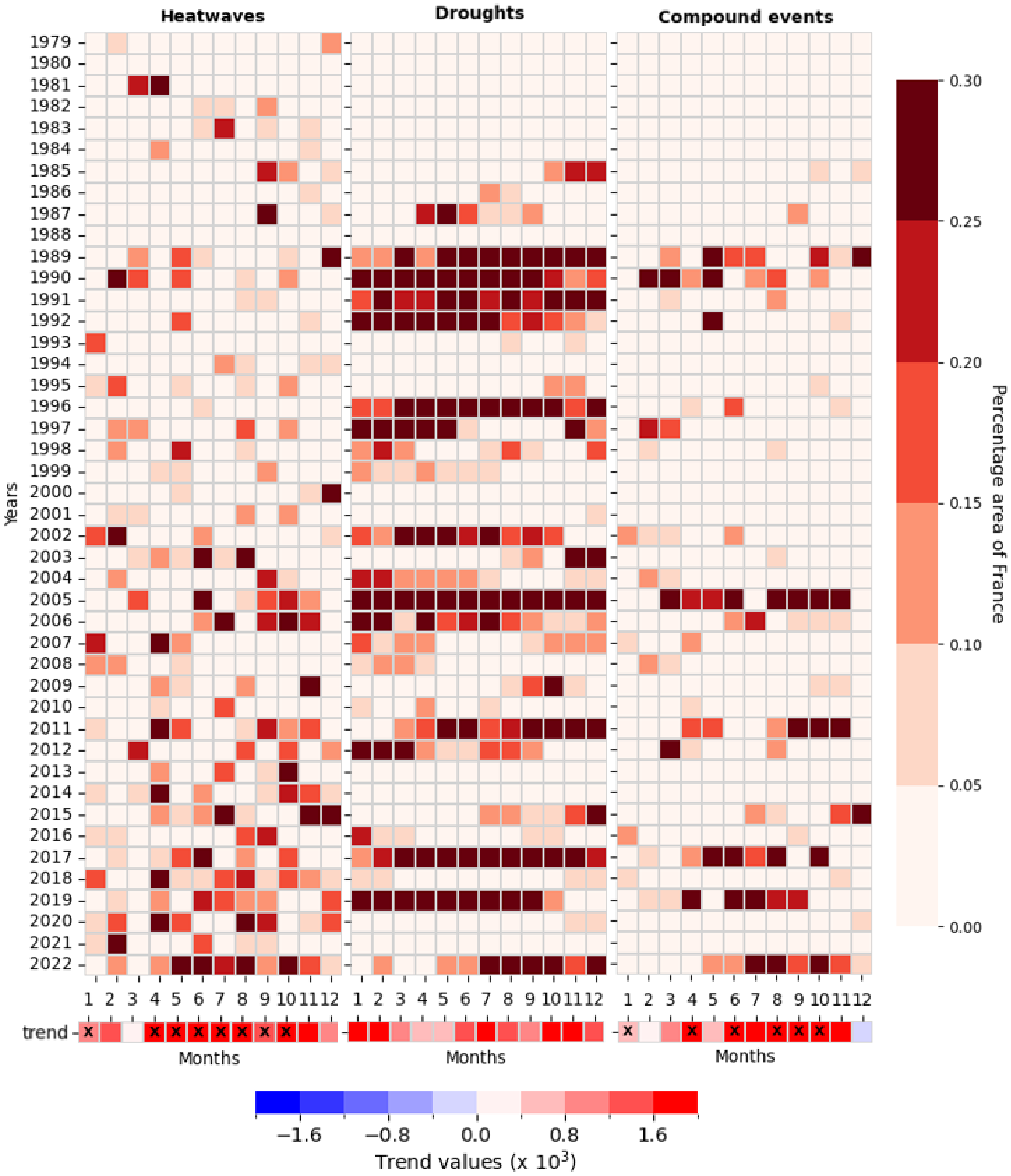

Figure S20: As in Fig. 12, but considering France.

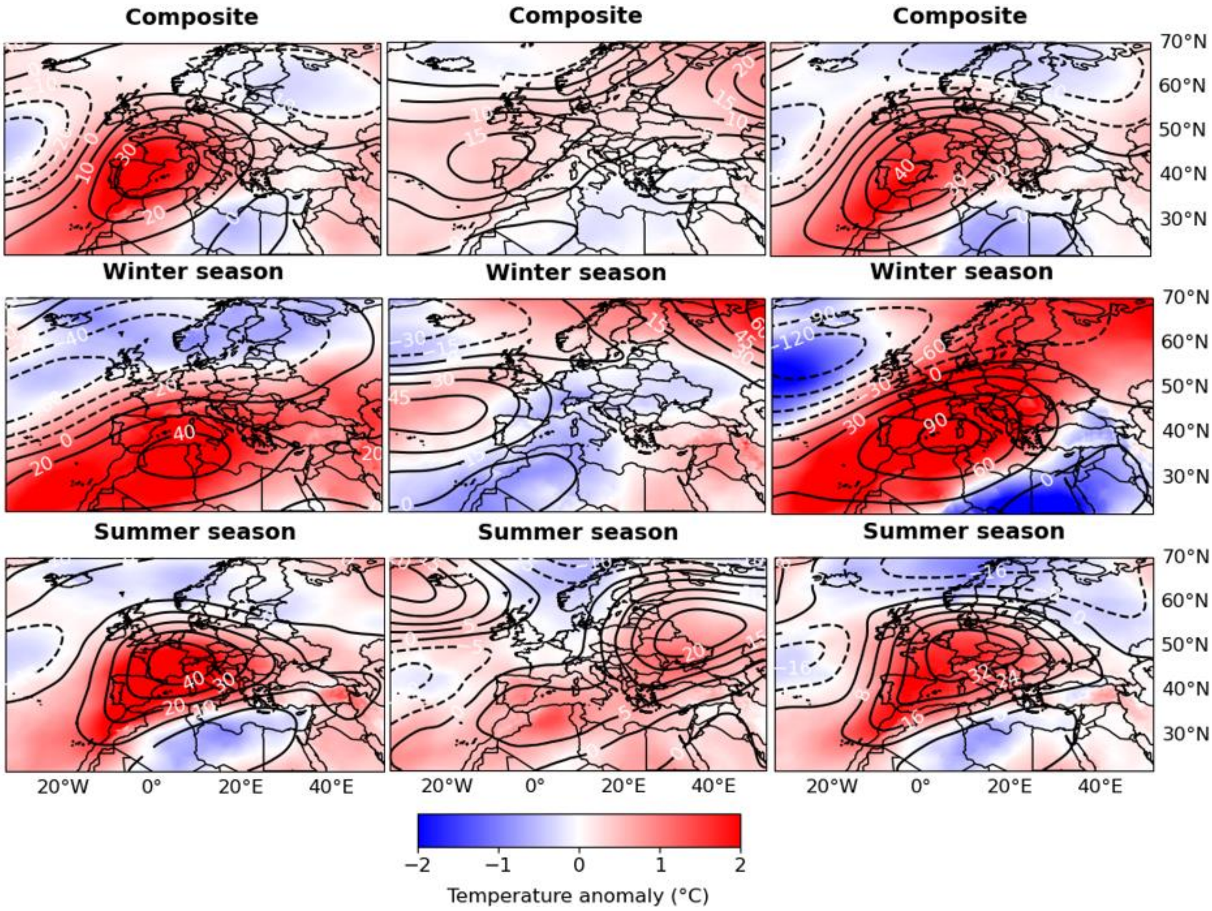

Figure S21: As in Fig. 13, but considering Iberia.

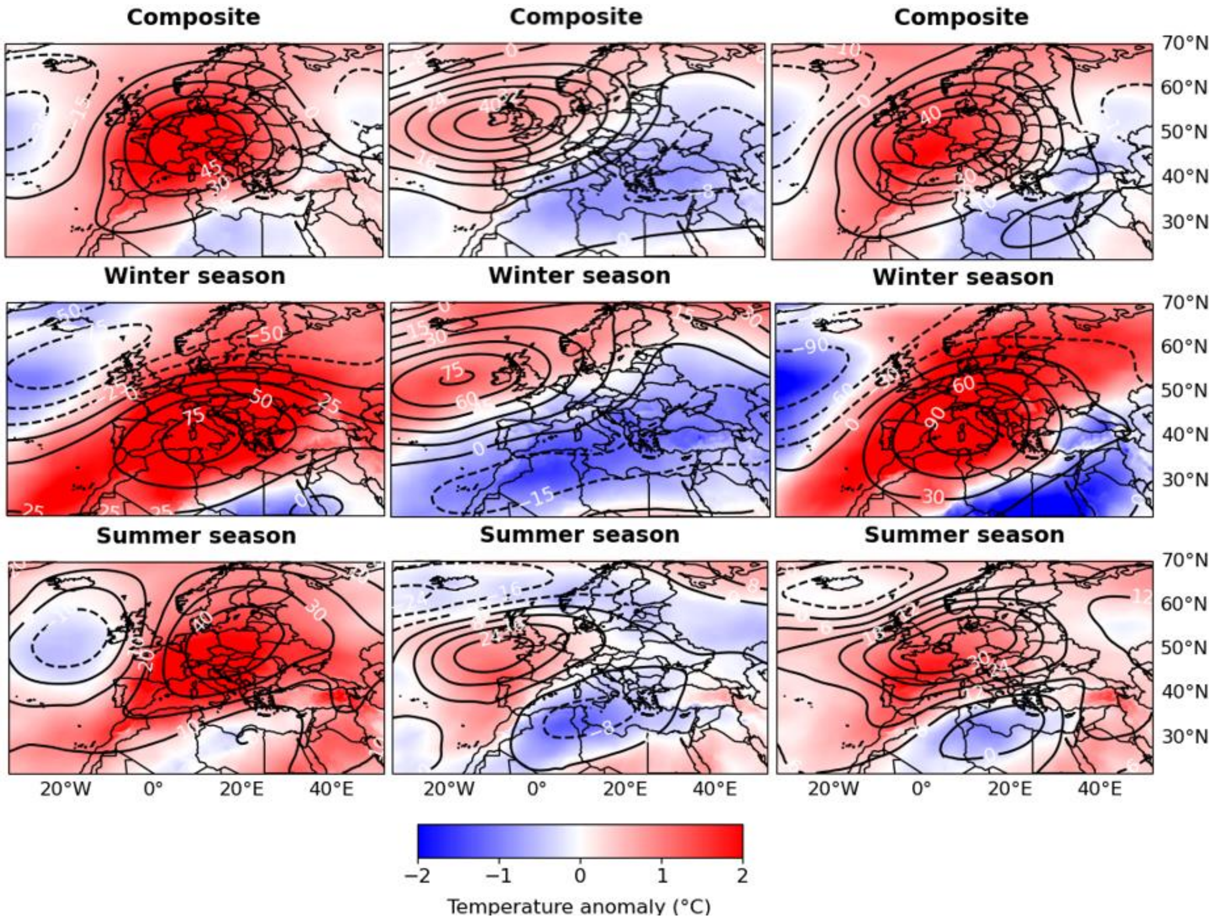

Figure S22: As in Fig. 13, but considering France.

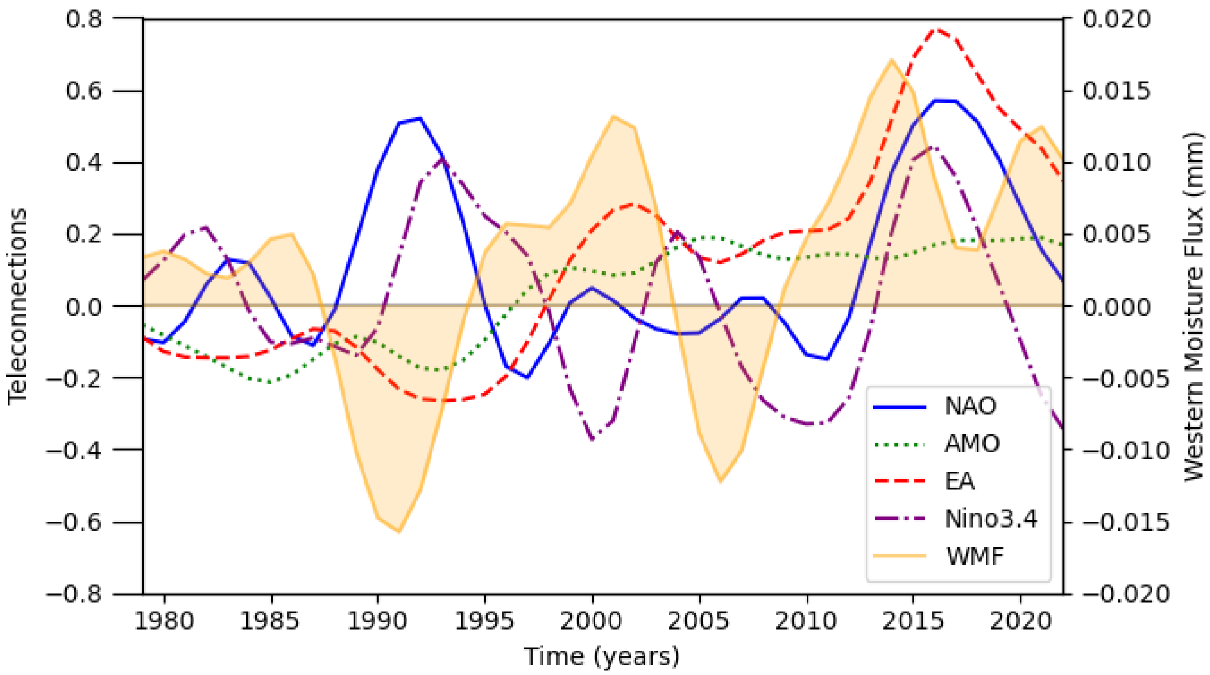

Figure S23: As in Fig. 14, but considering Iberia.

Table S1: As in Table 1, but considering Iberia.

	NAO+	*AMO*	*N3.4*	*EA*		*NAO+*	*AMO*	*N3.4*	*EA*
January	0.12	0.11	0.14	**0.56**	July	-0.13	0.11	-0.03	0.19
February	**0.39**	-0.18	0.07	**0.68**	August	-0.11	0.05	0.12	0.29
March	-0.01	0.14	-0.10	0.10	September	-0.04	0.06	-0.09	0.09
April	**-0.51**	0.04	0.08	**0.67**	October	**-0.40**	0.27	0.25	0.27
May	-0.22	0	0.02	**0.45**	November	-0.06	-0.16	**0.33**	**0.56**
June	**0.51**	0.14	0.29	0.20	December	0	0	0.14	**0.56**
Annual	-0.12	0.07	0.12	**0.39**	Annual (filt.)	-0.15	**0.37**	-0.16	**0.56**
DJF	0.18	-0.01	0.12	**0.59**	JJA	0.04	-0.11	0.13	**0.23**
MAM	-0.24	0.07	-0.02	**0.38**	SON	-0.14	**-0.19**	**0.21**	**0.28**

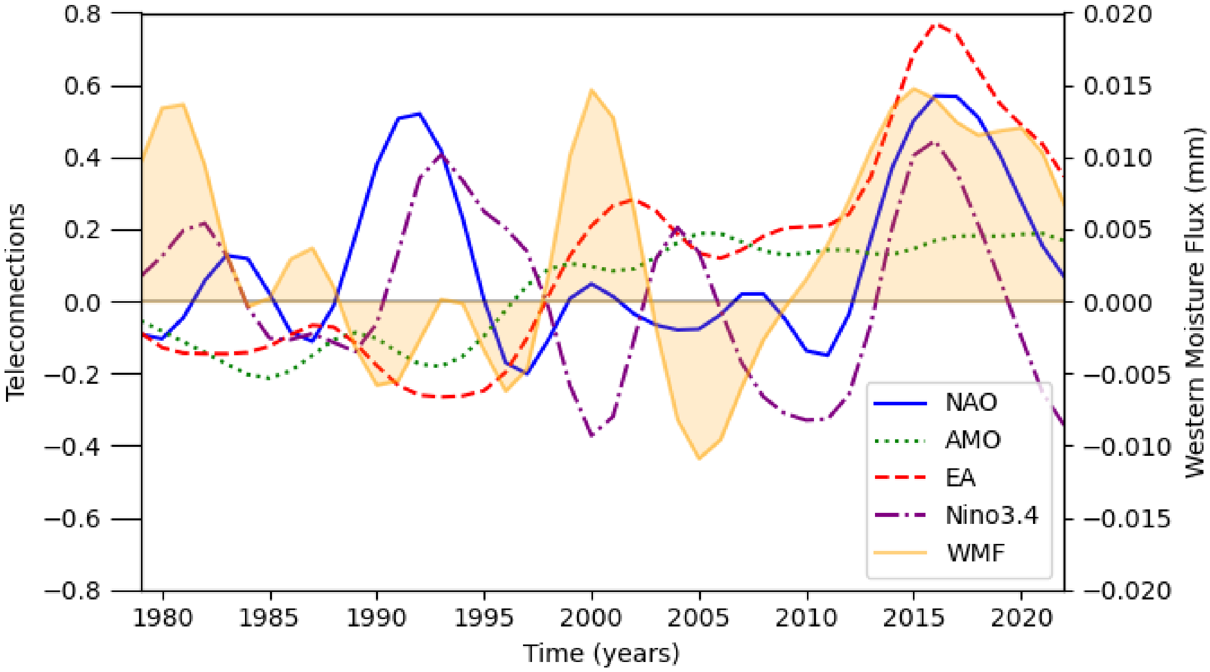

Figure S24: As in Fig. 14, but considering France.

Table S2: As in Table 1, but considering France.

	NAO+	*AMO*	*N3.4*	*EA*		*NAO+*	*AMO*	*N3.4*	*EA*
January	**0.45**	0.07	0.14	**0.44**	July	0.07	0.23	-0.05	**0.32**
February	**0.73**	0.20	0.02	**0.69**	August	0.29	0.02	0.06	**0.52**
March	**0.56**	-0.17	0.06	0.08	September	0.06	-0.08	-0.28	**0.40**
April	**-0.48**	-0.15	0.09	**0.62**	October	0.04	0.05	-0.03	**0.53**
May	-0.01	0.09	-0.05	**0.71**	November	0.35	-0.15	**0.44**	**0.82**
June	0.64	0.13	0.23	**0.38**	December	0.31	-0.17	0.20	**0.51**
Annual	0.17	0.03	0.11	**0.38**	Annual (filt.)	0.17	0.21	-0.01	**0.55**
DJF	**0.50**	0.03	0.12	**0.54**	JJA	0.27	0.13	0.07	**0.42**
MAM	0.19	-0.07	0.03	**0.45**	SON	0.17	-0.07	0.09	**0.54**

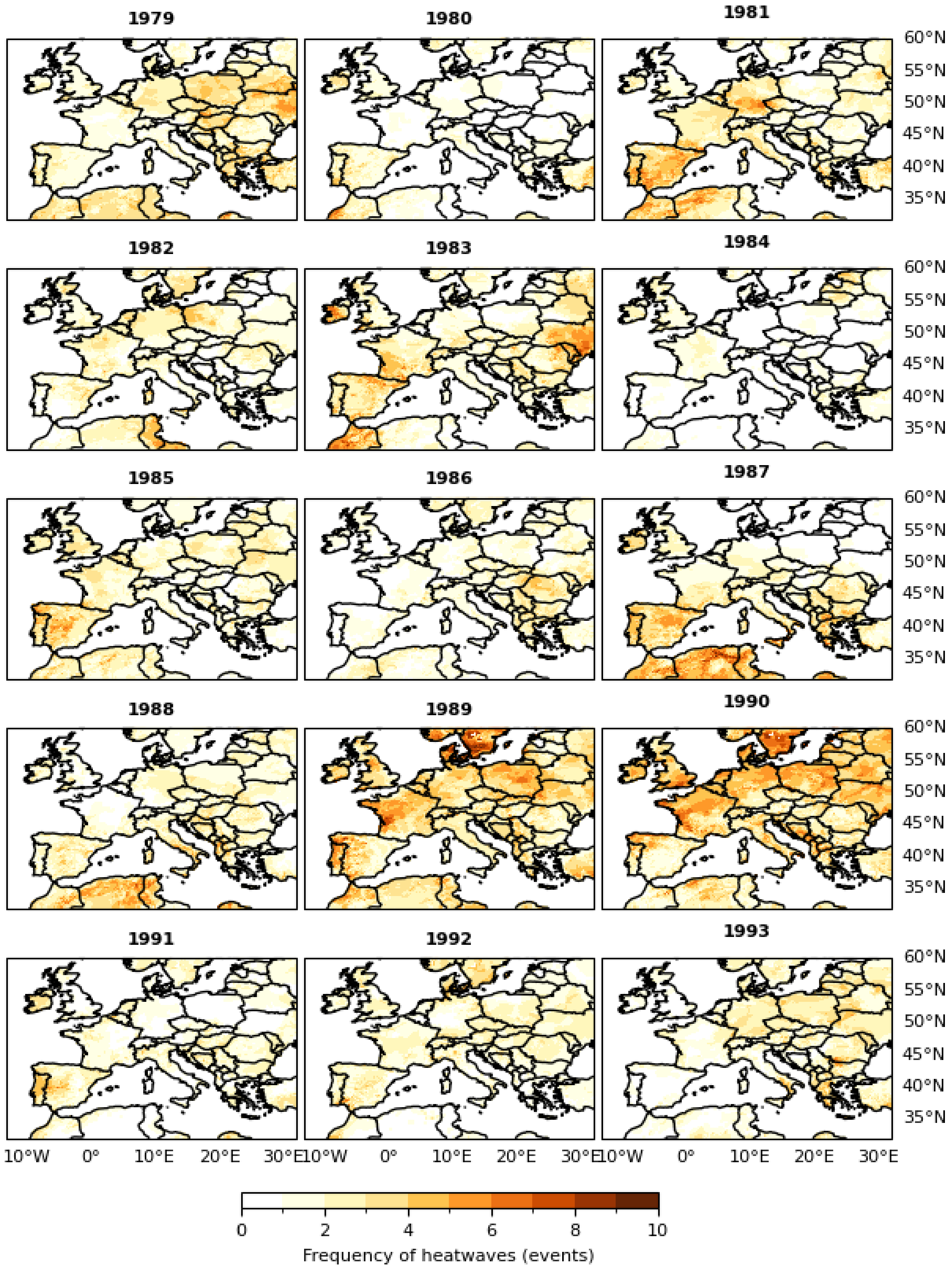

Figure S25: Annual spatial frequency of heatwaves between 1979 and 1993.

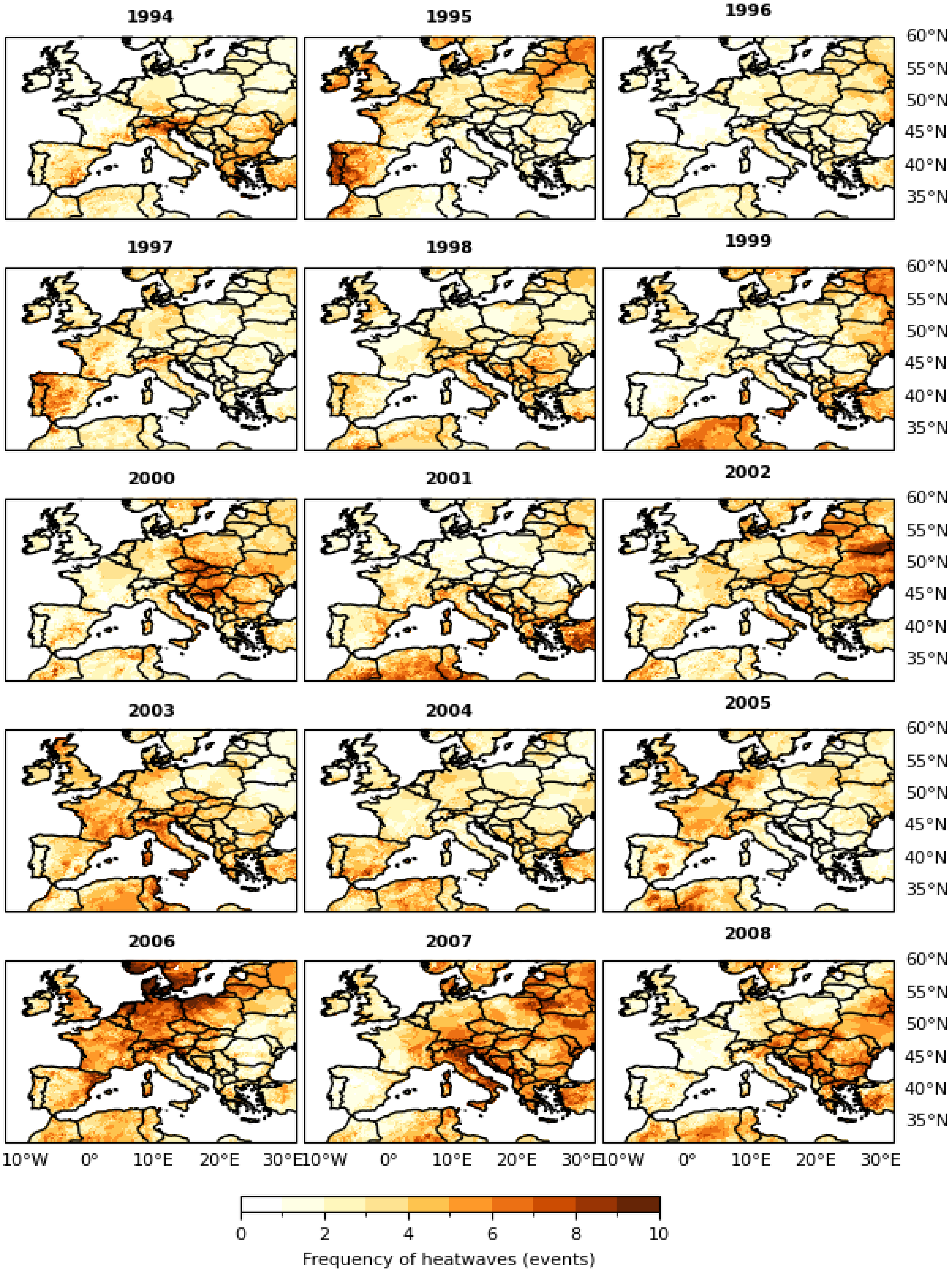

Figure S26: Annual spatial frequency of heatwaves between 1994 and 2008.

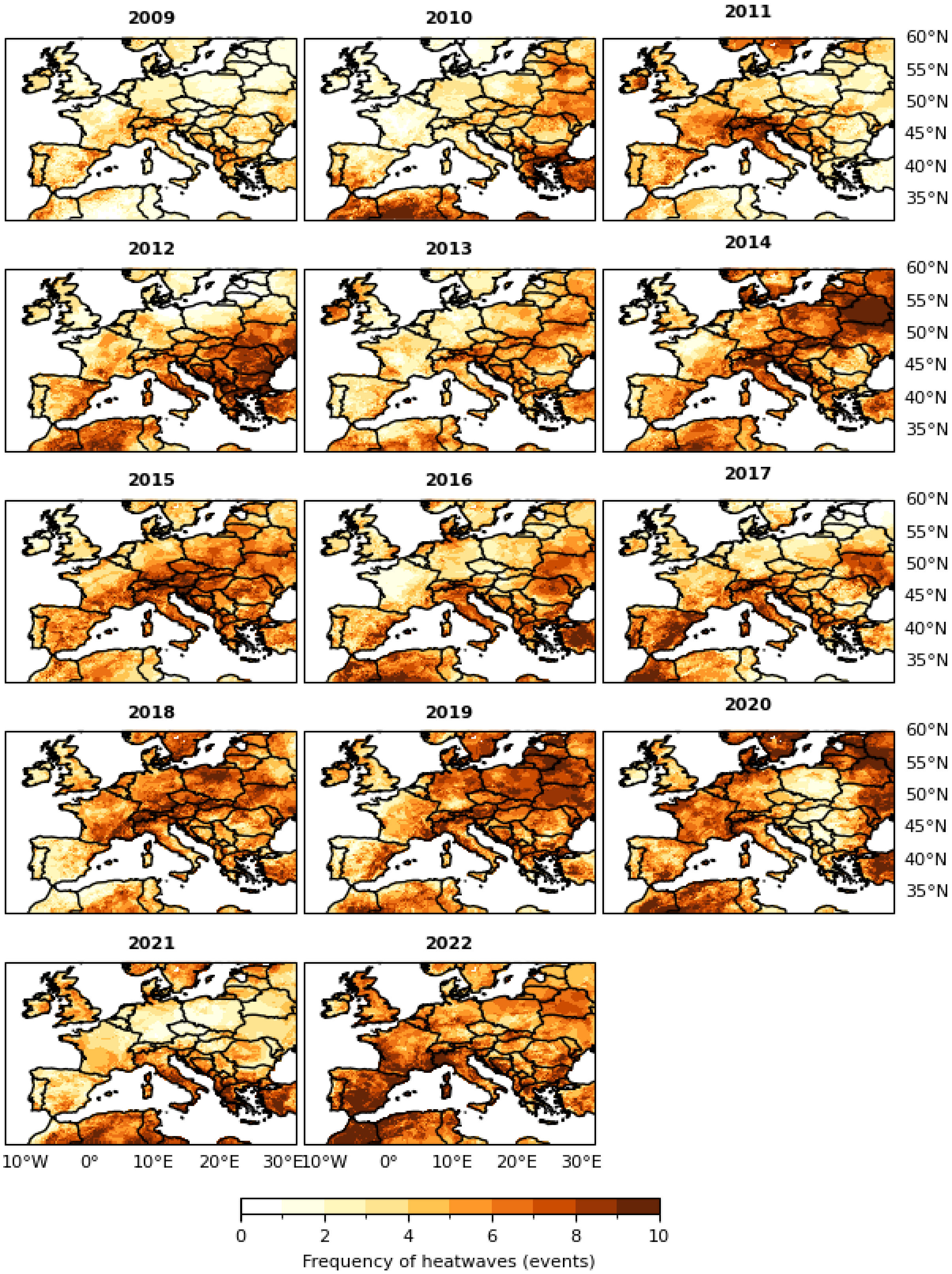

Figure S27: Annual spatial frequency of heatwaves between 2009 and 2022.

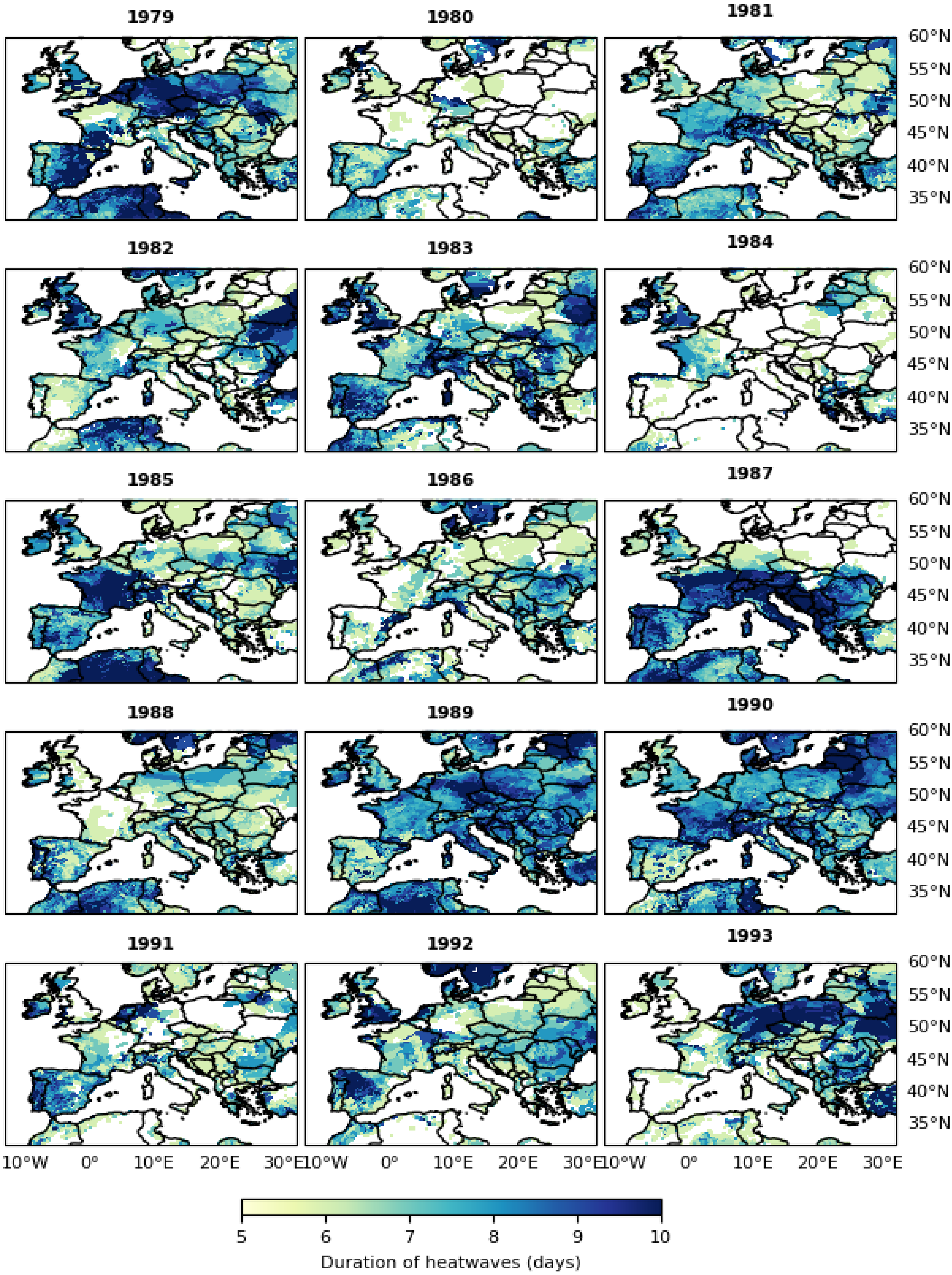

Figure S28: Annual spatial duration of heatwaves between 1979 and 1993.

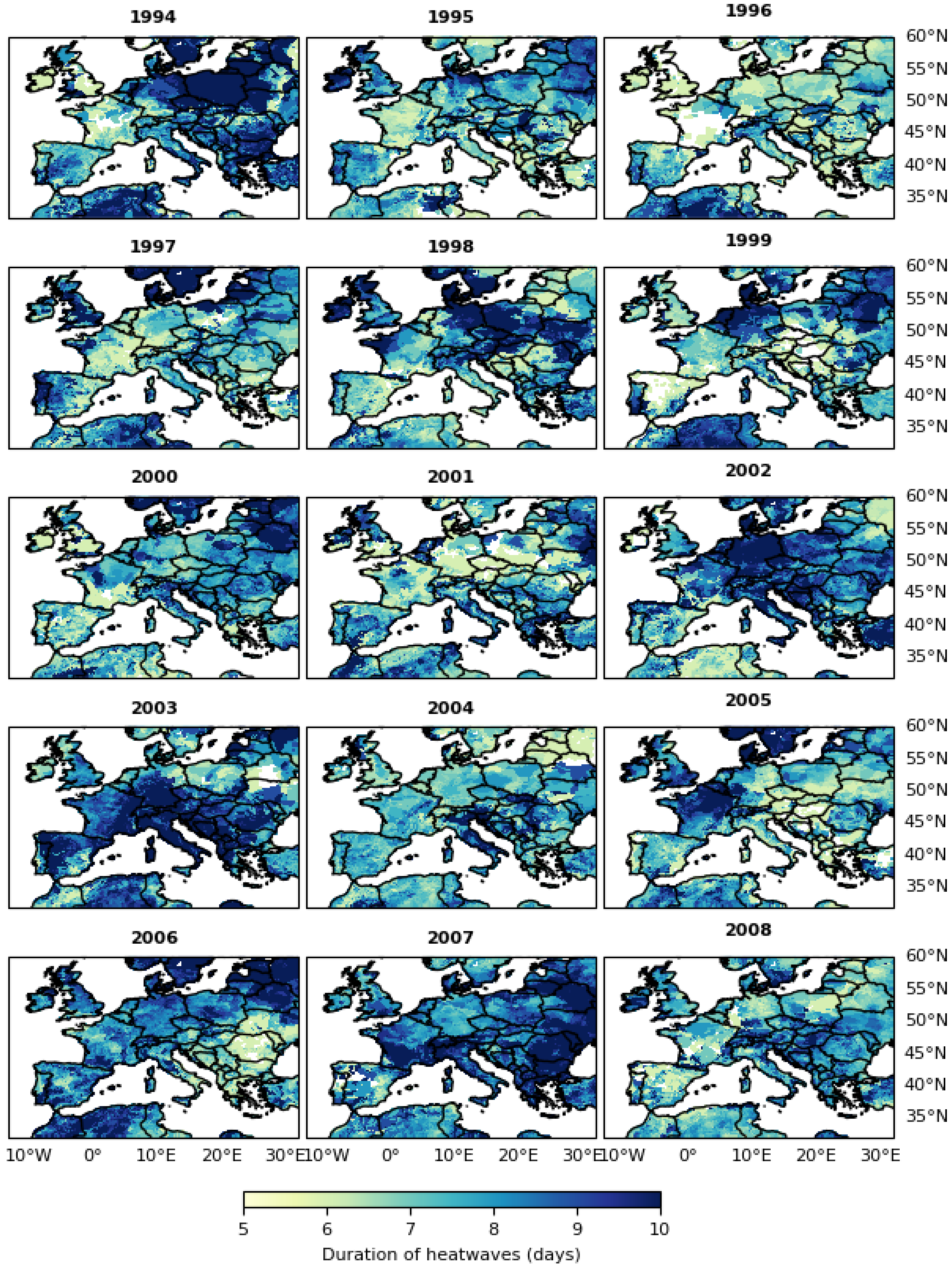

Figure S29: Annual spatial duration of heatwaves between 1994 and 2008.

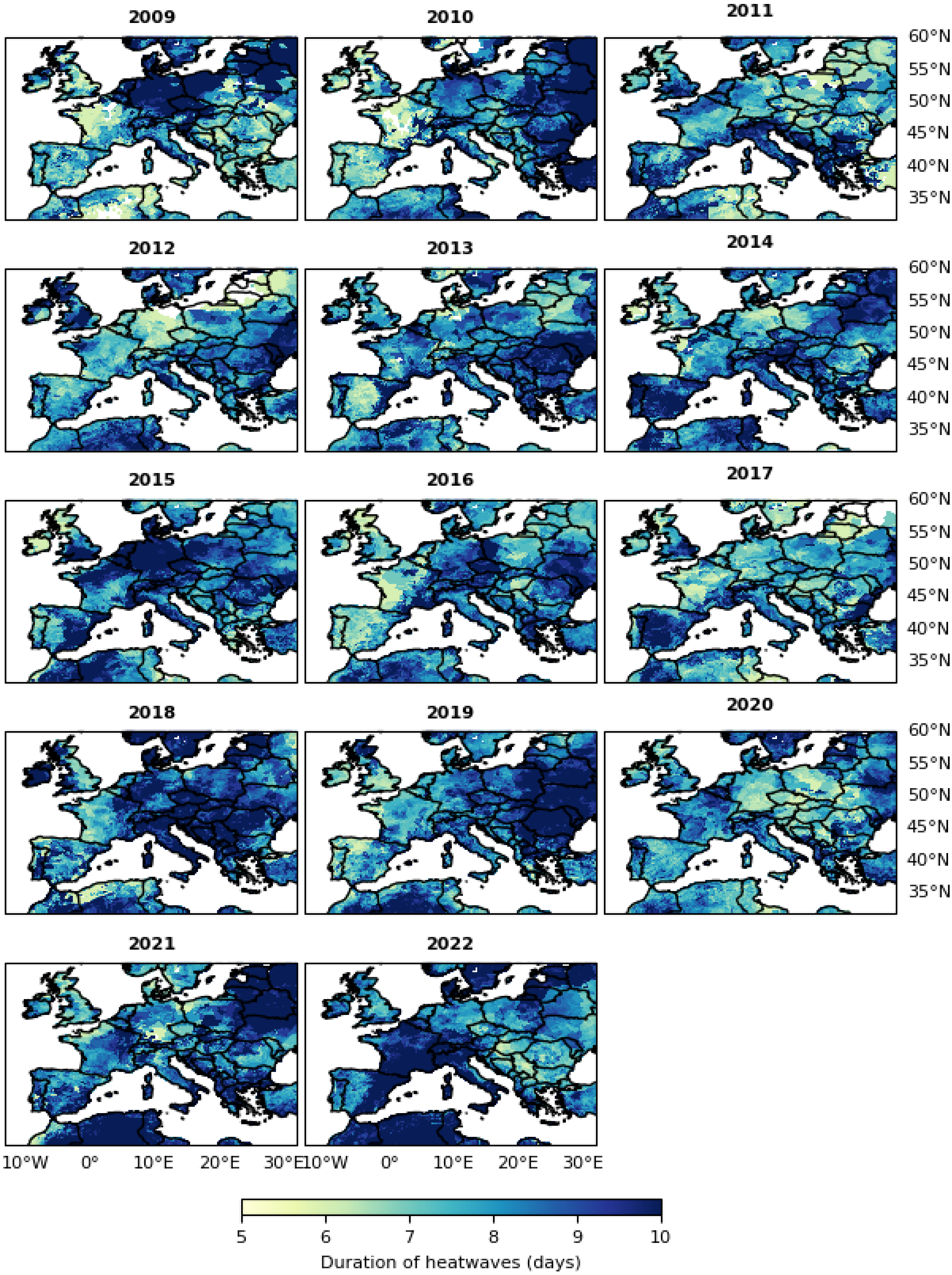

Figure S30: Annual spatial duration of heatwaves between 2009 and 2022.

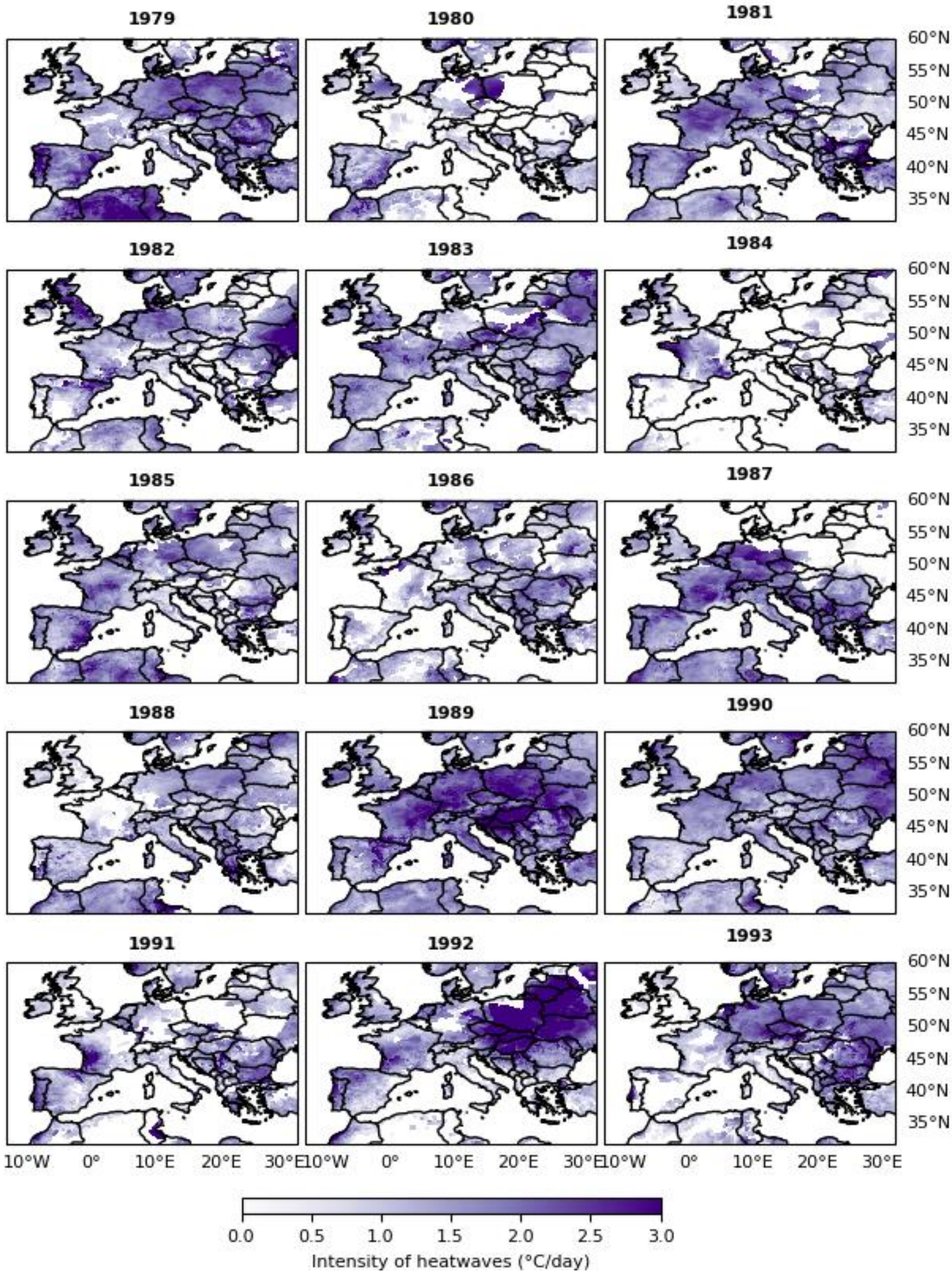

Figure S31: Annual spatial intensity between 1979 and 1993.

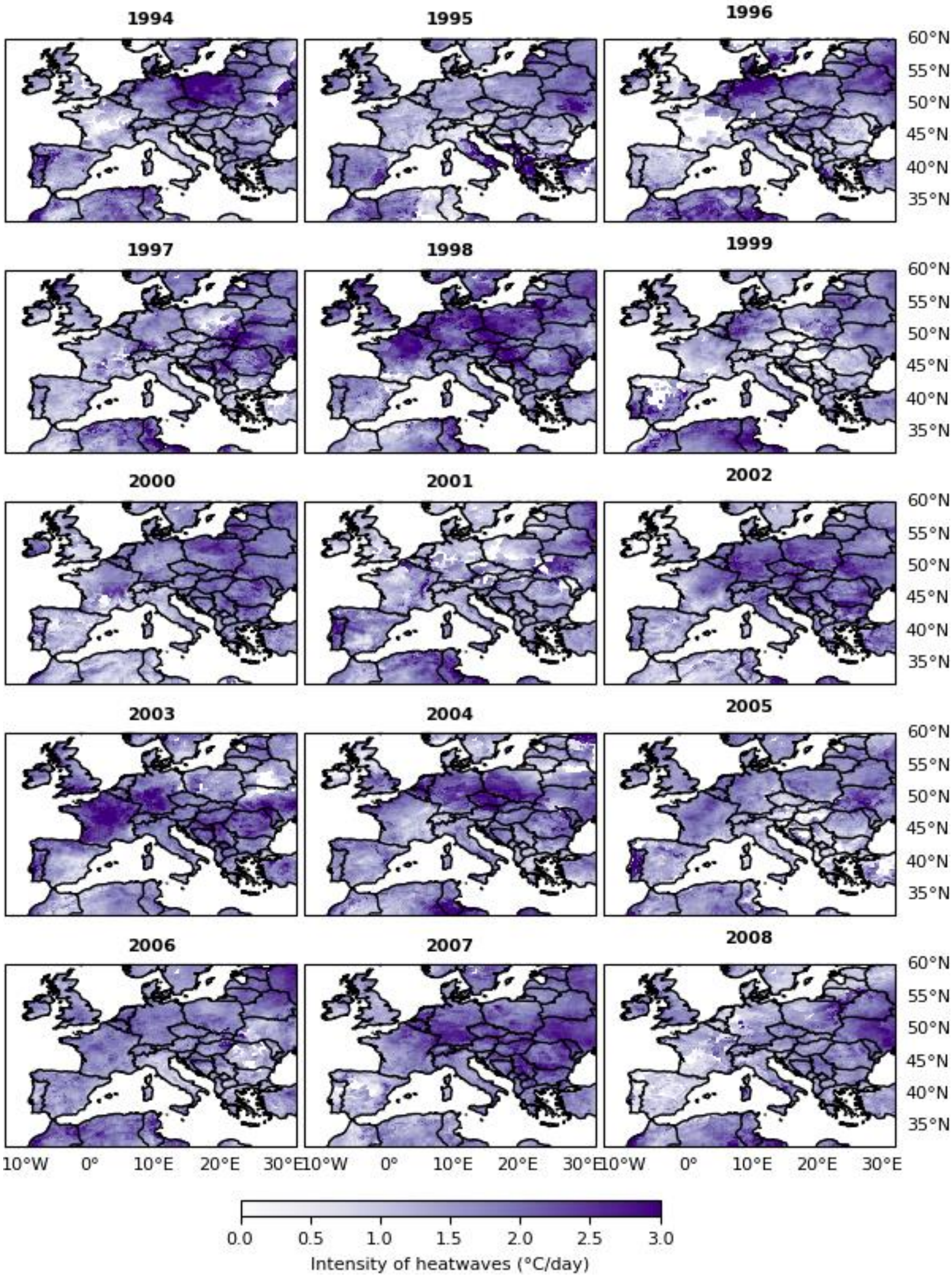

Figure S32: Annual spatial intensity between 1994 and 2008.

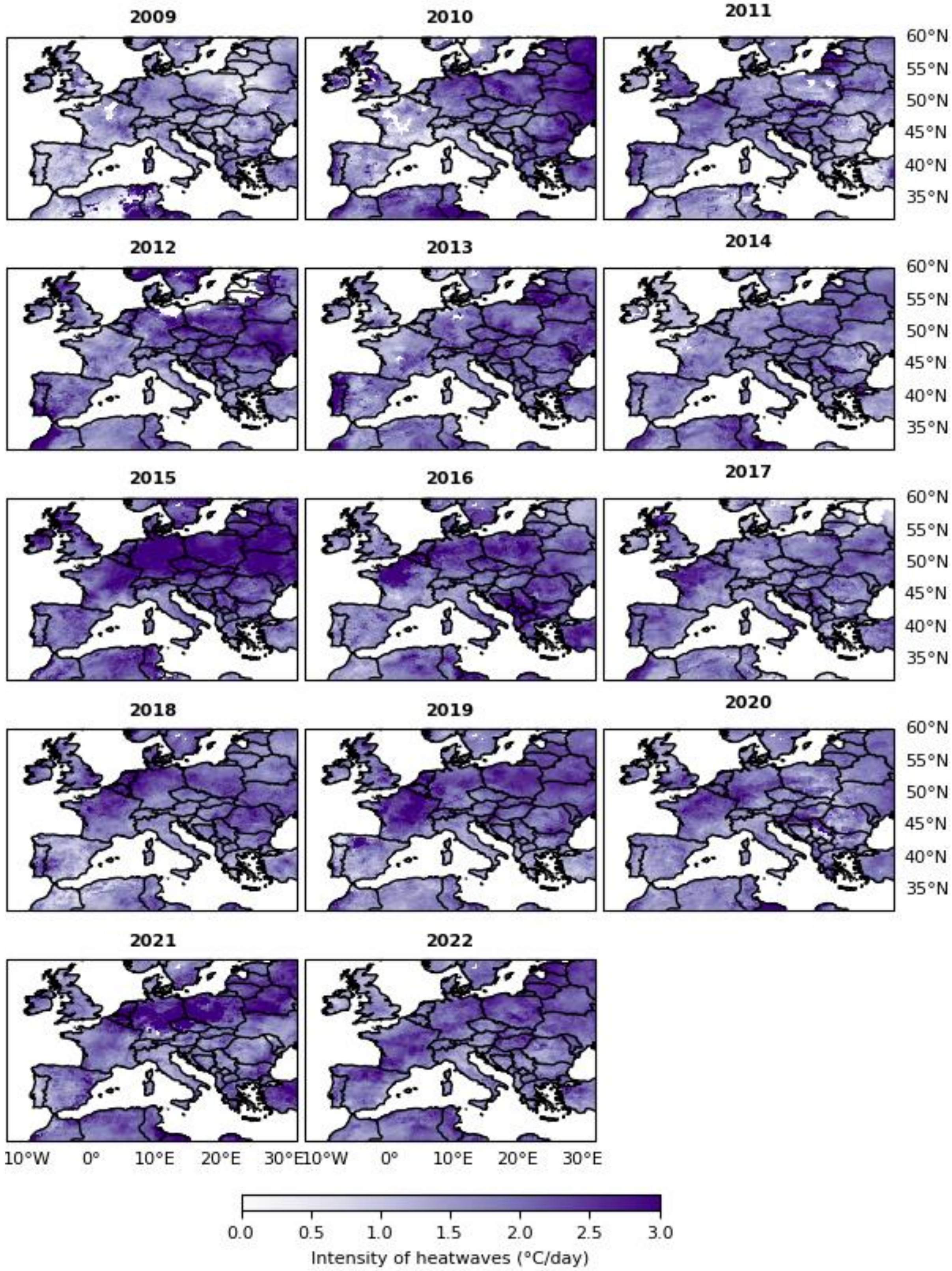

Figure S33: Annual spatial intensity between 2009 and 2022.

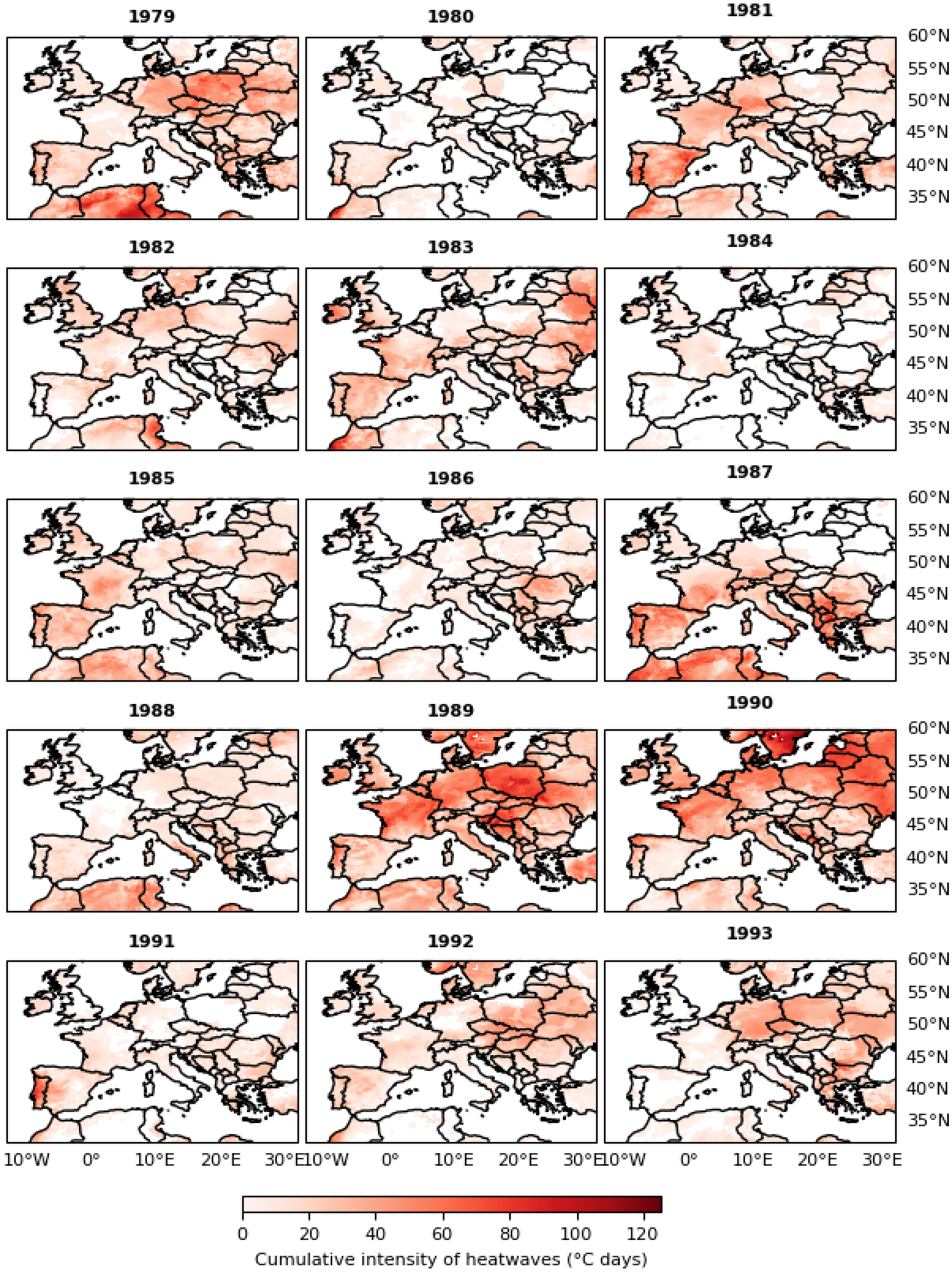

Figure S34: Annual spatial cumulative intensity between 1979 and 1993.

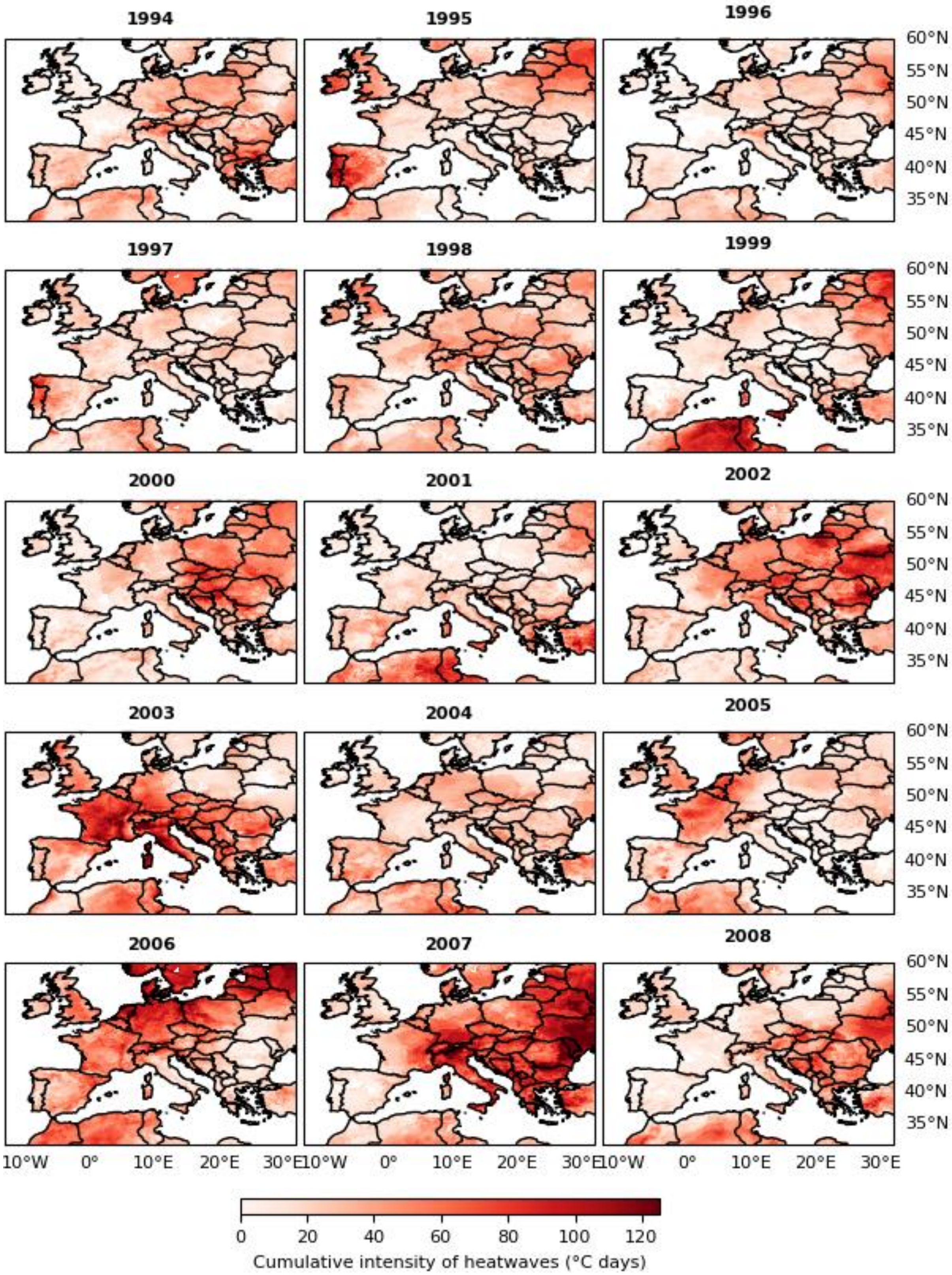

Figure S35: Annual spatial cumulative intensity between 1994 and 2008.

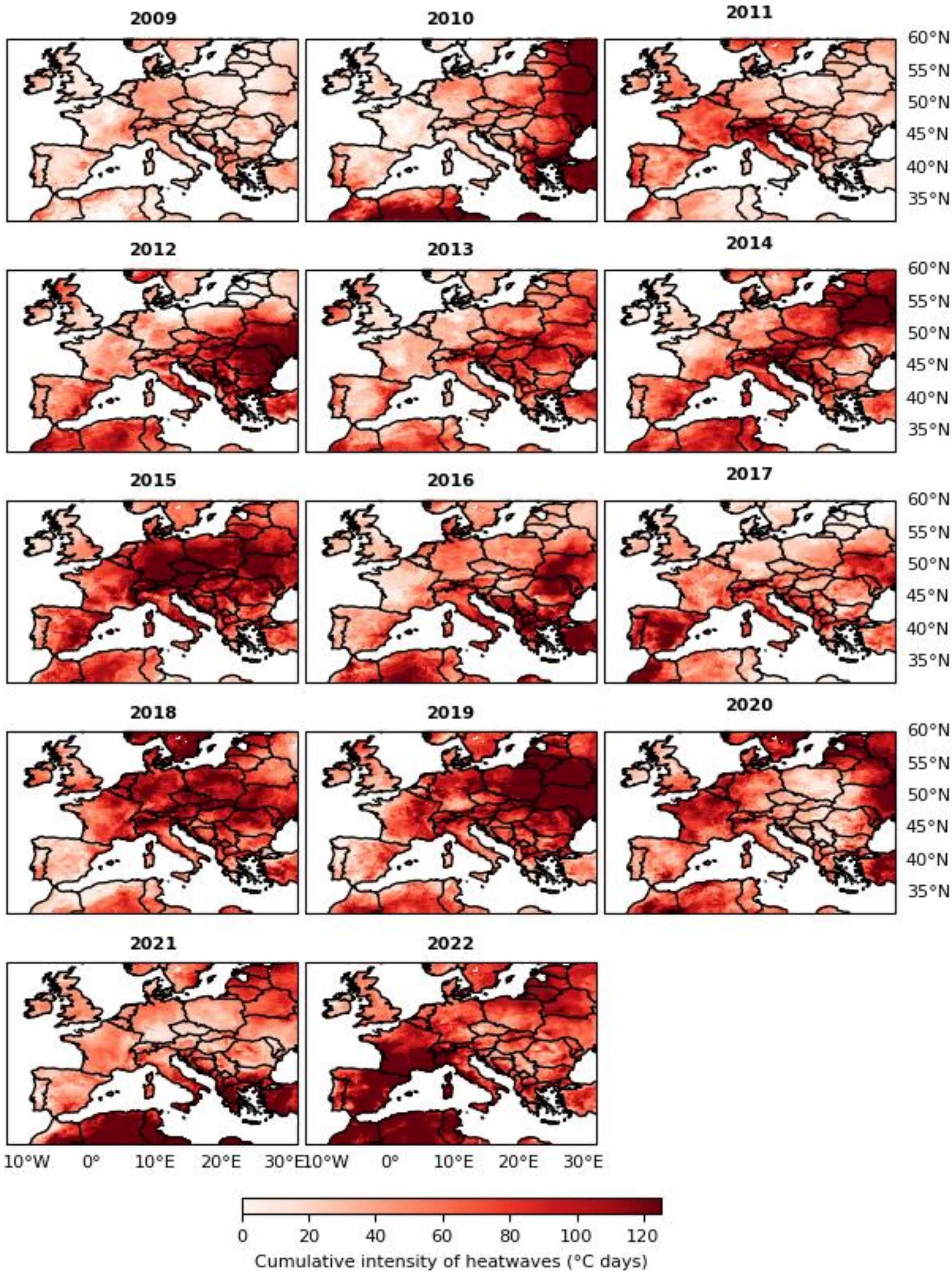

Figure S36: Annual spatial cumulative intensity between 2009 and 2022.

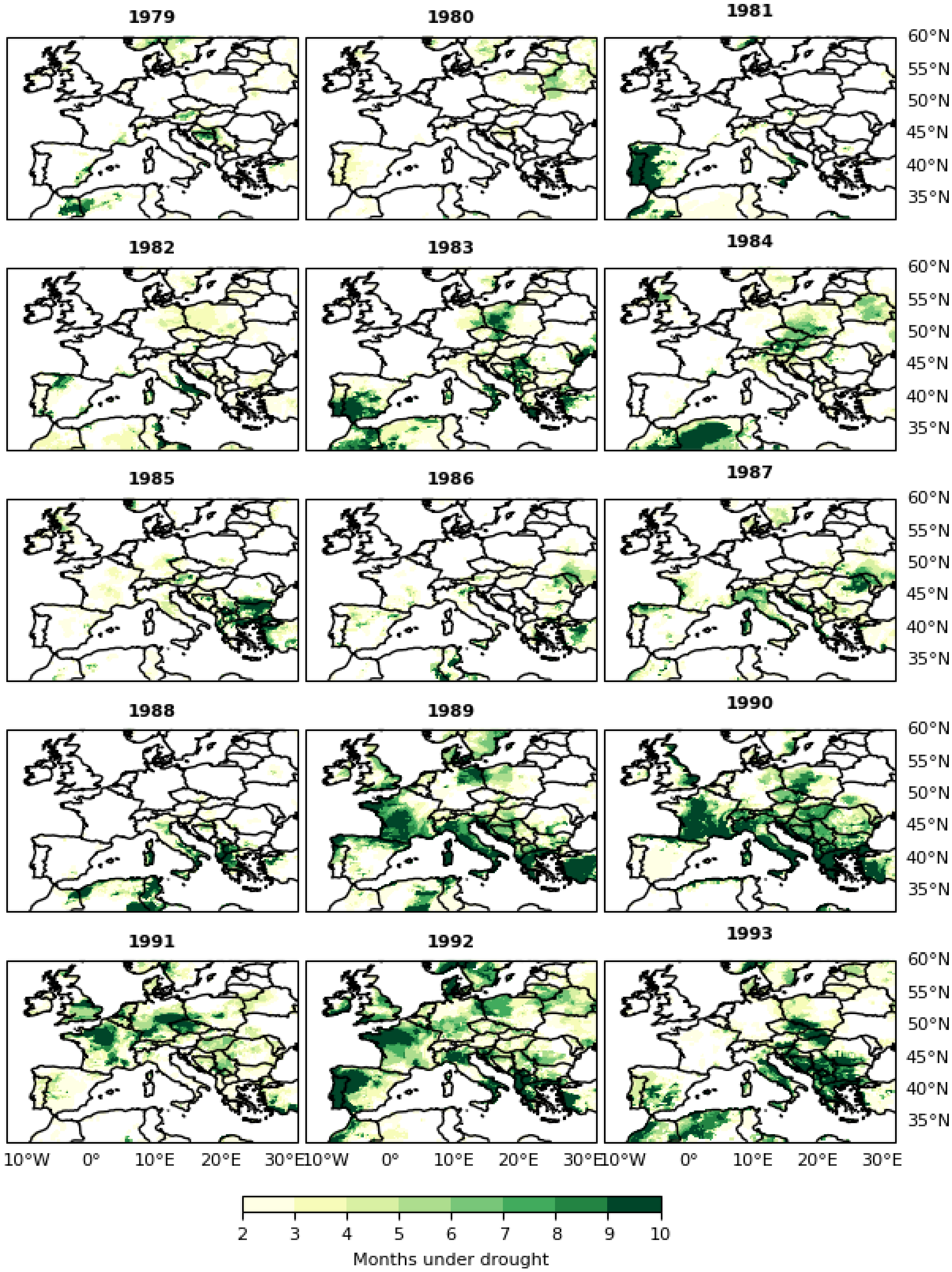

Figure S37: Annual spatial duration of droughts between 1979 and 1993.

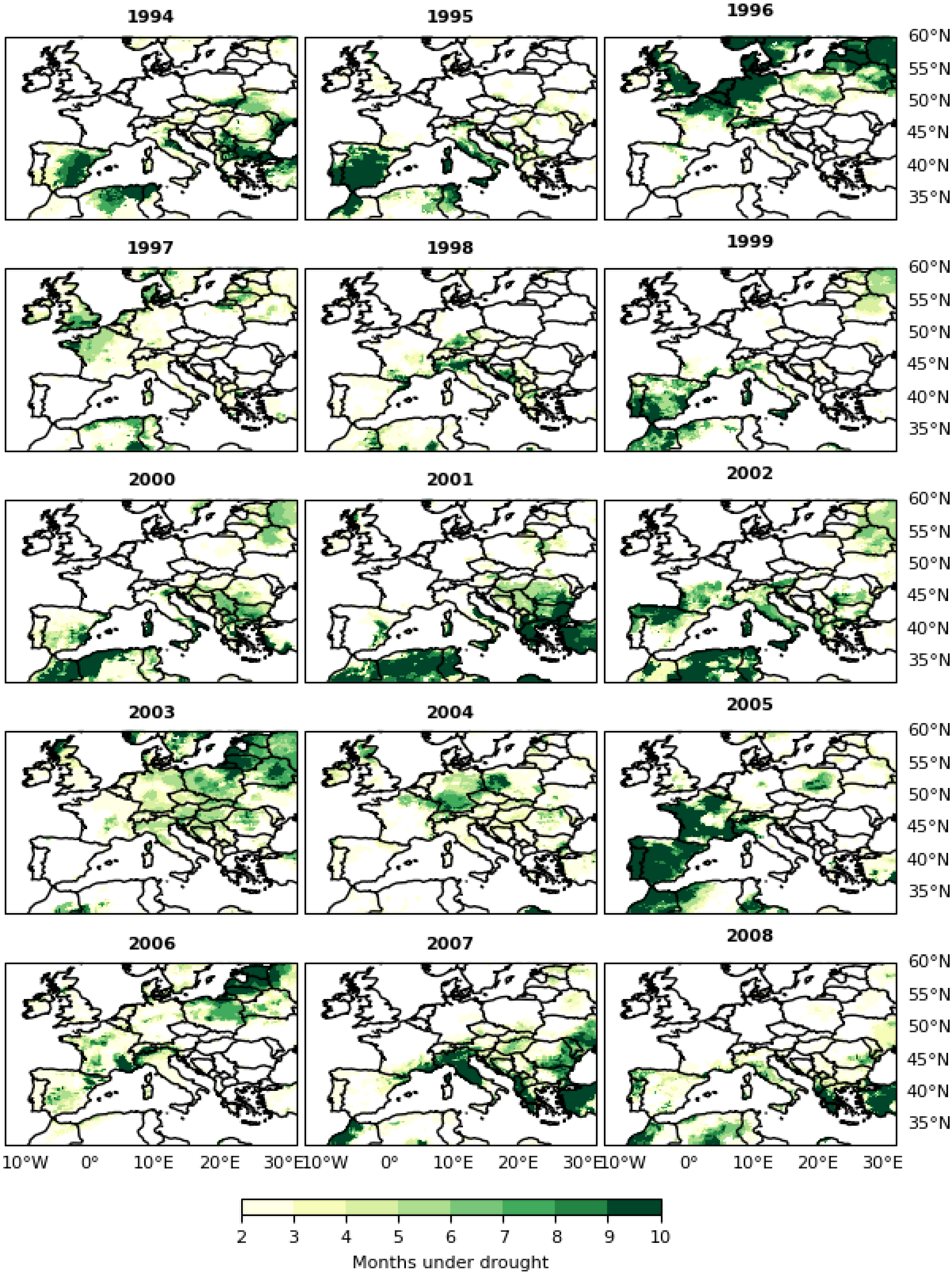

Figure S38

Figure S38: Annual spatial duration of droughts between 1994 and 2008.

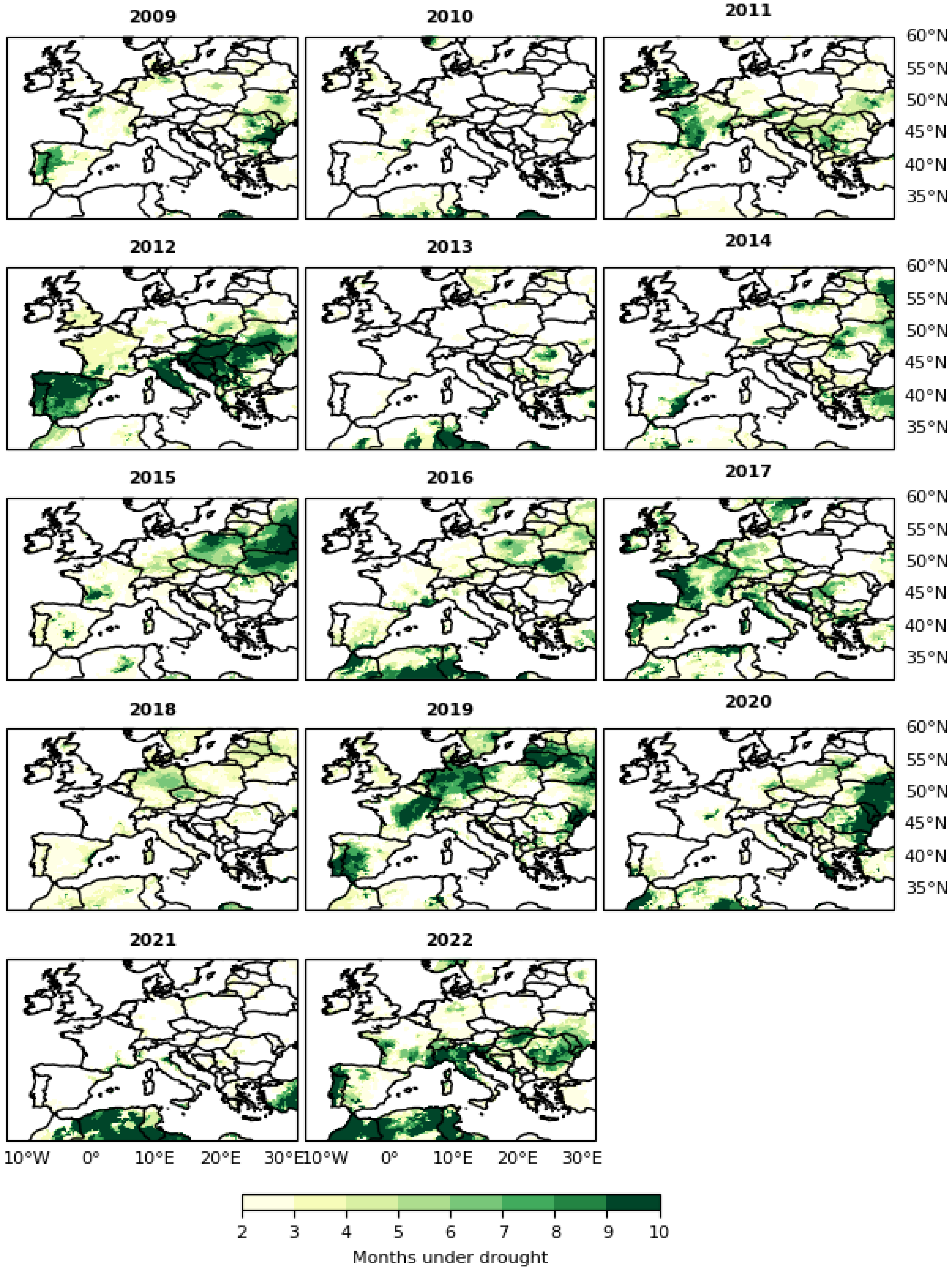

Figure S39: Annual spatial duration of droughts between 2009 and 2022.

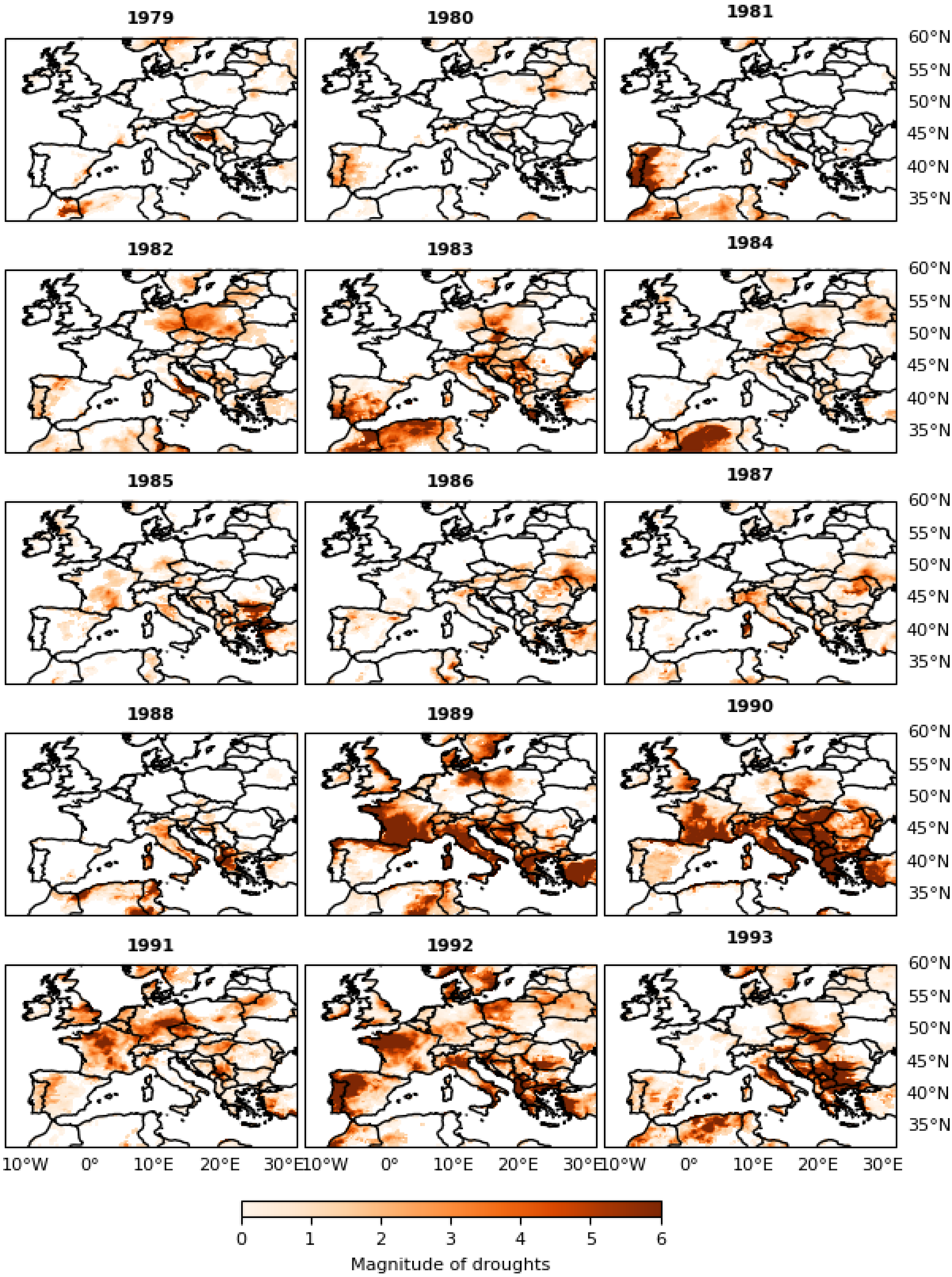

Figure S40: Annual spatial magnitude of droughts between 1979 and 1993.

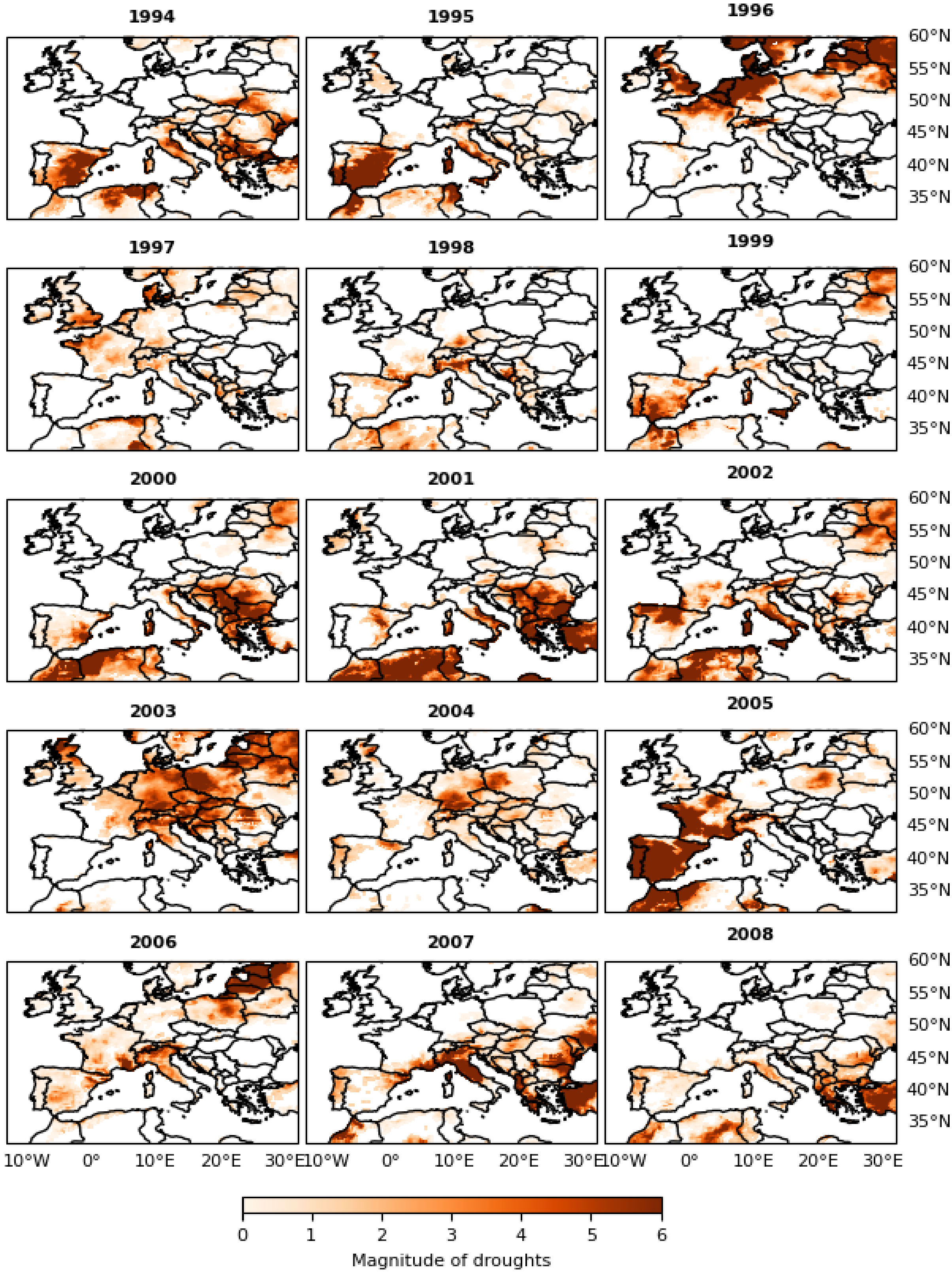

Figure S41: Annual spatial magnitude of droughts between 1994 and 2008.

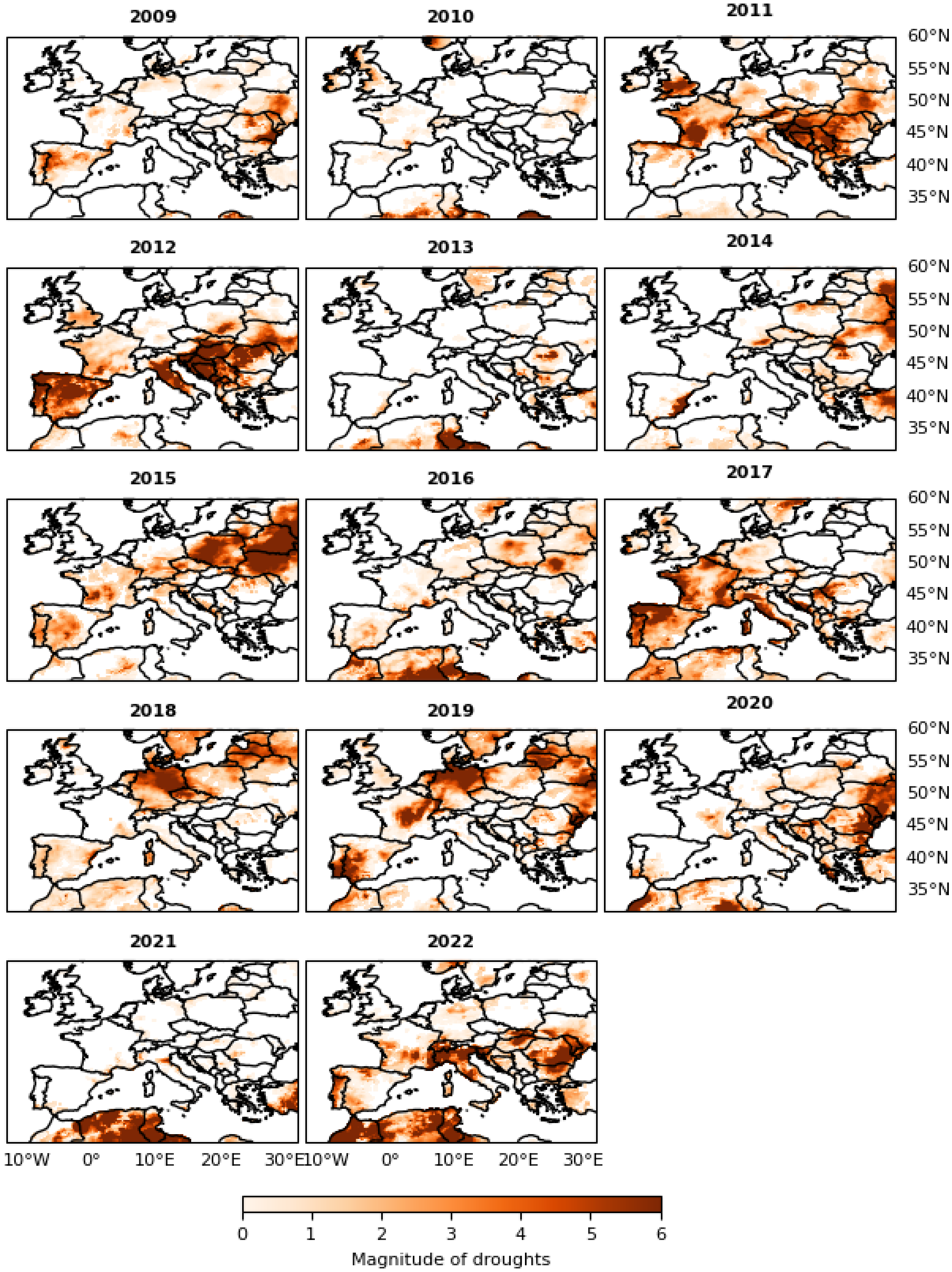

Figure S42: Annual spatial magnitude of droughts between 2009 and 2022.